NATIONAL AERONAUTICS AND SPACE ADMINISTRATION

The Deep Space Network
Progress Report 42-23

July and August 1974

JET PROPULSION LABORATORY
CALIFORNIA INSTITUTE OF TECHNOLOGY
PASADENA, CALIFORNIA

October 15, 1974

NATIONAL AERONAUTICS AND SPACE ADMINISTRATION

The Deep Space Network
Progress Report 42-23

July and August 1974

JET PROPULSION LABORATORY
CALIFORNIA INSTITUTE OF TECHNOLOGY
PASADENA, CALIFORNIA

October 15, 1974

Preface

Beginning with Volume XX, the Deep Space Network Progress Report changed from the Technical Report 32- series to the Progress Report 42- series. The volume number continues the sequence of the preceding issues. Thus, Progress Report 42-20 is the twentieth volume of the Deep Space Network series, and is an uninterrupted follow-on to Technical Report 32-1526, Volume XIX.

This report presents DSN progress in flight project support, tracking and data acquisition (TDA) research and technology, network engineering, hardware and software implementation, and operations. Each issue presents material in some, but not all, of the following categories in the order indicated:

Description of the DSN

Mission Support
  Ongoing Planetary/Interplanetary Flight Projects
  Advanced Flight Projects

Radic Science
  Radio Science Support
  Special Projects

Supporting Research and Technology
  Tracking and Ground-Based Navigation
  Communications—Spacecraft/Ground
  Station Control and Operations Technology
  Network Control and Data Processing

Network Engineering and Implementation
  Network Control System
  Ground Communications
  Deep Space Stations

Operations
  Network Operations
  Network Control System Operations
  Ground Communications
  Deep Space Stations

Planning and Facilities
  TDA Planning
  Facility Engineering

In each issue, the part entitled "Description of the DSN" describes the functions and facilities of the DSN and may report the current configuration of one of the five DSN systems (Tracking, Telemetry, Command, Monitor and Control, and Test and Training).

The work described in this report series is either performed or managed by the Tracking and Data Acquisition organization of JPL for NASA.

Contents

DESCRIPTION OF THE DSN

MISSION SUPPORT

Ongoing Planetary/Interplanetary Flight Projects

Advanced Flight Projects

SUPPORTING RESEARCH AND TECHNOLOGY

Communications—Spacecraft/Ground

PRECEDING PAGE BLANK NOT FILMED.

Network Control and Data Processing

NETWORK ENGINEERING AND IMPLEMENTATION

Deep Space Stations

OPERATIONS

Network Operations

PLANNING AND FACILITIES

TDA Planning

DSN Functions and Facilities

N. A. Renzetti

Office of Tracking and Data Acquisition

The objectives, functions, and organization of the Deep Space Network are summarized. Deep space station, ground communication, and network operations control capabilities are described.

The Deep Space Network (DSN), established by the National Aeronautics and Space Administration (NASA) Office of Tracking and Data Acquisition (OTDA) under the system management and technical direction of the Jet Propulsion Laboratory (JPL), is designed for two-way communications with unmanned spacecraft traveling approximately 16,000 km (10,000 mi) from Earth to the farthest planets of our solar system. It has provided tracking and data acquisition support for the following NASA deep space exploration projects, for which JPL has been responsible for the project management, development of the spacecraft, and conduct of mission operations:

(1) Ranger.

(2) Surveyor.

(3) Mariner Venus 1962.

(4) Mariner Mars 1964.

(5) Mariner Venus 1967.

(6) Mariner Mars 1969.

(7) Mariner Mars 1971.

(8) Mariner Venus/Mercury 1973.

The DSN has also provided tracking and data acquisition support for the following projects:

(1) Lunar Orbiter, for which the Langley Research Center carried out the project management, spacecraft development, and mission operations functions.

(2) Pioneer, for which the Ames Research Center carried out the project management, spacecraft development, and mission operations functions.

(3) Apollo, for which the Lyndon B. Johnson Space Center was the project center and the Deep Space Network supplemented the Spaceflight Tracking and Data Network (STDN), which is managed by the Goddard Space Flight Center (GSFC).

(4) Helios, a joint United States/West Germany project.

(5) Viking, for which the Langley Research Center provides the project management and Lander spacecraft, and conducts mission operations, and for which JPL provides the Orbiter spacecraft.

The Deep Space Network is one of two NASA networks. The other, the Spaceflight Tracking and Data Network, is under the system management and technical direction of the Goddard Space Flight Center. Its function is to support manned and unmanned Earth-orbiting and lunar scientific and advanced technology satellites. Although the DSN was concerned with unmanned lunar spacecraft in its early years, its primary objective now and into the future is to continue its support of planetary and interplanetary flight projects.

A development objective has been to keep the network capability at the state of the art of telecommunications and data handling and to support as many flight projects as possible with a minimum of mission-dependent hardware and software. The DSN provides direct support to each flight project through that project's tracking and data systems. This management element is responsible for the design and operation of the hardware and software in the DSN which are required for the conduct of flight operations.

As of July 1972, NASA undertook a change in the interface between the network and the flight projects. Since January 1, 1964, the network, in addition to consisting of the Deep Space Stations and the Ground Communications Facility, had also included the Mission Control and Computing Facility and had provided the equipment in the mission support areas for the conduct of mission operations. The latter facilities were housed in a building at JPL known as the Space Flight Operations Facility (SFOF). The interface change was to accommodate a hardware interface between the network operations control functions and the mission control and computing functions. This resulted in the flight project's picking up

the cognizance of the large general-purpose digital computers, which were used for network processing as well as mission data processing. It also assumed cognizance of all of the equipment in the flight operations facility for display and communications necessary for the conduct of mission operations. The network has already undertaken the development of hardware and computer software necessary to do its network operations control and monitor functions in separate computers. This activity became known as the Network Control System implementation. A characteristic of the new interface is that the network provides direct data flow to and from the stations via appropriate ground communications equipment to Mission Operations Centers, wherever they may be; namely, metric data, science and engineering telemetry, and such network monitor data as are useful to the flight project. It accepts command data from the flight project directly into the ground communications equipment for transmission to the station and thence to the spacecraft in a standardized format.

In carrying out its functions, the network activities can be divided into two general areas. The first includes those functions which are associated with the in-flight support and in tracking the spacecraft; its configuration can be characterized as follows:

(1) *DSN Tracking System.* Generates radio metric data; i.e., angles, one- and two-way doppler and range, and transmits raw data to mission control.

(2) *DSN Telemetry System.* Receives, decodes, records, and retransmits engineering and scientific data generated in the spacecraft to Mission Control.

(3) *DSN Command System.* Accepts coded signals from Mission Control via the Ground Communications Facility (GCF) and transmits them to the spacecraft in order to initiate spacecraft functions in flight.

The second category of activity supports testing, training, and network operations control functions and is configured as follows:

(1) *DSN Monitor and Control System.* Instruments, transmits, records, and displays those parameters of the DSN necessary to verify configuration and validate the network. Provides operational direction and configuration control of the network and primary interface with flight project mission control personnel.

(2) *DSN Test and Training System.* Generates and controls simulated data to support development, test, training, and fault isolation within the DSN. Participates in mission simulation with flight projects.

The capabilities needed to carry out the above functions have evolved in three technical areas:

(1) The Deep Space Stations that are distributed around Earth and which, prior to 1964, formed part of the Deep Space Instrumentation Facility. The technology involved in equipping these stations is strongly related to the state of the art of telecommunications and flight/ground design considerations and is almost completely multimission in character. Table 1 gives a description of the Deep Space Stations and the Deep Space Communications Complexes (DSCCs) they comprise.

(2) Ground communications. This technology supports the Earth-based point-to-point voice and data communications from the stations to the Network Operations Control Area at JPL, Pasadena, and to the Mission Operations Centers, wherever they may be. It is based largely on the capabilities of the common carriers throughout the world which are engineered into an integrated system by the Goddard Space Flight Center for support of all NASA programs. The term "Ground Communications Facility" is used for the sets of hardware and software needed to carry out the functions.

The Network Operations Control Center is the functional entity for centralized operational control of the network and interfaces with the users. It has two separable functional elements; namely, Network Operations Control and Network Data Processing.

The functions of the Network Operations Control Center are:

(1) Control and coordination of network support to meet commitments to network users.

(2) Utilization of the network data processing computing capability to generate all standards and limits required for network operations.

(3) Utilization of network data processing computing capability to analyze and validate the performance of all network systems.

The personnel who carry out the above functions are on the first floor of Building 230, wherein mission operations functions are carried out by certain flight projects. Network personnel are directed by an Operations Control Chief. The functions of the Network Data Processing are:

(1) Processing of data used by Network Operations Control for the control and analysis of the network.

(2) Display in Network Operations Control Area of data processed in Network Data Processing Area.

(3) Interface with communications circuits for input to and output from Network Data Processing Area.

(4) Data logging and production of the intermediate data records.

The personnel who carry out these functions are located in Building 202, which is approximately 200 m from Building 230. The equipment consists of minicomputers for real-time data system monitoring, two XDS Sigma 5's, display, magnetic tape recorders, and appropriate interface equipment with the ground data communications.

Table 1. Tracking and data acquisition stations of the DSN

| DSCC | Location | DSS | DSS serial designation | Antenna | | Year of initial operation |
				Diameter, m (ft)	Type of mounting	
Goldstone	California	Pioneer	11	26(85)	Polar	1958
		Echo	12	26(85)	Polar	1962
		(Venus)[a]	13	26(85)	Az-El	1962
		Mars	14	64(210)	Az-El	1966
Tidbinbilla	Australia	Weemala	42	26(85)	Polar	1965
		Ballima	43	64(210)	Az-El	1973
—	Australia	Honeysuckle Creek	44	26(85)	X-Y	1973
Madrid	Spain	Robledo	61	26(85)	Polar	1965
		Cebreros	62	26(85)	Polar	1967
		Robledo	63	64(210)	Az-El	1973

[a]A maintenance facility. Besides the 26-m (85-ft) diam Az-El mounted antenna, DSS 13 has a 9-m (30-ft) diam Az-El mounted antenna that is used for interstation time correlation using lunar reflection techniques, for testing the design of new equipment, and for support of ground-based radio science.

DSN Telemetry System, 1973–1976

E. C. Gatz
DSN Systems Engineering

This article provides a definition, functional description, and block diagram of the DSN Telemetry System. The characteristics of the capabilities being added during the 1973–1976 period are described. This system will be used to provide multiple-mission support to various flight projects.

I. Introduction

The Deep Space Network Telemetry System is being implemented by means of incremental additions and modifications, to provide multiple-mission support to a variety of planetary and interplanetary flight projects. Specifically, current system configurations are implemented to support:

(1) Pioneers 6 through 9

(2) Pioneers 10 and 11

(3) Mariner Venus/Mercury

(4) Helios A

(5) Viking

II. System Description

The DSN Telemetry System performs three main functions:

(1) Telemetry data acquisition and detection

(2) Telemetry data processing and transmission

(3) Telemetry System validation

Telemetry data acquisition and detection consist of those functions necessary to extract the telemetry information modulated on the downlink radio-frequency carrier(s) from the spacecraft and to detect the data bits. Telemetry data processing and transmission consist of those functions necessary to format, record, and transmit

the data to users. Telemetry System validation consists of those functions necessary to validate the performance of the Network and to verify that this performance meets specifications.

III. Key Characteristics

Key characteristics of the DSN Telemetry System evolve as new components and capabilities are added. For this reason, a succession of Telemetry System models is defined, each representing a new increment of capability. The following are key characteristics of the models through the period of 1973–1976.

A. Mark III-73 Model

(1) Multimission capability at each DSS for receiving and formatting uncoded telemetry and block-coded telemetry

(2) Mission-peculiar software for Pioneer convolutional-coded telemetry

(3) Centralized monitoring of Telemetry System performance by observation of project displays in the Mission Control and Computing Center (MCCC)

(4) Capability at each DSS for single carrier, dual subcarrier, and formatting for high-speed and wideband communication

(5) Recording of pre- and post-detection analog records with nonreal-time playback

(6) Production of digital Original Data Record (ODR) at each DSS, and playback via manual control or automatic response to project inputs

(7) Real-time reporting of telemetry status at the station to the DSS Monitor and Control Subsystem

B. Mark III-74 Model

Key characteristics of the Mark III-74 model are the same as those for Mark III-73, plus the following:

(1) Multimission capability for sequential decoding of convolutionally coded telemetry data (to accommodate both Pioneer and Helios coded data)

(2) Real-time monitoring of Telemetry System performance at the Network Operations Control Center (NOCC)

C. Mark III-75 Model

Key characteristics of the Mark III-75 are the same as those for Mark III-74, plus the following:

(1) Capability at the 64-m DSS to handle multiple carriers (up to four) and multiple subcarriers (up to six) with decoding, ODR, and formatting for communications circuits

(2) Centralized monitoring of Telemetry System performance at the NOCC, and reporting via the DSN Monitor and Control System

(3) Central log (Network Data Log) of all data received at the DSS, with gap accounting and automated recall of missing data from the DSS ODRs

(4) Generation of the Intermediate Data Record (IDR), a time-merged record of all received telemetry data

(5) Generation of Telemetry System predicts and configurations, and transmission to DSS for manual control of system elements

IV. Functional Description

A brief description of the operation of the DSN Telemetry System is presented in the remainder of this section. A simplified block diagram of the system is shown in Fig. 1.

At the Deep Space Station, spacecraft signals are received and amplified in the Antenna Microwave Subsystem. The RF carriers are then acquired and tracked by the receivers. A coherent reference and wideband signals are passed to the Subcarrier Demodulator Assemblies (SDA) where the subcarriers are regenerated, separated, and demodulated. Low-rate uncoded data are passed through analog-to-digital (A-D) converters to the Telemetry and Command Processor (TCP) for bit synchronization detection, and formatting for high-speed data transmission. All medium and high-rate streams are passed to a Symbol Synchronizer Assembly (SSA). Coded symbol streams are then forwarded to either a Block Decoder Assembly (BDA) or to a Digital Decoder Assembly (DDA) for decoding. Resulting data streams are outputted to high-speed data (HSD) or wideband (WBD) lines, depending upon data rate. Interlaced with these data are time tags and partial status.

Analog records of all receiver and SDA outputs are made at the DSS by the Pre/Post Detection Recording Subsystem; digital ODRs are made of all data after the bit synchronization and decoding processes.

The high-speed or wideband data are then transmitted to the MCCC or to a Remote Project interface at JPL, and to the Network Operations Control Center. All data inputs to the MCCC and Remote Project Interface are recorded on the Network Data Log. In the NOCC, the telemetry data are processed to analyze DSN Telemetry System performance. The performance is compared to expected values, and status and alarms are relayed to the Network Operations Control Area (NOCA). In addition, a permanent System Performance Record (SPR) is made of the DSN performance and a gap list of all missing or error data is prepared. In the Mark III-75 model, this gap list is used to recall missing data from the DSS ODRs. In the Mark III-73 and 74 models, the recall requests come from the MCCC or are manually inputted at the DSS.

In the Mark III-75 model, the Network Data Log and data recalled from the ODR can be combined in time sequence so that selected data blocks and their time intervals can be placed on an Intermediate Data Record. This record, which can contain data up to a full DSS pass, will be available to projects for their Master Data Record (MDR) processing.

In the Mark III-75 model, Telemetry System predicted signal levels are generated in the NOCC and transmitted to the DSS to be displayed as an aid in the manual control and configuration of the station. These predictions require project inputs concerning spacecraft configuration and data mode.

DSS

RECEIVER/EXCITER SUBSYSTEM

DSS TELEMETRY SUBSYSTEM

ODR

GCF
WI

ANTENNA
MICROWAVE
SUBSYSTEM

RECEIVER
ASSEMBLIES

SUBCARRIER
DEMODULATOR
ASSEMBLIES

SYMBOL
SYNCHRONIZER
ASSEMBLIES

BLOCK
DECODER
ASSEMBLIES

DATA
DECODER
ASSEMBLIES

ANTENNA
MECHANICAL
SUBSYSTEM

TEST AND
TRAINING DATA

TELEMETRY
DATA
SPECIAL
REQUESTS

TELEMETRY AND
COMMAND
PROCESSOR
ASSEMBLIES

ODR

TIME
TAGS

STATUS   STATUS   PREDICTS

PRE/POST
DETECTION RECORDING
SUBSYSTEM

DSS
MONITOR & CONTROL
SUBSYSTEM

FREQUENCY & TIMING
SUBSYSTEM

PREDICTS

FOLDOUT FRAME 1

GCF ———————————————— NOCC ————————————————

WIDEBAND

HIGH SPEED

MCC AND REMOTE
PROJECT INTERFACE

NETWORK OPERATIONS CONTROL
AREA DISPLAYS AND I/O

ODR

DATA
DECODER
ASSEMBLIES

TELEMETRY AND
COMMAND
PROCESSOR
ASSEMBLIES

ODR

TELEMETRY
DATA
SPECIAL
REQUESTS

**GCF HIGH-SPEED DATA AND
WIDEBAND SUBSYSTEMS**

STATION
WIDEBAND
DATA
ASSEMBLY

CENTRAL
WIDEBAND
DATA
ASSEMBLY

STATION
HIGH-SPEED
DATA
ASSEMBLY

CENTRAL
HIGH-SPEED
DATA
ASSEMBLY

**NETWORK
DATA PROCESSING
TERMINAL**

COMM LOG
PROCESSOR
ASSEMBLY

NC DISPLAY
SUBSYSTEM

DATA RECORD
SUBSYSTEM

NETWORK
DATA
LOG

TELEMETRY
IDR

**NETWORK
DATA PROCESSING
AREA**

NDPA COMM
PROCESSOR

NC TELEMETRY
SUBSYSTEM

NC SUPPORT
SUBSYSTEM

SYSTEM
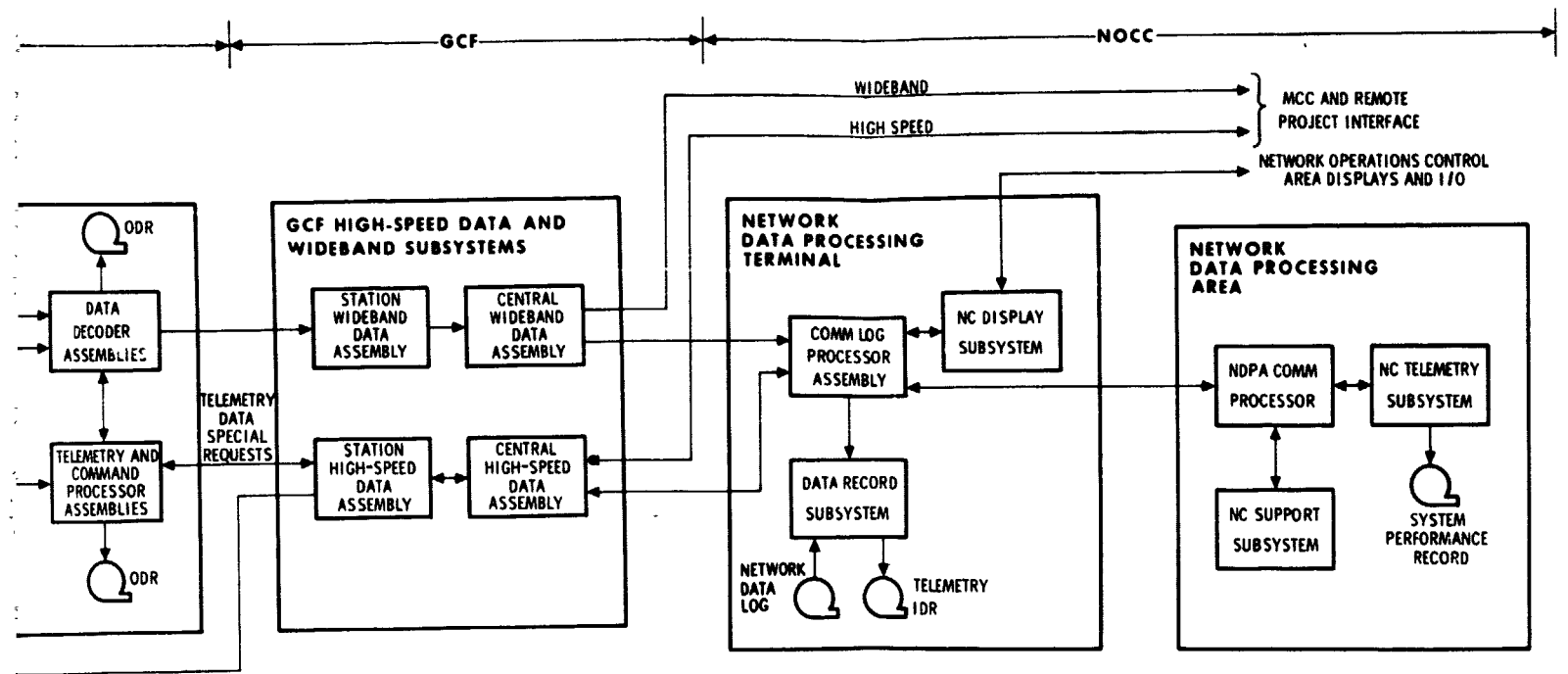PERFORMANCE
RECORD

Fig. 1. DSN Te'er etry System Mark III-75 block diagram

9

FOLDOUT FRAME 2

DSN Tracking System Predictions

W. D. Chaney
DSN Systems Engineering

O. B. Shows
Philco-Ford Corporation

The Deep Space Network Tracking System predictions include angles, frequencies and ranges for use by the Deep Space Stations in the acquisition and tracking of spacecraft. These predictions are also used to validate the radio metric data generated by the Deep Space Stations.

I. Introduction

The Network Operations Control Center Sigma 5 computer will assume the responsibility of generating the DSN predictions which are currently computed by the Mission Control and Computing Center. Since the Deep Space Network tracking prediction capability will be a phased implementation, the transfer of prediction capability from the Mission Control and Computing Center to the Network Operations Control Center will be incremental.

II. System 1: Network Operations Control Center, Block I

System 1 became operational March 1, 1974. In this phase the Sigma 5 computer assumes the responsibility of transmitting the predicts to the Deep Space Stations. The Mission Control and Computing Center generates the predictions and provides a magnetic tape of the prediction transmission file. The prediction tape is converted for high-speed data transmission on the off-line Sigma 5 computer and a high-speed data formatted tape is outputted for transmission by the on-line Sigma 5 computer (see Fig. 1).

III. System 2: Network Operations Control Center, Block II

The Sigma 5 computer will provide a capability of generating predictions from a project supplied "phi factor polynomial" magnetic tape interface. The predictions

generated on the Sigma 5 computer will contain the same prediction data output that was previously generated by the Mission Control and Computing Center.

The Sigma 5 batch process mode system (off-line computer) generates the predictions and converts these predictions to a high-speed data formatted magnetic tape. The predictions are then computed from the project-supplied phi factor polynomial tape. The prediction transmission on the on-line Sigma 5 will be the same as System 1 (see Fig. 1).

IV. System 3: Network Operations Control Center, Block III

System 3 will provide a capability of generating predictions from project-supplied state vector or probe ephemeris tape (Ref. 1). The state vector will simplify the DSN/Project interface from a magnetic tape interface to a six-parameter administrative interface. The state vector interface would be used for DSN acquisition studies and for DSN prediction generation in support of spacecraft tracking.

The DSN Tracking System predictions will utilize a special program designed specifically for generating accurate station prediction data. Economics, simplicity, size, and speed dictate its design. Program capabilities include the following:

(1) The ability to generate the trajectory of a spacecraft or landed probe utilizing adequate force models and to write a trajectory tape.

(2) The ability to process a trajectory tape generated by the Project's Double Precision Trajectory Program (DPTRAJ).

(3) The ability to write a tape with station observables and events (rise, set, occultations, etc.) for up to 10 stations.

(4) The ability to correct for range bias, antenna cone offsets, and angular observables correction (geodetic, aberration, refraction, and structural).

(5) The ability to utilize accurate time transformation and polar motion data.

The trajectory portion includes mathematical models of the forces which influence the space probe's motion. These forces are integrated numerically (Cowell method)

to generate a probe trajectory in the inertial 1950.0 Earth mean equator frame (EME 1950.0) utilizing planetary ephemerides generated in the same coordinate system. Accurate time and coordinate transformation capabilities provide the ability to represent the trajectory profile and probe's accelerations in their natural or desired frames.

A single "calibration station" is used in the interactive light times calculation instead of an actual station. Actual station light times are analytically related to the calibration station. The calibration or reference station is placed on the surface of a transparent Earth, and is located at longitude and latitude zero for maximum diurnal signature. Upleg and downleg light times are independently calculated at selected times corresponding to the natural frequencies of Chebyshev polynomials of the first kind and specified degree. This automatically yields the best least squares fit of the calculated qualities in polynomial form.

Analytic methods are introduced to calculate the viewability windows of up to 10 stations, the Chebyshev polynomial coefficients of the light time solutions and other useful quantities within the windows. The independent variable for all calculated polynomials is ephemeris time. Consequently, actual events and types of observables in any time scale can all be calculated from the polynomials.

Station observables such as range, range rate, transmitted frequency shifts, and angular data are all accurately calculated. The calculations include precise station location, antenna and media corrections, and relativistic effects on radio signals and coordinates of the time clock and probe. More efficiency is achieved by utilizing selective double precision as contrasted to blanket double precision in the calculations. The program generates a trajectory tape for later use or processes a trajectory tape generated by Project navigation programs. Reference station polynomials are saved for processing different sets of stations. The station polynomials are output and saved for processing observables at densities specified by the user.

The phi factors generated by the Fast Phi Factor Generation Program are stored on a phi factor file and a phi factor save tape. The phi factors stored on the phi factor file are interpolated to produce the prediction data. The prediction data are converted for high-speed data transmission to the Deep Space Stations and to the Network Operations Control Center radio metric monitor for system validation (Fig. 1).

V. Summary

System 1, which is operational, will transmit predictions to the DSSs. System 2 will complete acceptance testing in September 1974 and will generate predictions using a project-supplied phi factor polynomial tape. System 3 will generate phi factors from a state vector or project-supplied trajectory tape. The phi factors will be interpolated to produce predictions. The predictions will be transmitted to the Deep Space Stations and to the Network Operations Control Center.

Reference

1. Khatib, A. R., "The Fast Phi-Factor Generator Program," Document 900-628, Jet Propulsion Laboratory, Pasadena, Calif., July 7, 1973 (an internal document).

SYSTEM 0 - MCCC SYSTEM

1108 | 360/75

STATE VECTOR → DPTRAJ → PROBE EPHEMERIS TAPE → φ FACTORS → DSS OBSERVABLES PROGRAM → TTY OR HIGH SPEED DATA FORMATTING → TO DSS VIA HSD OR TTY

PLANETARY EPHEMERIS TAPE

SYSTEM 1 - NOCC BLOCK I

1108 | 360/75 ... 360/75 | Σ 5 OFFLINE ... Σ 5 ONLINE

STATE VECTOR → DPTRAJ → PROBE EPHEMERIS TAPE → φ FACTORS → DSS OBSERVABLES PROGRAM → PREDICT OBSERVABLES TAPE → HSD FORMATTING → HSD TRANS-MISSION TAPE → HSD TX → TO DSS VIA HSD

PLANETARY EPHEMERIS TAPE

SYSTEM 2 - NOCC BLOCK II

1108 | Σ 5 OFFLINE ... Σ 5 OFFLINE | Σ 5 ONLINE

STATE VECTOR → POEAS/ SOP → φ FACTOR POLY-NOMIAL TAPE → PREDICTS → PREDICTS TAPE OR DISC INTERFACE → HSD FORMATTING → HSD TRANS-MISSION TAPE → HSD TX → TO DSS VIA HSD

SYSTEM 3 - NOCC BLOCK III

1108 | Σ 5 ONLINE

TO RTM

STATE VECTOR → FAST PHI FACTOR PROGRAM → PHI FACTOR FILE → PREDICTS → PREDICTS FILE → HSD FORMATTING AND TRANSMISSION → TO DSS VIA HSD

PROBE EPHEMERIS TAPE | PLANETARY EPHEMERIS TAPE   PHI FACTOR SAVE TAPE   PREDICTS SAVE TAPE

Fig. 1. The DSN prediction configuration

Viking Mission Support

D. J. Mudgway
DSN Systems Engineering

D. W. Johnston
DSN Operations

In a previous article the basis for integration and data systems testing between the Compatibility Test Area (CTA 21) and the Viking Mission Control and Computing Center (VMCCC) was given, and the first eleven of these tests were described. This article describes the concluding tests in the system integration series and the results of a series of five data system compatibility tests. These tests provide an end-to-end 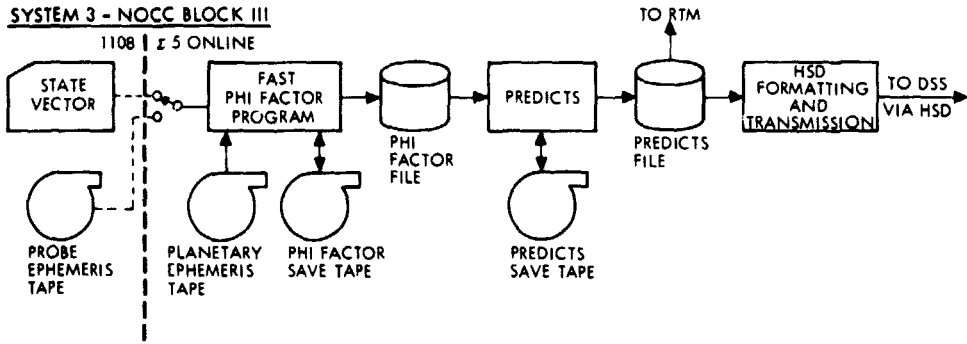verification of the integrity of the Ground Data System under typical mission loading conditions. Starting with the modulated RF carriers input to CTA 21, the data are sequentially processed through the station, passed across the Ground Communications Facility to VMCCC and finally displayed in the Mission Support Areas. For several of these tests, maximum data loading conditions were established which included six simultaneous telemetry data streams, two command streams, one monitor and one tracking data stream.

This report covers the final tests of the DSN/VMCCC System Integration Test series. It also covers the Data System Compatibility Test Series.

I. DSN/VMCCC System Integration

The interfaces, test plans, and responsibilities for the DSN/VMCCC System Integration Test (SIT) series were described in the last issue. This article gives results of the final test of this series.

A. SIT 12, June 24, 1974 — Two Orbiters and Lander Telemetry and Command

The primary objective of this test was to repeat the steps of SIT 11 and its objectives and to verify specific objectives of earlier SITs which had not been completed or against which liens existed. The secondary objective was to transfer Viking Orbiter and Lander telemetry and command data at maximum rates to determine if constraints existed as applicable to the Data System Compati-

bility Tests and as a result recommend operational work-arounds.

The test was to be conducted in four phases.

Phase 1. Transfer and process six telemetry data streams in real-time using the 28.5 kbps wideband line and the high speed data line.

Phase 2. To replay the 7- and 9-track digital original data records (DODRs) recorded during Phase 1 while continuing to process real-time data in one telemetry and command data (TCD) string.

Phase 3. To repeat Phase 1 while using the 50-kbps wideband line.

Phase 4. To repeat Phase 2 for data recorded during Phase 3.

Of the four test phases, only parts of Phases 1 and 2 were completed. Problems included hardware failures at CTA 21, simulation problems, and VMCCC processing problems. For Phase 2, 8-1/3 and 33-1/3 bps engineering data and command data were successfully replayed using telemetry and command processor (TCP) alpha from the 7-track DODR. Time did not permit the use of the DOI-5050-OP-C P-9 module and replay of the 9-track DODR. The test was considered to be only partially successful. The 6-channel simulation conversion assembly (SCA) and Data-Routing Operational Program (DROP)-F software package was used for the first time during this test.

B. GDS-1, 3 July 1974 — Two Orbiters and Lander Telemetry and Command

The primary difference between the SIT tests and the Ground Data System (GDS) test was the use of as much of the GDS as possible for GDS testing, whereas the SIT tests were primarily to test computer interfaces only. GDS 1 was to verify end-to-end telemetry processing of all Viking orbiter and Viking lander data rates. During the short-loop high-speed wideband communications portion of the test, problems with wideband simulation made it obvious that the test objectives could not be completed. The remainder of the test time was used to trouble-shoot these problems. After extensive checkout of wideband communications hardware (GCF and MCCF) it was determined that a problem existed in the MCCC (software) operating system which resulted in only the first 40 bits of each 2400-bit wideband data block being saved for use by other programs. A software correction was made in real-time and data were correctly processed in a short-loop configuration.

C. GDS Retest, July 20, 1974 — Two Orbiters and Lander Telemetry and Command

Objectives for this test were to complete the objectives of GDS-1. Telemetry and Command Systems were successfully tested. Minor problems were experienced in the operation of the 6-channel SCA and DROP-F software; however all were either corrected or suitable work-arounds were implemented. With the successful completion of this test, it was determined that the DSN/VMCCC were ready to support the Data System Compatibility testing effort.

II. Data System Compatibility

The primary purpose of these tests was to demonstrate compatibility between the Viking Flight Operations System (FOS) and the Viking spacecraft, Viking Orbiter, and Viking Lander, in response to requirements of the Viking Master Integrated Test Plan. The Data System Compatibility Test Program is divided into three phases as follows:

(1) Design compatibility test (DCT)

(2) Pathfinder compatibility test (PCT)

(3) Flight article compatibility test (FCT)

This report covers the first phase of testing conducted at JPL. Phases 2 and 3 to be conducted with the Spacecraft Compatibility/Monitor Station, STDN, Merritt Island, Florida will be covered in subsequent articles.

The design compatibility phase of testing demonstrated that the basic design of the Viking FOS was compatible with the Viking spacecraft. The tests were divided into six separate phases with results described in *Subsections II A to G.*

A. DCT-1, July 15, 1974 — Lander Direct Link Telemetry and Command

The objective of DCT-1 was to demonstrate that GDS design could support the Viking mission and is compatible with Viking lander data transmitted from the Viking lander S-band direct link. It was also to verify the direct S-band command capability. Engineering data at 8-1/3 bps was successfully processed simultaneously with commanding; however, frame lock could not be accomplished on the science data rates of 250, 500, and 1000 bps. After extensive trouble-shooting, it was determined that pre-recorded science on the flight tape recorder was in error. It was decided to terminate the test and utilize the contingency test period.

B. DCT-1 Retest, July 17, 1974 — Lander Direct Link Telemetry and Command

This test repeated the objectives of DCT-1. The objectives were successfully met. All Viking Lander data rates (8-1/3, 250, 500, 1000 bps) were successfully processed while simultaneously processing commands.

C. DCT-2, July 21, 1974 — Orbiter Telemetry and Command

DCT-2 was to demonstrate that the GDS, which was designed to support the Viking '75 mission, was compatible with the Viking Orbiter telemetry and command data systems. All objectives were met during this test. Telemetry data rates (8-1/3, 33-1/3, 1k, 2k, 4k, 8k, 16k bps) were successfully processed with simultaneously processing orbiter commands.

D. DCT-3, Uplink, July 22, 1974 — Viking Spacecraft Telemetry and Command

This test was to demonstrate that the GDS design was compatible with the Viking spacecraft (mated Viking Orbiter and Viking Lander hardware) telemetry and command data systems. The test was divided into two parts with the first part to demonstrate uplink design and part two to demonstrate downlink design compatibility. Part one was successfully completed. Commands were transmitted to the mated spacecrafts with verification and evaluation via the downlink telemetry stream.

E. DCT-3, Downlink, Aug. 8 — Viking Spacecraft Telemetry and Command

This second part of DCT-3 was to demonstrate GDS design compatibility with respect to processing Viking telemetry in the Viking spacecraft (mated) configuration. Telemetry data at mated configuration data rates (8-1/3, 33-1/3, 1K and 2k bps) were processed. Commanding was conducted simultaneously with telemetry processing.

F. DCT-4, Aug. 14, 1974 — Viking Lander (Relay) Telemetry and Command

DCT-4 was to demonstrate that the GDS is compatible with telemetry data transmitted by the Viking orbiter which contained both pre-recorded (Track 8) and real-time telemetry data relayed from the Viking Lander. Telemetry data rates (8-1/3, 33-1/3, 1k, 2k, 4k, 8k and 16k bps) for the pre-recorded data were processed. Telemetry at 8-1/3, 33-1/3 and 4k bps (uncoded) was also processed. Orbiter commanding was conducted simultaneously with the telemetry processing. A failure of channel 2 of the TCP at CTA 21 did not compromise the test. The redundant TCP was used following this failure. All objectives were met.

G. DCT-5, July 31/Aug. 1, 1974 — Two Orbiters and Lander Telemetry and Command

The test objective was to demonstrate that the GDS design was compatible with a multi-spacecraft environment. This test was completed in two days. Six simultaneous telemetry streams (8-1/3, 8-1/3, 33-1/3, 16k, 16k, and 1k bps) were successfully processed simultaneously with lander and orbiter commanding. Minor problems existed in simulation of one 8-1/3 bps data stream and the processing of 8-1/3 bps data. Inadequate time was allowed for data transfer tests prior to test start. The test was completed early, which permitted DODR recall of selected low and high data rates recorded during DCT-3. All test objectives were met.

Acknowledgment

References

1. *Viking '75 Project, Data System Detailed Compatibility Test Plan*, PL-3720341 (JPL internal document).

2. *Viking '75 Project, Test and Integration Plan for the Viking Mission Control and Computing Center System, Vol. IV, VMCCS/DSN Integration*, Doc. 619-6, May 1, 1974 (JPL internal document).

Helios Mission Support

P. S. Goodwin
Mission Support Office

The previous article, in The Deep Space Network Progress Report 42-22, discussed the Helios Prototype Model Spacecraft/DSN compatibility test effort conducted at the Jet Propulsion Laboratory, Pasadena. Since that time, the prototype has been transported to Cape Canaveral where it will serve both as a forerunner to the first flight spacecraft and as back-up. This article treats the compatibility verification tests that were performed after the prototype's arrival at Cape Canaveral, with particular emphasis upon the first use of the former Spacecraft Compatibility Station equipment in the consolidated Spacecraft Tracking and Data Network facility at Merritt Island, Florida.

I. Introduction

After completing environmental and DSN compatibility testing at JPL (Ref. 1), the Helios prototype model (PM) spacecraft and its associated support equipment were transported to Cape Canaveral, Florida, where they will serve as a back-up to the flight model spacecraft during the latter's launch preparations.

After unpacking and set-up in Building AO at Cape Canaveral, the condition of the PM spacecraft was checked by running a DSN compatibility verification test with the newly relocated Spacecraft Compatibility Station (formerly DSS 71) equipment within the STDN facility at Merritt Island, Florida now designated STDN (MIL-71). The tests between the PM spacecraft and

STDN (MIL-71) were conducted between July 31, and Aug. 2, 1974, and totaled 39 hours in length.

These tests, while successful, did reveal a few corrective actions that will be necessary prior to the start of the flight (F-1) model/DSN compatibility tests scheduled for the latter part of September 1974. The three most significant corrective actions are discussed.

II. Corrective Actions

A. Communications Distance

Because of the increased distance between Building AO and the STDN (MIL-71) facility over that between Building AO and the former DSS 71 facility, there was insufficient signal level to perform a two-way link range

calibration using the ranging zero delay device. This was temporarily circumvented by employing the STDN's 9-m-diam tracking antenna operating at 500 W of power for the up-link to the spacecraft, while maintaining the downlink from the spacecraft into the small, fixed-orientation roof-mounted antennas normally used with the DSN equipment housed at the STDN facility—denoted STDN (MIL-71). Since such an arrangement is non-standard for both the DSN and for STDN (when acting as a Near-Earth Phase Network (NEPN) support facility), it is desirable to add 32 dB to the STDN (MIL-71) link capability by either, or a combination of, higher trans-mitter power and larger fixed antennas on the roof. Both of these options are under current study with considera-tion being given to both the short-term (F-1 Compatibility Tests) and long-term (future flight project) needs.

B. Signal Level Fluctuations

The PM/DSN compatibility verification tests were the first involving a spacecraft and the newly relocated equip-ment STDN (MIL-71) using a microwave path over a body of water (Banana River). Signal level variations as much as ± 4 dB interfered with testing—most notably the command threshold tests and telemetry bit-error-rate tests at 32 and 8 bps. While a major contributor to these fluc-tuations was eventually traced to a faulty RF coupler (test adapter) at the spacecraft end of the link, there remained a ±1 dB link fluctuation. Serious consideration is being given to techniques for at least partially com-pensating these fluctuations in the microwave path.

C. Threshold Measurements

The unattenuated RF signal level from the PM space-craft (Building AO) as received via the existing small roof-top antennas at STDN (MIL-71) was −70 dBm. PIN modulators are used within the STDN (MIL-71) equip-ment to reduce the effective received signal level to the value specified for each particular portion of the com-patibility test sequence. These PIN modulators have a dynamic range of only 70 dB—thereby necessitating the use of additional (usually variable) attenuators in series with the receiver input for threshold tests. Some of the testing was impaired by RF leakage around these external attenuators and into the receiver. Effort is now underway to supply STDN (MIL-71) with a special, shielded atten-uator box which will permit independent attenuator adjustment of both the up- and down-links. Again, both the short-term and long-term aspects are being considered.

III. Tests

Despite the foregoing initial difficulties, sufficient tests were successfully completed at Cape Canaveral to verify that both the PM spacecraft and the relocated DSN equipment at STDN (MIL-71) were compatible. This verification test was a prelude to further ground data system (GDS) tests the Helios Project wished to perform in addition to the somewhat limited 2-day GDS testing that occurred at the conclusion of the PM/CTA 21 com-patibility tests during May 1974. The GDS tests with the PM at Cape Canaveral included an end-to-end test wherein PM telemetry was decoded at STDN (MIL-71), formatted onto high-speed data lines (HSDLs) and sent to the Mission Control and Computing Center (MCCC) at JPL, where it was processed and re-routed via other HSDLs to the German Control Center in Oberpfaffen-hofen (Southwest of Munich) where it was successfully displayed. A test of the reverse process, wherein com-mands originating at Oberpfaffenhofen were to be sent through the MCCC to the PM spacecraft at Cape Canav-eral was not successful due to procedural problems in Germany. However, commands originating at the MCCC were successfully executed via STDN (MIL-71) to the PM spacecraft, thereby verifying the proper operation of the DSN/MCCC portion of the command system inter-face. Since the MCCC interface with Germany had been previously verified, the command procedural problem that occurred during the Cape tests was not considered serious; however, the test will be repeated at a later date.

In addition to the preceding, the GDS tests involved the relocated DSN equipment at STDN (MIL-71) in an NEPN compatibility/data flow test. In this latter con-figuration, PM telemetry data were received by the STDN (MIL-71) 9-m antenna and fed into the STDN (MIL-71) receivers where it was detected and symbol-synchronized, then placed onto an HSDL. This HSDL, routed via the Goddard Space Flight Center, was one of two fed into the Automatic Switching Unit (ASU) com-puter in the (MIL-71) portion of that STDN facility. The other HSDL carried Helios telemetry received by the AFETR TEL-4 station. After data stream selection by the ASU, the data were passed into the standard DSN telem-etry system for decoding and formatting for transmission to the MCCC. This test successfully demonstrated the PM spacecraft's compatibility with the NEPN, thereby achieving another important milestone in the preparation for Helios-A launch.

Reference

1. Goodwin, P. S., "Helios Mission Support," in *The Deep Space Network Progress Report 42-22*, pp. 16–21, Jet Propulsion Laboratory, Pasadena, Calif., Aug. 15, 1974.

Helios Prototype Spacecraft Deep Space Network Compatibility Test Summary

A. I. Bryan
DSN Systems Engineering Office

Th? Helios Prototype Model Spacecraft/Deep Space Network (DSN) compatibility test program consisted of subsystem design, system design, and system verification tests in three phases, which were performed at the Jet Propulsion Laboratory and Cape Canaveral. Subsystem design tests were initiated on the Engineering Model in early 1972 and the program culminated in verification cf DSN/Helios Spacecraft compatibility on Aug. 2, 1974. This report describes the tests and test results that provided the basis for establishment of telecommunications system design compatibility and verification.

I. Introduction

Phase I of the DSN/Helios Spacecraft Compatibility Test Program began at the Spacecraft Compatibility Station (formerly DSS 71) in April 1972. The Engineering Model (EM) transponder was tested extensively for RF, command, and metric compatibility, but telemetry testing was limited because of the nonavailability of the spacecraft data handling unit and DSN operational software.

Several design deficiencies were discovered, principally interaction between the transmitter and receivers and interaction between the two receivers. Results of Phase I testing have been documented and are detailed in Ref. 1.

Phase II of the DSN/Helios Spacecraft Compatibility Test Program was performed with the Compatibility Test Area (CTA 21) in May 1974. CTA 21 is the DSN facility established to simulate an operational Deep Space

Station for verification of communications performance. The objectives of this series of tests was to establish system design compatibility between the Prototype Model (PM) Spacecraft and the DSN.

Phase III of the test program was performed at Cape Canaveral, Florida, between the DSN equipment at the Goddard Tracking Station at Merritt Island, Florida and the Helios PM. The DSN equipment is referred to as STDN (MIL 71). The objectives of these tests were two-fold: (1) to verify continued interface integrity and maintenance of compatibility following transportation of the PM Spacecraft to Florida, and (2) to verify the capability of STDN (MIL 71) to support Flight Project/DSN compatibility testing.

Procedures for conducting these tests were prepared by the DSN and included DSN test parameters and criteria. Spacecraft test parameters and design criteria were provided by the Helios Telecommunications Project of the German Society for Space Research (GfW). The final procedures were approved by a joint DSN/Helios Project test team.

II. Test Report

Initial testing with the Engineering Model Transponder at DSS 71 in April 1972 uncovered several design incompatibilities between the transponder and the DSN. The transponder exhibited lag in sensitivity, pushing effects at strong uplink signal levels, instability of the voltage-controlled crystal oscillator (VCXO) and improper shielding. Despite these incompatibilities, meaningful engineering tests were performed as documented in Ref. 1. The last two phases of the DSN/Helios Spacecraft Compatibility Test Program were successful in establishing telecommunications compatibility between the DSN and the Helios Prototype Spacecraft.

A. Prototype CTA 21 Testing

1. Test objectives. The objectives of these tests were to prove system design compatibility between the DSN and the PM spacecraft and to demonstrate that compatibility deficiencies in the EM had been resolved. All tests were accomplished in accordance with the DSN test/training plan described in Ref. 2.

2. Test conditions. The Helios Prototype Spacecraft was located in Building 248 (10-ft solar simulator) and an RF link was established to CTA 21 in Building 125 at JPL. CTA 21 was configured as a standard DSS utilizing oper-

ational hardware and software including Telemetry and Command Processor (TCP) software, DOI-5050 (OP-B, modified). The Helios spacecraft was configured for flight operation.

On May 17, the RF link was tested and the amplitude stability was measured to be ± 0.2 dB over a 24-hour period. The formal tests started on May 18 and the test duration was approximately 120 hours. Excellent support from the spacecraft team and CTA 21 provided a smooth and continuous flow of testing. Decommutation of spacecraft telemetry via high-speed data blocks to the Simulation Conversion Assembly (SCA) provided real-time spacecraft operating parameters, such as receiver automatic gain control (AGC) and receiver static phase error, (SPE). This configuration performance of the DSN Telemetry System through the DSN Ground Communications Facility (GCF) High-Speed Data Subsystem.

3. Test results. Table 1 provides in summary form the test results. Significant events and/or items in the areas of RF telemetry, command and metric data are described below:

a. Radio frequency. The standard DSN RF tests of tracking range, rate and acquisition under doppler conditions were very successful. In particular, very limited pushing or pulling effects were noted over a range of plus and minus 32.5 kHz in the spacecraft transponder. All RF thresholds corresponded to predicted values and were very stable. The redesign of the Helios transponder was successful.

b. Command. Station-to-spacecraft command operation performance for DSN-generated commands was successfully tested at threshold levels, for a total of 1500 commands with and without ranging and under simulated mission conditions (i.e., under spacecraft low-gain antenna amplitude and phase variations in the uplink).

The mission critical command performance during the Step II maneuver was successfully verified.

c. Metric data. A series of tests was performed utilizing the Planetary Ranging Assembly (PRA) for both the continuous and discrete modes. In addition, verification of the PRA and the Mark I A range delay measurements through the spacecraft was performed. The difference between the two ranging systems' measurements was approximately 2 ns.

The acquisition times, spacecraft range delay at simulated 1.6 and 2.0 AU conditions, range stability, and DRVID stability tests were performed with the spacecraft at ambient temperatures.

No interference between ranging, command, and telemetry was observed with the discrete mode of ranging. In particular, an 8-hour DRVID test indicated a very stable spacecraft transponder. The variation of the DRVID number due to the transponder was measured to be less than 5 ns.

d. Telemetry. The telemetry tests were designed to verify both coded and uncoded telemetry performance of the DSN with the Helios spacecraft. Uncoded telemetry performance was tested by determining the bit error rate (utilizing test software DOI-5087-TP) and decommutating HSD blocks. Coded telemetry performance was verified by measuring the frame deletion rate for 8, 256, and 2048 bps, and a review of the HSD block integrity was made. Both the coded and uncoded telemetry performance met the test criteria of bit error and frame deletion rate, with the exception of bit error tests performed at 8 bps and 32 bps uncoded. The 8 and 32 bps uncoded modes are not critical to the Helios mission; however, tests with the Helios PTM spacecraft were planned with STDN (MIL-71) to provide operational performance estimates at these rates.

The 128-bps uncoded tests (critical for Step II maneuver) were successfully performed.

B. Prototype Spacecraft/STDN (MIL 71) Testing

1. Test objectives. The objectives of the tests were to verify design compatibility between the DSN and the Helios Prototype Spacecraft after transportation from JPL and to provide training in preparation for compatibility tests with the flight article at Cape Canaveral, Florida. All tests were accomplished in accordance with the DSN Test/Training Plan for Helios Project, 613-4; Rev. A.

2. Test conditions. The Helios Prototype Spacecraft was configured to represent a flight model and STDN (MIL 71) was configured to represent a 26-meter antenna DSS. The spacecraft was located in the clean room of Building AO, Cape Canaveral, Florida. An S-band RF air link was established between a 1.85-meter antenna at Building AO and a 1.2-meter antenna at the ground station.

The ground station telemetry and command software utilized in these tests was the released version of Telemetry and Command Data (TCD) DOI-5050-OP-C. This package is the final revision of station operational software which will be used to support the Helios mission. Bit error rate testing was supported utilizing the multiple-mission telemetry (MMT) test software, DOI-5087-TP. The total time to accomplish the Helios Prototype Spacecraft/STDN (MIL 71) compatibility tests was 39 hours. The test schedule was on the basis of a 12-hour shift. The successful accomplishment of the RF compatibility tests was due in large measure to the outstanding cooperation and coordination between the Helios Project Spacecraft test team and the STDN (MIL 71) Team.

3. Test results. Table 2 provides in summary form the test results. Significant events and/or items in the areas of RF, telemetry, command and metric data are described below:

a. Radio frequency. Short-term RF link fluctuations throughout the test period were observed and recorded to be ± 4.0 dB on the downlink and ± 3.0 dB on the uplink. These fluctuations were primarily caused by a faulty three-way directional coupler used for test purposes at the spacecraft antenna inputs. Elimination of this coupler reduced link fluctuations to ± 1.5 dB on the downlink and ± 1.5 dB on the uplink.

No observable degradation to downlink and uplink threshold performance was observed despite link fluctuations. All RF acquisition and tracking rate tests were well within the expected tolerances.

The subcarrier phase jitter measurement at STDN (MIL 71) was significantly improved over the same measurement performed at CTA 21. The measurement at CTA 21 (8 deg rms) is assumed to be due to an error in CTA 21 test instrumentation.

b. Commands. Command performance testing was attempted five times and was successfully accomplished after a noisy directional coupler at the spacecraft complex was replaced toward the end of the test period. Experience with the noisy uplink revealed that the actual command threshold of the spacecraft was approximately 3 dB below the specified value of − 144 dBm.

c. Metric. All metric data testing proceeded flawlessly. Both discrete and continuous ranging delay measurements were as expected.

d. Telemetry. All telemetry erasure rate tests for the coded telemetry were performed as expected. All test criteria were met or exceeded.

Bit error rate measurements for the uncoded mode of operations were slightly outside the expected limits. This deviation from the May 1974 test results at CTA 21 was attributable to the unstable RF link performance observed during these tests.

The 8 and 32 bps uncoded performance problems described previously in the Prototype Spacecraft/CTA 21 testing were not observed. With the exception of the RF link stability problem, the 8 and 32 bps uncoded telemetry performed flawlessly.

III. Conclusions

The successful completion of Helios Spacecraft telecommunications test activities at Pasadena and Cape Canaveral represents a significant project event. It can be assumed with high probability that the telecommunications design compatibility established with the PM will also be established with the Helios Flight (F-1) Spacecraft.

The importance of the performance of a formal compatibility test program is clearly demonstrated by the problem areas uncovered, verified and resolved during the DSN/Helios Prototype Spacecraft Test Program.

References

1. *DSN Test/Training Plan for Helios Project; Vol. III, Part A, DSN/Helios Spacecraft Telecommunications Compatibility Test Report*, Document 613-8, July 1, 1972 (JPL internal document).

2. *DSN/Test Training Plan for Helios Project, Vol. I, Part A, DSN/Helios Spacecraft Telecommunications Compatibility Test Plan*, Document 613-4; Rev. A, June 15, 1973 (JPL internal document).

3. *DSN Test/Training Plan for Helios Project, Vol. II, Part A, DSN/Helios Spacecraft Telecommunications Compatibility Test Procedures*, Document 613-5, June 15, 1972 (JPL internal document).

4. *Deep Space Network/Helios Spacecraft Telecommunications Interface Definition*, Document 613-6; Rev. A, Feb. 1, 1974 (JPL internal document).

Test date	Test title	Test No.	BLK III RCV	EXC	PRA RNG	CMD	Uplink doppler	Uplink offset	CMA SUBC offset	SDA SUBC offset	CAR SUP	Bit rate	EXC
5-18-74	S, maximum sweep and acquisition rate	I.1	1	1	Off	Off	500 Hz/sec	−30.0 kHz	NA	NA	High	2048	1
		I.1	1	1	Off	Off	500 Hz/sec	+30.0 kHz	NA	NA	High	2048	1
		I.2	1	1	Off	Off	80 Hz/sec	−10.0 kHz	NA	NA	High	2048	1
		I.2	1	1	Off	Off	80 Hz/sec	+10.0 kHz	NA	NA	High	2048	1
		I.3	1	1	Off	Off	500 Hz/sec	−30.0 kHz	NA	NA	High	2048	1
		I.3	1	1	Off	Off	500 Hz/sec	+30.0 kHz	NA	NA	High	2048	1
		I.4	1	1	Off	Off	80 Hz/sec	−10.0 kHz	NA	NA	High	2048	1
		I.4	1	1	Off	Off	80 Hz/sec	+10.0 kHz	NA	NA	High	2048	1
5-17-74	Noncoherent downlink spectrum analysis	II.1	1	NA	Off	Off	NA	NA	NA	NA	Low	32	1
		II.2	1	NA	Off	Off	NA	NA	NA	NA	High	2048	1
		II.3	1	NA	Off	Off	NA	NA	NA	NA	Low	32	1
5-18-74	Noncoherent downlink spectrum analysis	II.4	1	NA	Off	Off	NA	NA	NA	NA	High	2048	1
		II.5	1	NA	Off	Off	NA	NA	NA	NA	High	128	1
5-18-74	Coherent downlink spectrum analysis	II.6	1	1	Off	Idle on	NA	NA	NA	NA	Low	32	1
		II.7	1	1	Off	Idle on	NA	NA	NA	NA	Low	32	1
		II.8	1	1	Off	Idle on	NA	NA	NA	NA	High	2048	1

Table header spanning: Deep Space Network

Table 1. Helios Prototype Spacecraft telecommunications compatibility test data from CTA 21

Spacecraft						Test data		Test time	Test comment
RCV	ANT (PWR)	TWT	RNG	S/C DM	S/C FM	Performance	Criteria		
1 & 2 (VCX01)	MGA (High)	1	Off	0	4	Acquired @ −100.0 dBmW; Tracked to +32.5 kHz	Acquire @ −100.0 dBmW; Track to +32.5 kHz	1 hr 15 min	Acquired U/O @ best lock (VCX01) 2115.699552 MHz
1 & 2 (VCX01)	MGA (High)	1	Off	0	4	Acquired @ −100.0 dBmW; Tracked to −32.5 kHz	Acquire @ −100.0 dBmW; Track to −32.5 kHz		Acquired L @ best lock (VCX01) 2115.699552 MHz
1 & 2 (VCX01)	MGA (High)	1	Off	0	4	Acquired @ −141.0 dBmW; Tracked to +32.5 kHz	Acquire @ −141.0 dBmW; Track to +32.5 kHz		Acquired U/L @ best lock (VCX01) 2115.699552 MHz
1 & 2 (VCX01)	MGA (High)	1	Off	0	4	Acquired @ −141.0 dBmW; Tracked to −32.5 kHz	Acquire @ −141.0 dBmW; Track to −32.5 kHz		Acquired U/L @ best lock (VCX01) 2115.699552 MHz
1 & 2 (VCX02)	MGA (High)	1	Off	0	4	Acquired @ −100.0 dBmW; Tracked to +32.5 kHz	Acquire @ −100.0 dBmW; Track to +32.5 kHz	0 hr 45 min	Acquired U/L @ best lock (VCX02) 2115.697344 MHz
1 & 2 (VCX02)	MGA (High)	1	Off	0	4	Acquired @ −100.0 dBmW; Tracked to −32.5 kHz	Acquire @ −100.0 dBmW; Track to −32.5 kHz		Acquired U/L @ best lock (VCX02) 2115.697344 MHz
1 & 2 (VCX02)	MGA (High)	1	Off	0	4	Acquired @ −141.0 dBmW; Tracked to +32.5 kHz	Acquire @ −141.0 dBmW; Track to +32.5 kHz		Acquired U/L @ best lock (VCX02) 2115.697344 MHz
1 & 2 (VCX02)	MGA (High)	1	Off	0	4	Acquired @ −141.0 dBmW; Tracked to −32.5 kHz	Acquire @ −141.0 dBmW; Track to −32.5 kHz		Acquired U/L @ best lock (VCX02) 2115.697344 MHz
1	MGA (Med)	1	Off	0	4	No spurs observed	No spurious signal within 30 dB of the carrier	53 min	
1	MGA (Med)	1	Off	0	4	No spurs observed	No spurious signal within 30 dB of the carrier	6 min	
1	MGA (High)	1	Off	0	4	No spurs observed	No spurious signal within 30 dB of the carrier	10 min	
1	MGA (High)	1	Off	0	4	No spurs observed	No spurious signal within 30 dB of the carrier	7 min	
1	LGA (Low)	NA	Off	0	4	No spurs observed	No spurious signal within 30 dB of the carrier	11 min	
1	MGA (Med)	1	Off	0	4	No spurs observed	No spurious signal within 30 dB of the carrier	28 min	U/L level −144 dBmW
1	MGA (High)	1	Off	0	4	No spurs observed	No spurious signal within 30 dB of the carrier	14 min	U/L level −144 dBmW
1	HGA (High)	1	Off	0	4	No spurs observed	No spurious signal within 30 dB of the carrier	19 min	U/L level −103 dBmW

Test date	Test title	Test No.	Deep Space Network										
			BLK III RCV	EXC	PRA RNG	CMD	Uplink doppler	Uplink offset	CMA SUBC offset	SDA SUBC offset	CAR SUP	Bit rate	EXC
5-18-74	Coherent down-link spectrum analysis (contd)	II.9	1	1	Off	Idle on	NA	NA	NA	NA	High	2048	1
		II.10	1	1	Off	Idle on	NA	NA	NA	NA	High	2048	1
5-18-74	Uplink threshold	III.1	1	1	Off	Off	NA	NA	NA	NA	High	2048	1
5-20-74	Residual carrier phase jitter	IV.1	1	1	Off	Off	NA	NA	NA	NA	High	2048	1
			1	1	Off	On	NA	NA	NA •	NA	High	2048	1
		IV.2	1	1	Off	Off	NA	NA	NA	NA	High	2048	1
			1	1	Off	On	NA	NA	NA	NA	High	2048	1
		IV.3	1	1	Off	Off	NA	NA	NA	NA	High	2048	1
5-20-74	Residual carrier phase jitter	IV.4	1	1	Off	Off	NA	NA	NA	NA	High	2048	1
		IV.5	1	1	Off	Off	NA	NA	NA	NA	High	2048	1
		IV.6	1	1	Off	Off	NA	NA	NA	NA	Off	Off	1
			1	1	Off	Off	NA	NA	NA	NA	High	2048	1
		IV.7	1	1	Off	Off	NA	NA	NA	NA	Off	Off	1
			1	1	Off	Off	NA	NA	NA	NA	High	2048	1
		IV.8	1	1	Off	Off	NA	NA	NA	NA	High	2048	1
		IV.9	1	1	Off	Off	NA	NA	NA	NA	High	2048	1
5-20-74	Noncoherent downlink threshold	V.1	1	1	NA	NA	NA	NA	NA	NA	Low	32	1
		V.2	1	1	NA	NA	NA	NA	NA	NA	High	2048	1
5-20-74	Coherent down-link threshold	V.3	1	1	Off	Off	NA	NA	NA	NA	Low	32	1
		V.4	1	1	Off	Off	NA	NA	NA	NA	High	2048	1
		V.5	1	1	On	Off	NA	NA	NA	NA	High	2048	1
		V.6	1	1	On	Off	NA	NA	NA	NA	Low	32	1
5-20-74	S/C ranging polarity	VI.1	1	1	On	Off	NA	NA	NA	NA	High	2048	1

Table 1 (contd)

	Spacecraft					Test data		Test time	Test comment
RCV	ANT (PWR)	TWT	RNG	S/C DM	S/C FM	Performance	Criteria		
1	HGA (Med)	1	Off	0	4	No spurs observed	No spurious signal within 30 dB of the carrier	25 min	U/L level −144 dBmW
1	HGA (High)	1	On	0	4	No spurs observed	No spurious signal within 30 dB of the carrier	1 hr 42 min	U/L level −132.5 dBmW
1	MGA (High)	1	Off	0	4	−154.35 dBmW	−155.0 ± 1.0 dBmW	45 min	Average of three measuren.ents
1	MGA (Med)	1	Off	0	4	5.7 deg rms	2.86 deg rms	3 hr 26 min	U/L level −100 dBmW
1	MGA (Med)	1	Off	0	4	6.2 deg rms	↓		D/L level −100 dBmW
1	MGA (Med)	1	Off	0	4	17.98 deg rms	22.9 deg rms		U/L level −144 dBmW
1	MGA (Med)	1	Off	0	4	18.1 deg rms	↓		D/L level −100 dBmW
1	MGA (High)	1	Off	0	4	5.23 deg rms	2.86 deg rms	↓	U/L level −100 dBmW; D/L level −100 dBmW
1	MGA (High)	1	Off	0	4	17.29 deg rms	22.9 deg rms	3 hr 26 min	U/L level −144 dBmW; D/L level −100 dBmW
1	MGA (High)	1	Off	0	4	1.78 deg rms	5.7 deg rms		D/L level −100 dBmW; Noncoherent mode
1	MGA (Med)	1	Off	0	4	0.78 deg rms	5.7 deg rms		TLM modulation Off; Noncoherent mode
1	MGA (Med)	1	Off	0	4	1.66 deg rms	↓		D/L level −100 dBmW; Noncoherent mode
1	LGA (Low)	NA	Off	0	4	4.96 deg rms	2.86 deg rms		TLM modulation Off; Coherent mode
1	LGA (Low)	NA	Off	0	4	5.12 deg rms	↓		U/L level −100 dBmW; D/L level −100 dBmW
1	LGA (Low)	NA	Off	0	4	16.77 deg rms	22.9 deg rms		U/L level −144 dBmW; D/L level −100 dBmW
1	LGA (Low)	NA	Off	0	4	1.65 deg rms	5.7 deg rms	↓	D/L level −100 dBmW; Noncoherent mode
1	HGA (High)	1	Off	0	4	−159.7 dBmW	−159.0 ± 3.0 dBmW	20 min	Avg. three runs
1	HGA (High)	1	Off	0	4	−158.8 dBmW	−159.0 ± 3.0 dBmW	14 min	Avg. three runs
1	MGA (High)	1	Off	0	4	−161.8 dBmW	−159.0 ± 3.0 dBmW	13 min	Avg. three runs
1	MGA (High)	1	Off	0	4	−158.5 dBmW	−159.0 ± 3.0 dBmW	13 min	Avg. three runs
1	MGA (High)	1	On	0	4	−157.8 dBmW	−159.0 ± 3.0 dBmW	18 min	Continuous spectrum; Avg. three runs
1	MGA (High)	1	On	0	4	−160.6 dBmW	−159.0 ± 3.0 dBmW	13 min	Discrete spectrum; Avg. three runs
1	HGA (High)	1	On	0	4	Not inverted	Polarity not inverted	15 min	Continuous spectrum

| Test date | Test title | Test No. | Deep Space Network | | | | | | | | | | |
			BLK III RCV	EXC	PRA RNG	CMD	Uplink doppler	Uplink offset	CMA SUBC offset	SDA SUBC offset	CAR SUP	Bit rate	EXC
5-20-74	S/C ranging delay	VI.2	1	1	On	Off	NA	NA	NA	NA	High	2048	1
		VI.3	1	1	On	Off	NA	NA	NA	NA	High	2048	1
5-21-74	Ranging system acquisition time	VII.1	1	1	On	Off	NA	NA	NA	NA	High	2048	1
		VII.2	1	1	On	Off	NA	NA	NA	NA	Low	32	1
5-21-74	Bit error rate	VIII.1	1	1	Off	Off	NA	NA	NA	NA	High	2048	1
		VIII.2	1	1	Off	Off	NA	NA	NA	NA	High	64	1
		VIII.3	1	1	Off	Off	NA	NA	NA	NA	Low	32	1
		VIII.4	1	1	Off	Off	NA	NA	NA	NA	Low	8 UNC	1
		VIII.5	1	1	On	Off	NA	NA	NA	NA	High	2048	1
		VIII.6	1	1	Off	Off	NA	NA	NA	NA	High	128	1
5-23-74	Telemetry erasure rate	IX.1	1	1	Off	On	NA	NA	NA	NA	High	2048	1
		IX.1a	1	1	Off	On	NA	NA	NA	NA	High	2048	1
		IX.2	1	1	Off	On	NA	NA	NA	NA	High	256	1
		IX.3	1	1	On	On	NA	NA	NA	NA	High	2048	1
		IX.4	1	1	Off	On	NA	NA	NA	NA	High	128	1
		IX.7	1	1	On	On	NA	NA	NA	NA	Low	8	1
		IX.8	1	1	On	On	NA	NA	NA	NA	High	2048	1
5-18-74	Subcarrier frequency and phase jitter	X.1	1	1	Off	Off	NA	NA	NA	NA	High	2048	1
5-22-74	Spacecraft command threshold	XI.1	1	1	Off	On	0	0	0	NA	High	2048	1
		XI.2	1	1	On	On	0	0	0	NA	High	2048	1

Table 1 (contd)

	Spacecraft					Test data		Test time	Test comment
RCV	ANT (PWR)	TWT	RNG	S/C DM	S/C FM	Performance	Criteria		
1	HGA (High)	1	On	0	4	1409 ns	To be measured	33 min	Continuous spectrum
1	HGA (High)	1	On	0	4	1407 ns	To be measured	22 min	Discrete spectrum
1	HGA (High)	1	On	0	4	23 min	Less than 45 min 1.6 AU case	1 hr 30 min	Continuous spectrum U/L level -133.0 dBmW D/L level -132.1 dBmW
1	HGA (High)	1	On	0	4	1.8 min	Less than 0.8 min 2.0 AU case	29 min	Discrete spectrum U/L level -134.5 dBmW D/L level -135.0 dBmW
1	MGA (Med)	1	Off	0	4	2.1×10^{-5}	10^{-5}	10 min	D/L level -128.2 dBmW
1	MGA (Med)	1	Off	0	4	0	10^{-4}	57 min	D/L level -140.8 dBmW
1	MGA (Med)	1	Off	0	4	1.5×10^{-6}	10^{-4}	2 hr 7 min	D/L level -141.7 dBmW
1	MGA (Med)	1	Off	0	4	No results	10^{-3}	4 hr 12 min	D/L level -147.7 dBmW
1	MGA (Med)	1	On	0	4	3.1×10^{-5}	10^{-5}	17 min	Discrete spectrum D/L level -128.2 dBmW
1	MGA (Med)	1	Off	0	4	3.55×10^{-5}	10^{-5}	25 min	D/L level -138.4 dBmW
1	MGA (Med)	1	Off	0	4	2.1×10^{-4}	10^{-4}	1 hr 30 min	D/L level -131.8 dBmW
1	MGA (Med)	1	Off	0	4	1.9×10^{-2}	$>10^{-1}$	1 hr	D/L level -134.9 dBmW
1	MGA (Med)	1	Off	0	4	0	10^{-4}	7 hr	D/L level -139.3 dBmW
1	MGA (Med)	1	On	0	4	0	10^{-4}	2 hr	D/L level -131.5 dBmW
1	MGA (Med)	1	Off	0	4	0	10^{-5}	2 hr	D/L level -132.1 dBmW
1	MGA (Med)	1	On	0	4	0	Process 200 frames	7 hr 30 min	D/L level -153.3 dBmW
1	MGA (Med)	1	On	0	4	0	Process 3200 frames	11 hr 30 min	D/L level -142.0 dBmW
1	MGA (Med)	1	Off	0	4	32.768 kHz @ 8.0 deg rms	32.768 kHz To be measured	1 hr 38 min	
1	MGA (High)	1	Off	0	4	1.3×10^{-5}	10^{-5}	8 hr 15 min	512-Hz subcarrier
1	MGA (High)	1	On	0	4	0	10^{-5}	32 min	512-Hz subcarrier, discrete spectrum

| Test date | Test title | Test No. | Deep Space Network | | | | | | | | | | |
			BLK III RCV	EXC	PRA RNG	CMD	Uplink doppler	Uplink offset	CMA SUBC offset	SDA SUBC offset	CAR SUP	Bit rate	EXC
5-23-74	Command bit error rate with uplink spin modulation	XII.1	1	1	Off	On	Freq. modulation: ±35 Hz @ 1 Hz/sec Phase modulation: ±40 deg @ 20 Hz/sec Amp. modulation: 10 dB p-p @ 20 Hz/sec	None	NA	High	128	1
		XII.2	1	1	Off	On	Phase modulation: ±40 deg @ 20 Hz/sec Amp. modulation: 16 dB p-p @ 20 Hz/sec	None	NA	High	128	1
6-1-74	Differenced ranging versus integrated doppler (DRVID)	XIII.1	1	1	On	Off	0	0	NA	NA	High	2048	1

Table 1 (contd)

Spacecraft						Test data		Test time	Test comment
RCV	ANT (PWR)	TWT	RNG	S/C DM	S/C FM	Performance	Criteria		
1	MGA (High)	1	Off	0	4	0	10^{-5}	1 hr	U/L level −128 dBmW
1	MGA (High)	1	Off	0	4	0	10^{-1}	30 min	U/L level −114 dBmW
1	MGA (High)	1	On	0	4	3 ns drift	<5-ns drift	8 hr	U/L level −100 dBmW D/L level −113 dBmW

Test date	Test title	Test No.	BLK III RCV	EXC	PRA RNG	CMD	Uplink doppler	Uplink offset	CMA SUBC offset	SDA SUBC offset	CAR SUP	Bit rate	EXC
									Deep Space Network				
7-31-74	S/C maximum sweep and acquisition rate	I.1	1	1	Off	Off	500 Hz/sec	−30.0 kHz	NA	NA	High	2048	1
		I.1	1	1	Off	Off	500 Hz/sec	+30.0 kHz	NA	NA	High	2048	1
		I.2	1	1	Off	Off	80 Hz/se·	−10.0 kHz	NA	NA	High	2048	1
		I.2	1	1	Off	Off	80 Hz/sec	+10.0 kHz	NA	NA	High	2048	1
7-31-74	Downlink spectrum analysis	II.1	1	NA	Off	Off	NA	NA	NA	NA	High	128	1
		II.2	1	NA	Off	Off	NA	NA	NA	NA	High	2048	1
		II.3	1	1	Off	On	NA	NA	NA	NA	High	2048	1
		II.4	1	1	Off	On	NA	NA	NA	NA	Low	32	1
7-31-74	Uplink threshold	III.1	1	1	Off	Off	NA	NA	NA	NA	High	2048	1
7-31-74	Carrier residual phase jitter	IV.3	1	1	Off	Off	NA	NA	NA	NA	High	2048	1
		IV.4	1	1	Off	Off	NA	NA	NA	NA	High	2048	1
		IV.5	1	1	Off	Off	NA	NA	NA	NA	High	2048	1
7-31-74	Coherent downlink threshold	V.5	1	1	On	Off	NA	NA	NA	NA	High	2048	1
7-31-74	S/C ranging polarity and delay	VI.2	1	1	On	Off	NA	NA	NA	NA	High	2048	1
		VI.3	1	1	On	Off	NA	NA	NA	NA	High	2048	1
8-2-74	Bit error rate	VIII.3	1	1	Off	Off	NA	NA	NA	NA	Low	32 Uncoded	1
		VIII.4	1	1	Off	Off	NA	NA	NA	NA	Low	8 Uncoded	1
8-1-74	Telemetry erasure rate	IX.1	1	1	Off	Off	NA	NA	NA	NA	High	2048	1
		IX.2	1	1	Off	Off	NA	NA	NA	NA	High	256	1
		IX.8	1	1	Off	Off	NA	NA	NA	NA	High	128	1
8-2-74	Subcarrier frequency and phase jitter	X.1	1	1	Off	Off	NA	NA	NA	NA	High	2048	1
8-2-74	Spacecraft command threshold	XI.1	1	1	Off	On	NA	NA	NA	NA	High	2048	1

Spacecraft							Test data		Test time	Test comment
RCv	PWR	ANT	TWT	RNG	S/C DM	S/C FM	Performance	Criteria		
1 & 2	High	MGA	1	Off	0	4	Acquire @ −100 dBmW; tracked to +32.5 kHz	Acquire @ −100 dBmW; track to +32.5 kHz	2 hr 43 min	Acquire U/L @ best lock 2115.705024 MHz
1 & 2	High	MGA	1	Off	0	4	Acquired @ −100 dBmW; tracked to −32.5 kHz	Acquire @ −100 dBmW; track to −32.5 kHz		Acquired U/L @ best lock 2115.705024 MHz
1 & 2	High	MGA	1	Off	0	4	Acquired @ −141 dBmW; tracked to +32.5 kHz	Acquire @ −141 dBmW; track to +32.5 kHz		Acquired U/L @ best lock 2115.705024 MHz
1 & 2	High	MGA	1	Off	0	4	Acquired @ −141 dBmW; track to −32.5 kHz	Acquire @ −141 dBmW; track to −32.5 kHz		Acquired U/L @ best lock 2115.705024 MHz
1	Med	MGA	1	Off	0	4	No spurs observed	No spurious signal within 30 dB of the carrier	48 min	
1	High	MGA	1	Off	0	4	No spurs observed	No spurious signal within 30 dB of the carrier	9 min	
1	High	MGA	1	Off	0	4	No spurs observed	No spurious signal within 30 dB of the carrier	17 min	
1	Med	MGA	1	Off	0	4	No spurs observed	No spurious signal within 30 dB of the carrier	17 min	
1	High	MGA	1	Off	0	4	−154.3 dBmW	−155.0 ± 1.0 dBmW	1 hr 16 min	
1	High	MGA	1	Off	0	4	1.74 deg rms	To be measured	58 min	U/L level −100.0 dBmW
1	High	MGA	1	Off	0	4	18.67 deg rms	To be measured		U/L level −144.0 dBmW
1	High	MGA	1	Off	0	4	1.55 deg rms	To be measured		Spacecraft in noncoherent mode
1	High	MGA	1	On	0	4	−159.5 dBmW	−159.0 ± 3.0 dBmW	1 hr 1 min	
1	High	HGA	1	On	0	4	1410.8 ns	To be measured	33 min	Polarity not inverted, continuous spectrum
1	High	HGA	1	On	0	4	1389.3 ns	To be measured		polarity not inverted, discrete spectrum
1	Med	MGA	1	Off	0	4	4.3 × 10⁻⁴	10⁻⁴	2 hr 47 min	8 dB Peak-to-peak RF link variation
1	Med	MGA	1	Off	0	4	1.6 × 10⁻³	10⁻³	3 hr 31 min	8 dB Peak-to-peak RF link variation
1	Med	MGA	1	Off	0	4	0.0%	0.01%	3 hr 10 min	10⁴ Frames
1	Med	MGA	1	Off	0	4	0.0%	0.01%	1 hr 25 min	2 × 10³ Frames
1	High	HGA	1	On	0	4	0.06%	0.1%	4 hr 33 min	1.6 × 10³ Frames
1	Med	MGA	1	Off	0	4	32.768 kHz @ 0.38 deg rms	32.768 kHz To be measured	16 min	
1	High	MGA	1	Off	0	4	Ground station transmitted 120 commands, all confirmed at spacecraft	Spacecraft receive all commands	1 hr	U/L level −144.0 dBmW

Table 3. Definitions for Tables 1 and 2

BLK III receiver	The standard DSN S-band receiving equipment
BLK III exciter	The standard DSN S-band exciter equipment
PRA RNG	Planetary ranging assembly modulation
CMD	Telemetry and command data handling command modulation
Uplink doppler	Ramp rate of the uplink carrier frequency
Uplink offset	Uplink carrier frequency offset relative to the spacecraft receiver rest frequency
CMA SUBC offset	Command modulation assembly subcarrier frequency offset relative to nominal
SDA SUBC offset	Subcarrier demodulator assembly subcarrier frequency offset relative to nominal
CAR SUP	Downlink carrier suppression due to telemetry modulation
Bit rate	Clock frequency of the telemetry bit information
EXC	Spacecraft S-band exciter equipment
RCV	Spacecraft S-band receiving equipment
PWR	Spacecraft transmitter power mode
ANT	Spacecraft antenna
LGA	Low-gain antenna
MGA	Medium-gain antenna
HGA	High-gain antenna
TWT	Traveling wave tube amplifier
RNG	Spacecraft ranging channel
S/C DM	Spacecraft data mode
S/C FM	Spacecraft data format

Pioneer Venus 1978 Mission Support

R. B. Miller

DSN Systems Engineering

Significant aspects of the multiprobe portion of the Pioneer Venus Mission are described.

I. Introduction

The Pioneer Venus 1978 Project will consist of two missions: an orbiter mission and a multiprobe mission. Both missions will utilize an Atlas SLV-IIID Centaur D-1AR launch vehicle with about 160-km parking-orbit trajectory. The orbiter mission will launch in May 1978 using a type II trajectory and will have a Venus orbital design lifetime of at least 243 Earth days. The multiprobe mission will launch in August 1978 using a type I trajectory. Both missions will arrive at Venus in December 1978. The type I and type II trajectories are used in order to separate the launch dates of the two missions. The spacecraft will be constructed by the Hughes Aircraft Company under contract to Ames Research Center, which has project management responsibilities. This article will concentrate on describing some significant aspects of the multiprobe mission as it is currently understood. Note that much of this material is subject to further refinement and change.

II. Multiprobe Physical Characteristics

The multiprobe mission consists of a bus, one large probe, and three small probes, all five of which will enter the Venusian atmosphere. A schematic drawing of the spacecraft is shown in Fig. 1. The spacecraft will be spin-stabilized and have a launch weight, including the probes and all science instruments, of just over 816 kg (1800 lb). There will be a total of 60 kg (133 lb) of instruments, 18 kg (40 lb) of which will be on the bus.

The bus consists of a basic cylindrical structure, the surface of which is covered with solar cells. The large probe sits on top of the cylinder centered on the spin axis. The three small probes sit equally spaced around the circumference of the large probe. The probes are deployed from the bus by means of springs about 20 days before entering the Venusian atmosphere. The large probe will be deployed first and then the three small probes will be deployed simultaneously. The bus will then execute a maneuver to retard its time of flight so that the bus will enter the Venusian atmosphere after the probes have reached the surface of Venus. In this way, the bus will serve as a frequency reference for an interferometry experiment, which will be performed in order to determine wind velocities during the probe's descent.

Since the probes will be on battery power after release from the bus, there will be no RF signal from them until just prior to entry in order to conserve power. Commands will be sent to the bus while the probes are still attached to set the epoch for the coast timers in each of the probes. The probes will have an on-board sequence programmer which, together with the coast timer, will control the entry sequence. The RF signal from each of the probes will be turned on 22 min prior to entry, where entry is defined as 200 km above the surface of Venus, which is the approximate altitude at which maximum dynamic stress and blackout will occur.

All of the probes consist of a sphere pressurized with an inert gas and sitting in a high-drag aeroshell which also serves as a thermal shield for the entry. The aeroshell and afterbody heat shields of the large probe will be jettisoned at about 68 km altitude, at which point parachutes will be deployed to slow the descent through the lower atmosphere. The parachute will be jettisoned at an altitude of approximately 44 km. The total descent time for the large probe will be about $1\frac{1}{2}$ hr. The small probes will not utilize a parachute nor will they jettison their heat shield; they will depend solely upon aerodynamic drag to slow their descent. The small probe descent will last on the order of 1 hr.

The entry sequence programmers on the small probes will be able to store on the order of 15 commands. The programmer on the large probe will store 64 commands. In addition, there will be spacecraft-detected events which will back up the stored sequence. For example, if the coast timer should fail to turn on the RF system 22 min prior to entry, an accelerometer on the probe will detect the occurrence of entry and initiate the entry sequence. In order to recover science data during the blackout region, the probes will have a storage capability. The large probe will be able to store on the order of 2500 bits of formatted data; the small probes will have a 1500-bit capacity. During the blackout, this storage will be filled with low-rate data, and these data will be transmitted interspersed with the real-time data during the remainder of the descent.

III. Science Payload

The large probe will be carrying on the order of 32 kg (70 lb) of instruments. Each small probe will carry about 2.3 kg (5 lb) of instruments, and the bus will carry approximately 18 kg (40 lb) of instruments. The instruments and chief scientists for the multiprobe mission have been officially designated and are listed below:

Large probe	Experimenter
Neutral mass spectrometer	J. Hoffman/University of Texas, Dallas
Gas chromatograph	V. Oyama/Ames Research Center
Atmosphere structure	A. Seiff/Ames Research Center
Solar radiometer	M. Tomasko/University of Arizona
Infrared radiometer	R. Boese/Ames Research Center
Cloud particle size spectrometer	R. Knollenberg/Particle Measurement Systems
Nephelometer	B. Ragent/Ames Research Center

Small probe	Experimenter
Atmosphere structure	A. Seiff/Ames Research Center
Nephelometer	B. Ragent/Ames Research Center
Net flux radiometer	V. Suomi/University of Wisconsin

Bus	Experimenter
Neutral mass spectrometer	U. Van Zahn/University of Bonn
Ion mass spectrometer	H. Taylor/Goddard Space Flight Center

In addition, the following Earth-based experiments have been approved:

Earth-based radio experiments	Experimenter
DVLBI	G. Pettengill/Massachusetts Institute of Technology
Tracking, turbulence	R. Woo/Jet Propulsion Laboratory
Tracking, propagation	T. Croft/Stanford University
Tracking, winds	A. Kliore/Jet Propulsion Laboratory

The individual experiments listed above will be described in more detail in subsequent *DSN Progress Report* articles on the Pioneer Venus 1978 Mission.

IV. Telecommunications

The signals from each of the probes will be recei via a direct link with Earth rather than via a relay through the bus. This means that during the descent there will be a total of five signals, the bus plus four probes, which must be acquired and tracked simultaneously. This aspect of the mission, together with the current DSN plans for handling the five simultaneous signals, was described in a previous article (Ref. 1).

Current concepts call for the use of long-constraint-length sequential decoding (essentially identical to that used on Pioneers 10 and 11) for all the signals from the bus and the probes. The small probes will be in one-way, using on-board very stable oscillators as the frequency reference during their entire descent. The downlink signal from the small probes will turn on 22 min prior to entry, although the oscillators themselves may be turned on earlier to allow them to warm up.

The small probes will be using very low subcarrier frequencies, on the order of 4 kHz. In order to aid in the initial acquisition at 22 min prior to entry, the small probes may be programmed to transmit carrier-only for the first 5 min. This will provide a stronger carrier to look for and will reduce the chances of locking the closed-loop receivers onto a sideband.

On the large probe, an attempt will be made to acquire and maintain two-way lock (where the frequency transmitted by the probe is determined by a coherent multiple of a frequency received from Earth) during the entire descent. This will necessitate acquiring an uplink to the large probe at probe turn on 22 min prior to entry and reacquiring the uplink after exit from the blackout. Blackout will last on the order of 20 sec; however, a large doppler shift will have taken place during that period.

Both the large and small probes will have various telemetry format changes during the descent; however, each telemetry format will have the same frame length, so that it should not be necessary to reconfigure the station portion of the ground system with each telemetry format change. The probes will change to a lower telemetry bit rate for a few minutes surrounding the expected blackout, and the small probes will switch to a lower bit rate for the lower 30 km of the descent. These bit rate changes will require reinitialization in real-time of the station portion of the Ground Data System, which will result in a few minutes of lost real-time data which will have to be recovered from the open-loop telemetry recordings which will be made.

Current planning calls for the transmitter power of the large probe to be 40 watts and for the small probes to be 10 watts each, utilizing solid-state amplifiers. The antennas on the large and small probes will be identical. During the final stages of descent, the probes will be descending essentially perpendicular to the local surface of the planet. This, coupled with the plan to disperse the probes over widely different latitudes and longitudes on the planet, means that the communication angle from the spin-stabilized probes will be as great as 60 to 65 deg. The antennas carried on the probes will therefore be required to have a fairly wide beamwidth and corresponding relatively low gain. Current antenna design is an approximately 10-cm (4-in.) diam plastic hemisphere with a turnstile-shaped conductive strip on its surface.

Obtaining sufficient telemetry margin to achieve the desired bit rates with the constraints of antenna size and transmitter power is one of the principal design challenges of this mission. How soon the RF systems can be turned on prior to entry and the total transmitter power are highly constrained by the battery size which, in turn, is highly constrained by weight limitations. The DSN will have less than 20 min to acquire all four of these signals, signals which have not been seen since launch. It will be possible to do a telemetry check on all of the probes one at a time while they are still attached to the bus via a hardwire connection with the bus telemetry subsystem. However, it will not be possible to do a direct or indirect RF check with the probes after launch until the RF turnon 20 min prior to entry.

Reference

1. Miller, R. B., "Pioneer-Venus 1978 Mission Support," in *The Deep Space Network Progress Report 42-20*, pp. 17–19, Jet Propulsion Laboratory, Pasadena, California, Apr. 15, 1974.
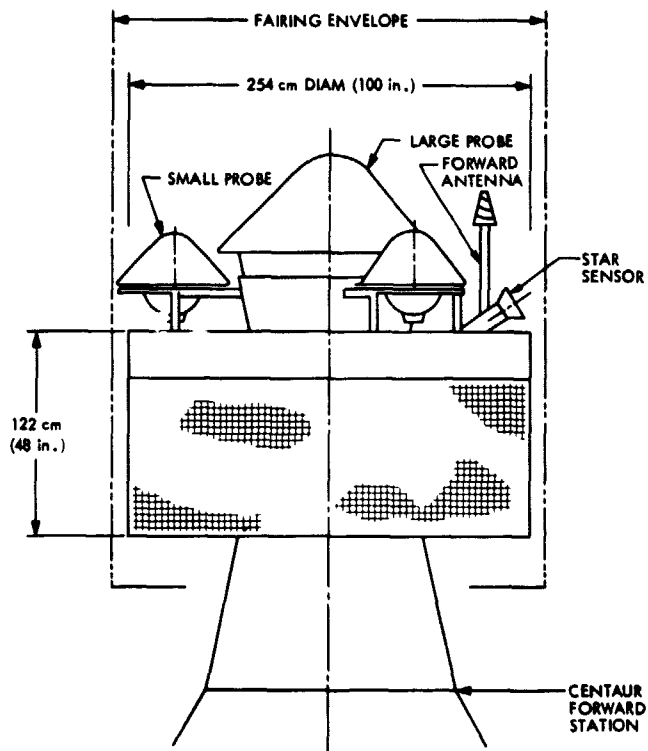
Fig. 1. Pioneer Venus 1978 multiprobe spacecraft

Low-Noise Receivers: Microwave Maser Development

R. B. Quinn
Communications Elements Research Section

Low-pass microwave filters have been built and tested in the laboratory and are now ready for installation in the 14.3- to 16.3-GHz traveling wave maser presently being used on the 64-m antenna at Goldstone Deep Space Communications Complex. These filters, when placed in the input and output lines of the traveling wave maser, will prevent possible calibration errors caused by traveling wave maser gain changes resulting from pump frequency radiation into the signal waveguides. These filters are matched at the signal frequency of the traveling wave maser, have low insertion loss, and will operate at 4.5 K. Therefore, no significant degradation in system performance results.

I. Introduction

Two low-pass filters with pump frequency rejection have been completed and tested in the laboratory. They are ready for installation in the 14.3- to 16.3-GHz traveling wave maser (Ref. 1) presently installed on the 64-m antenna at Goldstone Deep Space Communications Complex. Differences in traveling wave maser (TWM) gain of as much as 0.5 dB have been recorded and are a function of impedance changes at the pump frequencies as seen at the input of the TWM. Calibration errors can occur due to changes in gain caused by pump frequency radiation into the signal waveguides. These gain changes will be substantially reduced by the use of low-pass filters that are placed in the signal frequency waveguide to coaxial line transitions which operate at 4.5 K. The small physical size of the filter permits it to be located within the existing transition.

II. Filter Description

The filter is of a coaxial type with eleven semi-lumped elements. The design data for this type of filter were obtained from Ref. 2 and have been used successfully in the construction of a pair of low-pass filters that have been incorporated into the X-band TWM system (Ref. 3). The X-band filter, with a 12-GHz cutoff, has a rejection at the pump frequencies (18.4 to 19.6 and 22.6 to 24.8 GHz) of over 30 dB and a reflection coefficient at the signal frequency (7700 to 8800 MHz) of better than -21 dB. Because of these favorable rejection and match characteristics, a scaling factor of $\frac{2}{3}$ was used to obtain an 18-GHz cutoff for use with the Ku-band TWM.

A removable metal centering sleeve was used to establish adequate concentricity of the filter elements to

the outer conductor. It was found that the reduced clearance between the capacitive elements and the outer conductor in the scaled-down filter required a higher degree of concentricity to obtain a satisfactory match. To solve this problem a Teflon dielectric centering sleeve (Fig. 1) was incorporated. The element diameters were reduced to compensate for the difference in dielectric constant, and a Teflon sleeve was made to fit tightly over five of the six capacitive elements.

In building this filter, as with the X-band filter, the match was optimized by cut-and-try methods. The final tuning for best match at the TWM signal frequency (14.3 to 16.3 GHz) is done by adjusting the length of the two 2-56 screws holding the coupling loop to the transition body (Fig. 2). The filter section is located in the transition body between the coupling loop and the center contact of the SMA connector, a space previously occupied by a straight section of coaxial center conductor. Since the transition body, coupling loop, and SMA connector fitting are identical to those now installed in the Ku-band TWM, the transition/filter assembly has the same outside appearance and dimensions and is directly interchangeable with the present transition. Implementation of these filters will require no modification of the traveling wave maser/closed cycle refrigerator (TWM/CCR) system.

III. Filter Performance

These filters are designed to have low insertion loss at the Ku-band signal frequency and have an 18-GHz cutoff. Rejection at the pump frequencies (25.4 to 27.4 and 35.4 to 39.3 GHz) is more than 20 dB.

Loss and match measurements have been made on both filters in the laboratory and, on the basis of these measurements, the filter with the best reflection coefficient has been chosen for use in the TWM input line. The reflection coefficient at the signal frequency of this filter is better than −20 dB across the entire TWM tuning range (Fig. 3). The reflection coefficient of the filter chosen for the output line has been recorded at better than −15 dB across the same frequency range. The installation of the filters is not expected to degrade the match of the TWM.

While "identical" parts were used in both assemblies, small machining differences account for the considerable difference in the characteristics of the two filters.

The insertion loss at the signal frequency of the filter chosen for the TWM input is less than 0.2 dB at room temperature. These transition/filter assemblies, when installed, will be bolted directly to the 4.5 K station of the CCR. Operation at this temperature will decrease the noise contribution caused by the insertion loss of the filter to less than 0.2 K.

References

1. Clauss, R. C., and Quinn, R. B., "Low Noise Receivers: Microwave Maser Development," in *The Deep Space Network Progress Report*, Technical Report 32-1526, Volume V, pp. 102–108, Jet Propulsion Laboratory, Pasadena, Calif., Oct. 15, 1971.

2. Matthaei, G. L., Young, L., and Jones, E.M.T., *Microwave Filters, Impedance-Matching Networks, and Coupling Structures*, McGraw-Hill Book Company, Inc., New York, 1964, pp. 102, 365–380.

3. Clauss, R., Wiebe, E., and Quinn, R., "Low Noise Receivers; Microwave Maser Development," in *The Deep Space Network Progress Report*, Technical Report 32-1526, Volume XI, pp. 71–80, Jet Propulsion Laboratory, Pasadena, Calif., Oct. 15, 1971
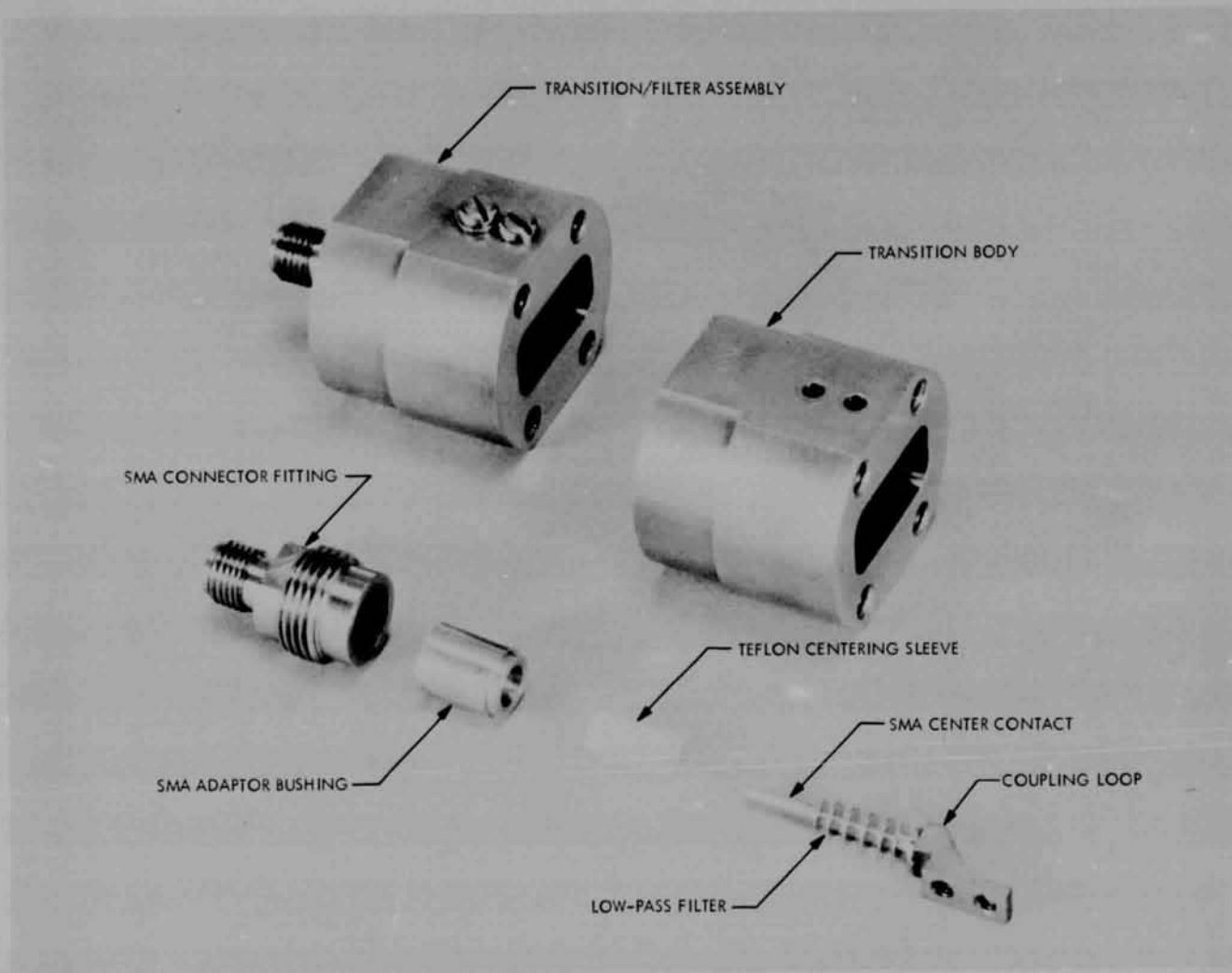
Fig. 1. Photo of transition/filter parts and assembly
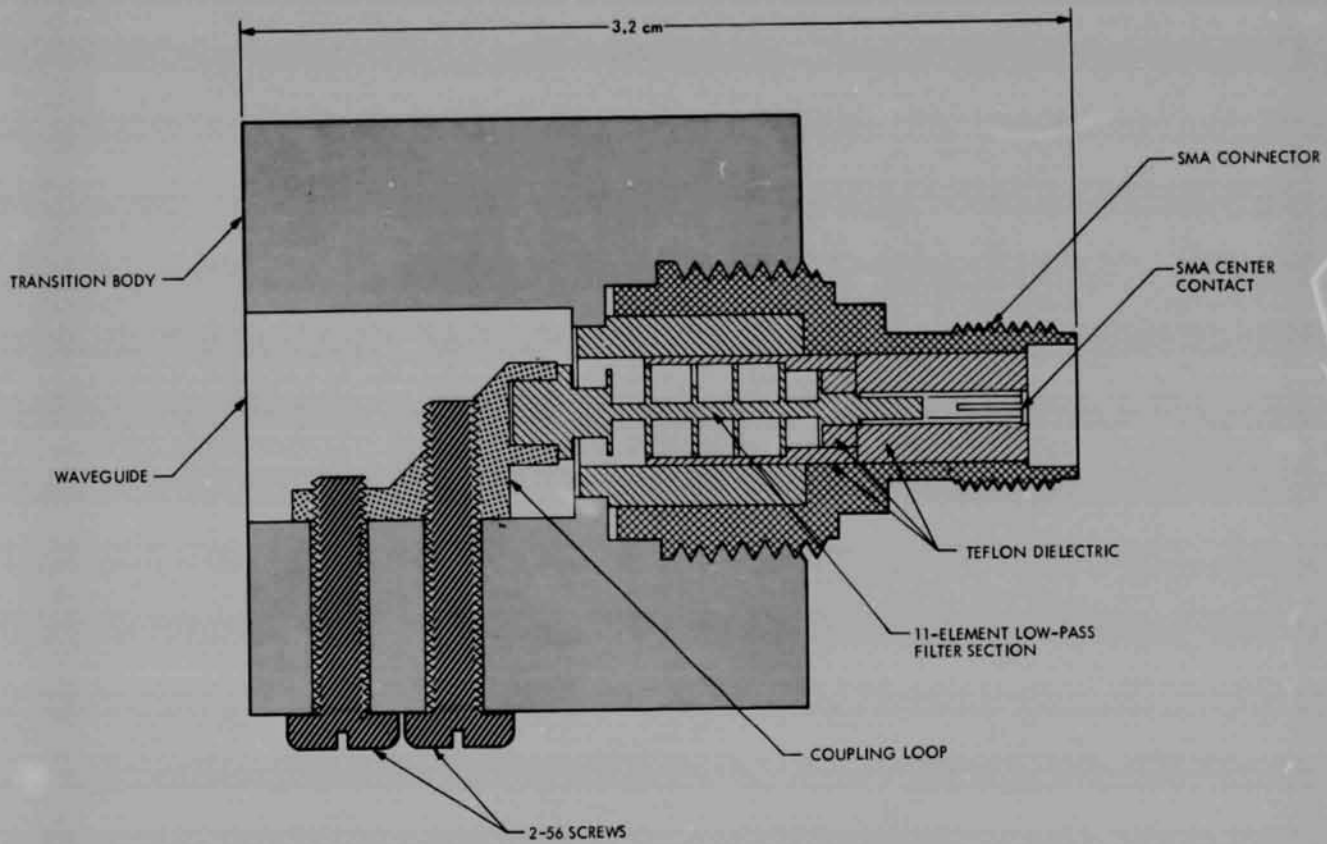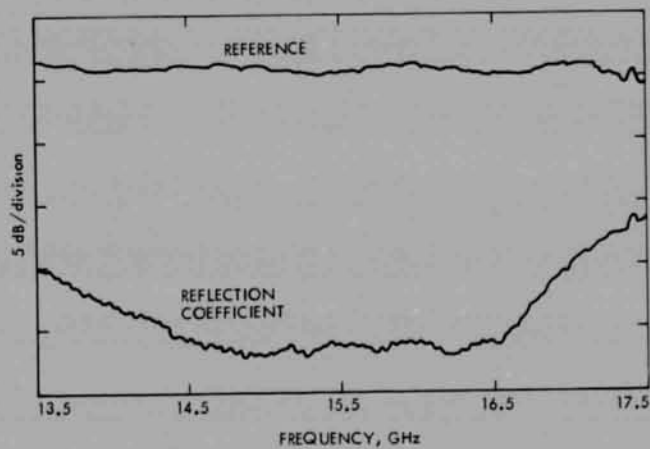
Fig. 2. Section view of transition/filter assembly

Fig. 3. Match diagram (input filter)

S/X Experiment: A Study of the Effects of Ambient Temperature on Ranging Calibrations

T. Y. Otoshi
Communications Elements Research Section

*A study has been made of the effects of the outside air temperature at DSS 14
on ground system range calibrations. Some correlation was found on range data
obtained with the 20-kW transmitter system configuration, but no correlation was
found for the 100-kW transmitter system configuration.*

I. Introduction

In a previous report (Ref. 1), Mariner 10 pre- and post-tracking pass range calibration data were presented for 1974 Day 12 through Day 150. A cursory examination of the data showed that differences between pre- and post-calibration data for the same day's track could be attributed to ambient temperature changes. Since outside air temperatures at DSS 14 have been tabulated in the ranging calibration log book, it was possible to perform a correlation analysis of these data. This article presents the result of this study.

II. Calibration Configuration

Ranging calibrations on the ground system at DSS 14 are currently being performed with the zero delay device (ZDD) in the cable configuration that was described in Ref. 2. The ranging calibrations are normally done during pre- and post-calibration periods of Mariner 10 tracking passes at the signal levels and frequencies applicable to the particular tracking pass. These ZDD pre- and post-calibration data are used along with the ground station

Z-correction (Ref. 3) and spacecraft radio system bias correction to enable determination of the true range to the spacecraft (Ref. 4).

A block diagram of the present ZDD configuration for the S/X ground system calibrations at DSS 14 is shown in Fig. 1. As was described in Ref. 2, the ZDD is a ground station antenna-mounted transponder that samples the uplink 2113 MHz from the transmitter and generates coherent downlink S- and X-band test signals of 2295 and 8415 MHz. These test signals are transmitted to the respective masers through calibrated cables of known delay.

Figures 2 and 3 show the ZDD in the cable configuration as it is currently installed in the Mod-3 section of the 64-m antenna at DSS 14. Since this ZDD assembly is located in the air-conditioned environment of the Mod-3 area, this portion of the range calibration system should not be affected by outside air temperature changes. It is believed that most of the range changes attributed to outside air temperature changes will occur in the uplink and downlink cables between the tricone

area and the control room. Only about 97.5 m (320 ft) round trip cable length is actually exposed to the outside air temperature environment. Most of this cable run is Spiroline RG 252 cable, but about 12.2 m (40 ft) of round trip RG 214 cable is used in the elevation cable wrapup.

III. Test Results

As was discussed in previous reports (Refs. 1 and 5), the Block 4 range calibration data are also a function of signal level and differ when using the 20-kW or the 100-kW transmitters. Therefore, it was necessary to group the data as those belonging to either the 20-kW or 100-kW transmitter calibrations. Through the use of range change versus signal level curves presented in Ref. 5 it was possible to correct the data and normalize them to a common signal level reference, which was arbitrarily chosen to be −145 dBm. Only calibration data from 1974 Day 85 to Day 172 were used; it was only after Day 85 when both the doppler and system configurations were left unaltered.

The ranging calibration data are shown plotted as functions of outside air temperature in Figs. 4 through 7. It can be seen that some correlation of range change to temperature is evident for the 20-kW transmitter system for both S- and X-band.

For the purposes of comparison, X-band group delay data as a function of temperature are shown in Figs. 8 and 9 for 3.05-m (10-ft) lengths of Spiroline RG 252 and RG 214 cables, respectively. These data were obtained in a temperature-controlled oven and group delay measured by a phase versus frequency measurement tech-

nique with a network analyzer. It can be seen that the Spiroline RG 252 characteristics are similar to those measured for the 20-kW data. As was mentioned previously, most of the DSS 14 ranging system cable run consists of RG 252 cable.

No correlation was seen for the data plotted for the 100-kW transmitter system data. This lack of correlation for the 100-kW transmitter data is difficult to explain. It is possible that there are more random noise and range changes associated with the 100-kW transmitter itself. The effect on connector and cable mismatches could also cause departure from expected trends.

IV. Discussion and Conclusions

The results presented in this article show that some correlation of range change with ambient temperature changes was found. However, the results should be interpreted to show trends only and not be used as a correction curve. The data quality is understandably poor for this type of analysis since it is based on two data points a day for a period of about three months. Many systematic and random errors could easily be introduced. It would have been preferable to obtain ranging stability data in one continuous run over a period of about 12 hours. This test should begin in the early morning hours and continue to nighttime hours so as to include the large temperature change periods.

Although time at DSS 14 had been scheduled for performing some of this type of testing, other system problems and test requirements made it difficult to obtain a long continuous run of good ranging stability data.

References

1. Otoshi, T. Y., "S/X Experiment: DSS 14 Pre- and Post-Track Ranging Calibrations for Mariner 10 Tracking Passes and Associated Problems," in *The Deep Space Network Progress Report 42-22*, pp. 81–89, Jet Propulsion Laboratory, Pasadena, California, August 15, 1974.

2. Otoshi, T. Y., and Stelzried, C. T., "S/X Experiment: A New Configuration for Ground Range Calibrations With the Zero Delay Device," in *The Deep Space Network Progress Report 42-20*, pp. 57–63, Jet Propulsion Laboratory, Pasadena, California, April 15, 1974.

3. Batelaan, P. D., "S/X-Band Experiment: Zero Delay Device Z Correction," in *The Deep Space Network Progress Report 42-20*, pp. 78–83, Jet Propulsion Laboratory, Pasadena, California, April 15, 1974.

4. "TRK-2-8 Module of DSN System Requirements Detailed Interface Design Document 820-13, Rev. A.," July 1, 1973 (JPL internal document).

5. Otoshi, T. Y., and Batelaan, P. D., "S/X Experiment: DSS 14 S/X Ground System Ranging Tests," in *The Deep Space Network Progress Report 42-22*, pp. 90–100, Jet Propulsion Laboratory, Pasadena, California, August 15, 1974.
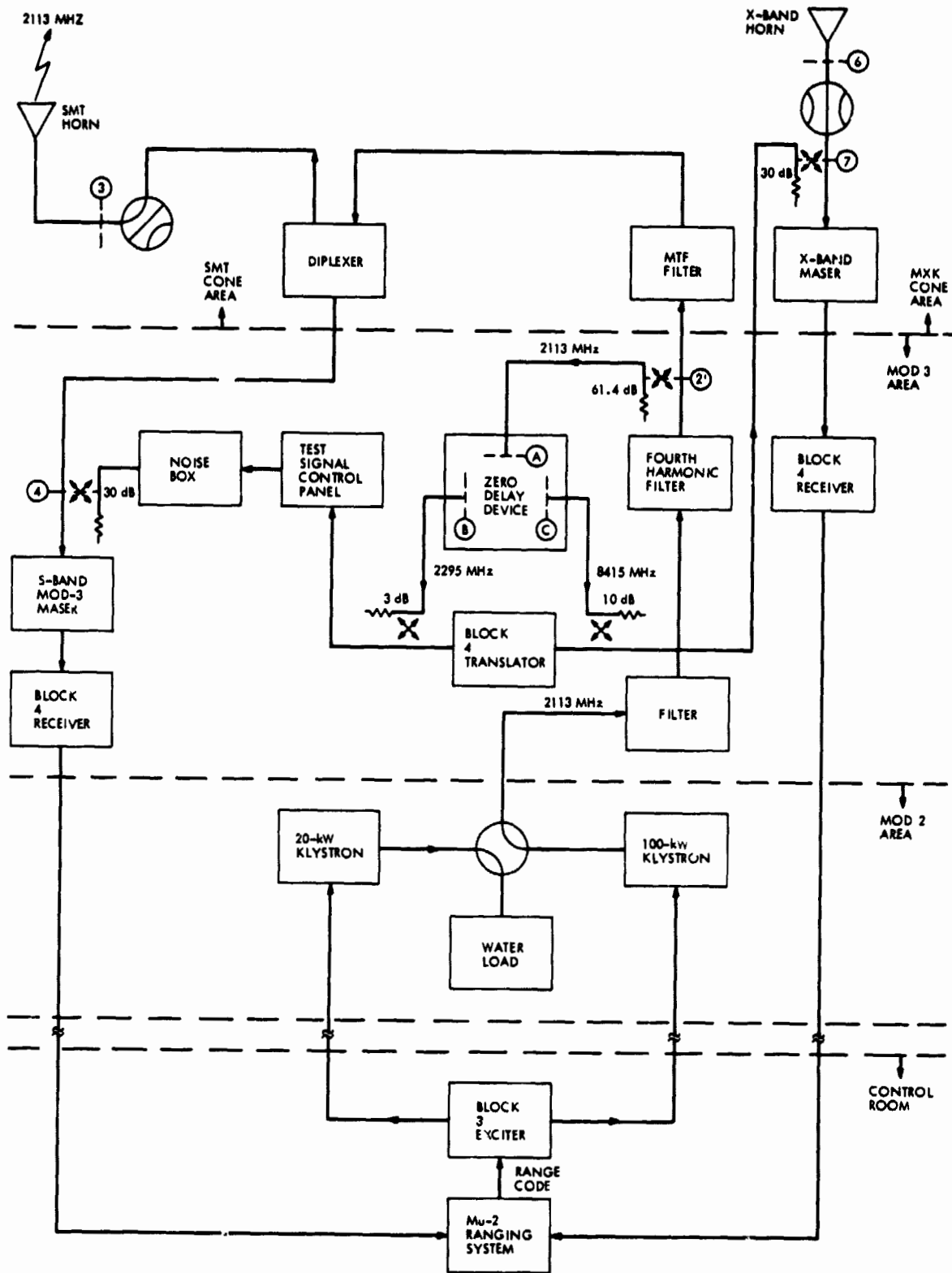
Fig. 1. Block diagram of the new configuration at DSS 14 for ground system range calibrations
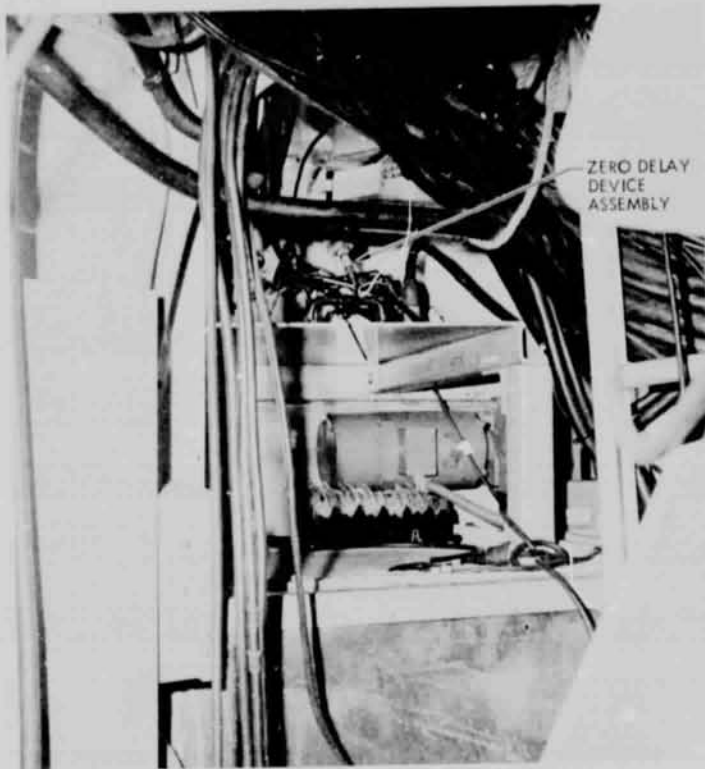
Fig. 2. Zero delay device assembly as seen inside the Mod 3 area
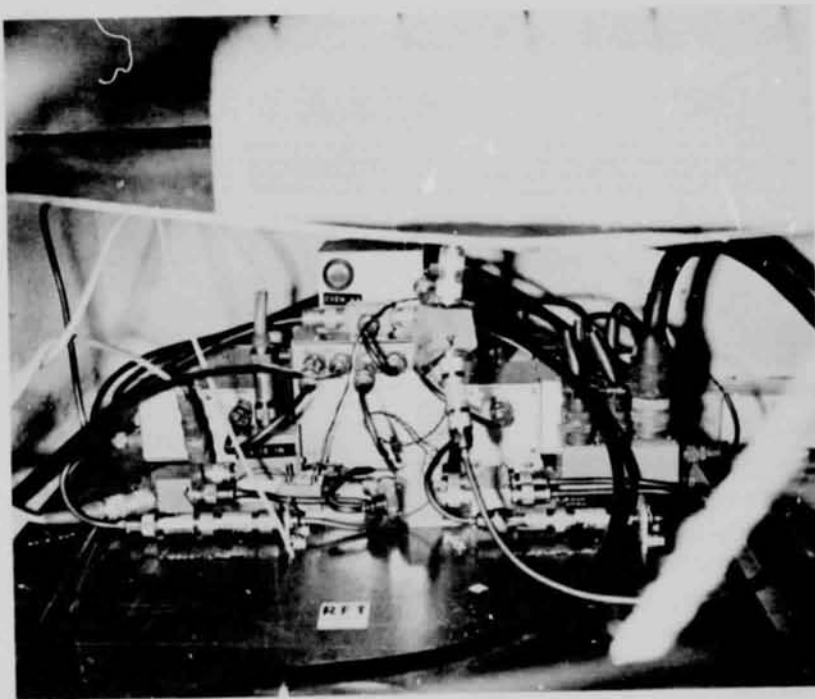
Fig. 3. Closeup view of the zero delay device assembly as currently installed in the Mod 3 area
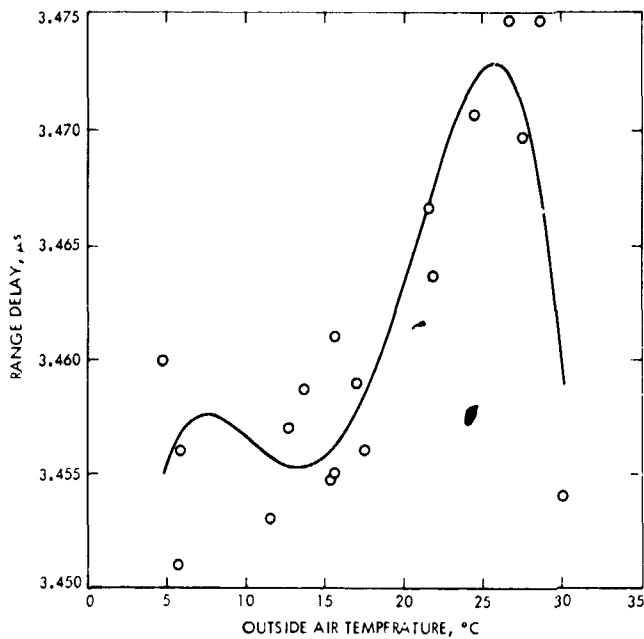
Fig. 4. S-band range as a function of outside air temperature at DSS 14. Data taken after 1974 Day 85 for 20-kW transmitter configuration and corrected to the −145-dBm signal level
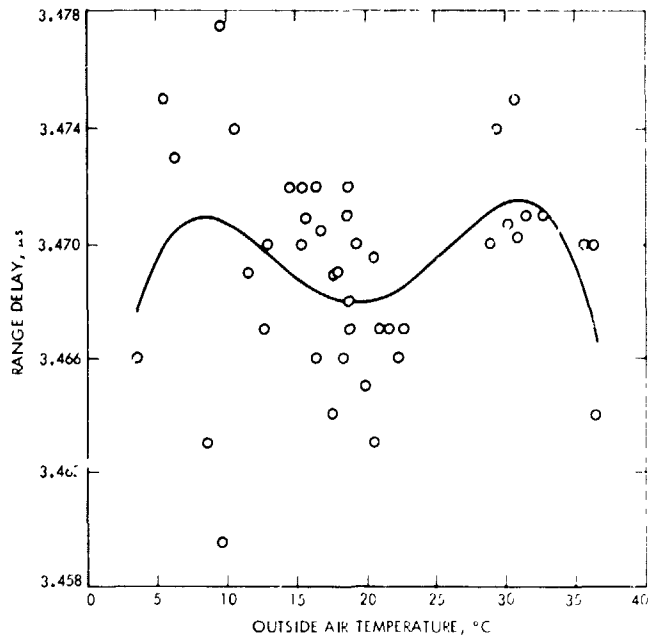
Fig. 6. S-band range as a function of outside air temperature at DSS 14. Data taken after 1974 Day 85 for 100-kW transmitter configuration and corrected to the −145-dBm signal level
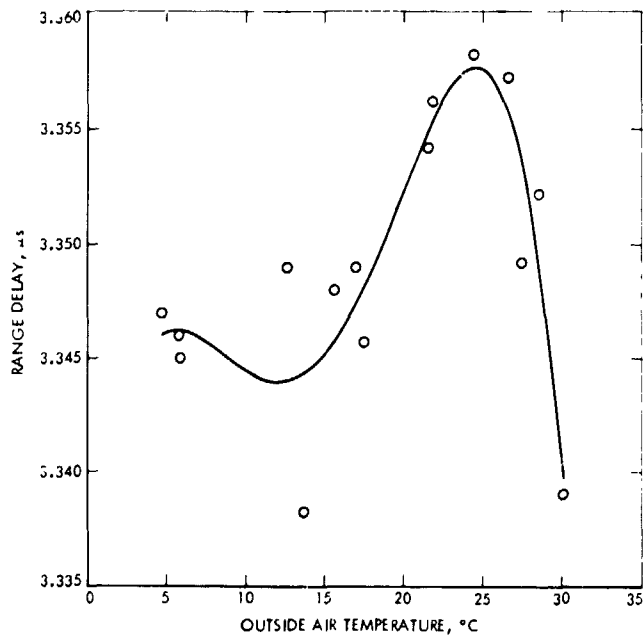
Fig. 5. X-band range as a function of outside air temperature at DSS 14. Data taken after 1974 Day 85 for 20-kW transmitter configuration and corrected to the −145-dBm signal level
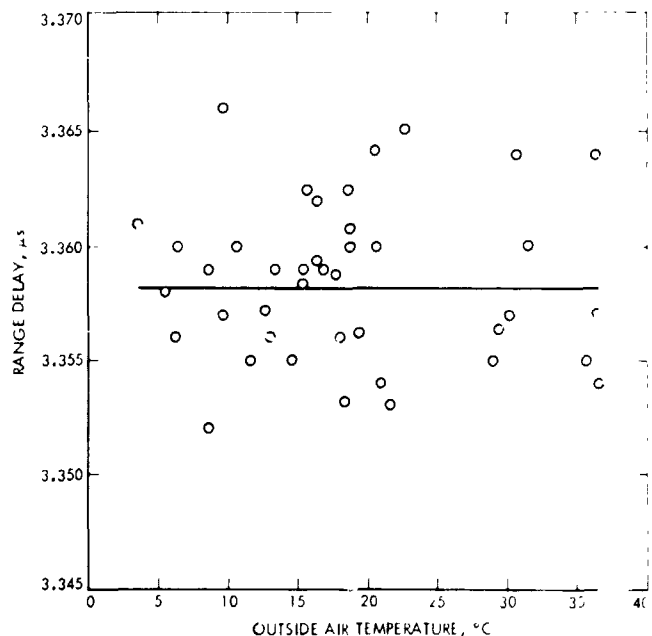
Fig. 7. X-band range as a function of outside air temperature at DSS 14. Data taken after 1974 Day 85 for 100-kW transmitter configuration and corrected to the −145-dBm signal level
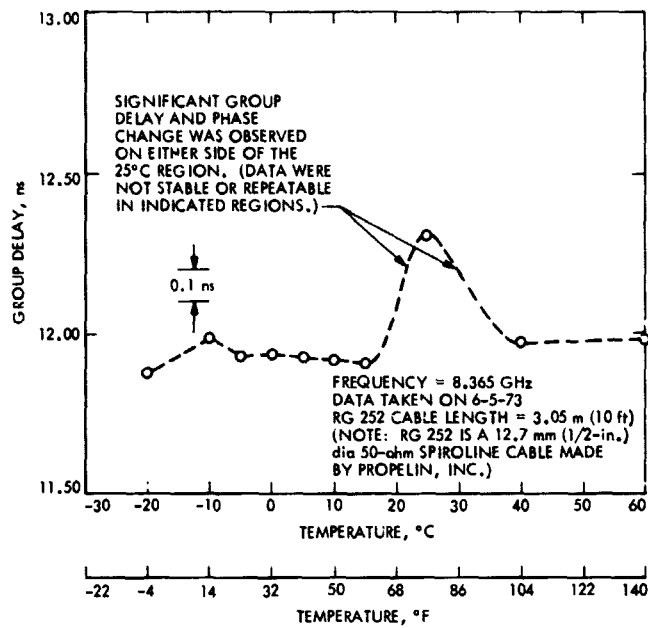
Fig. 8. X-band group delay as a function of temperature for
3.05-m (10-ft) length of Spiroline RG 252 cable
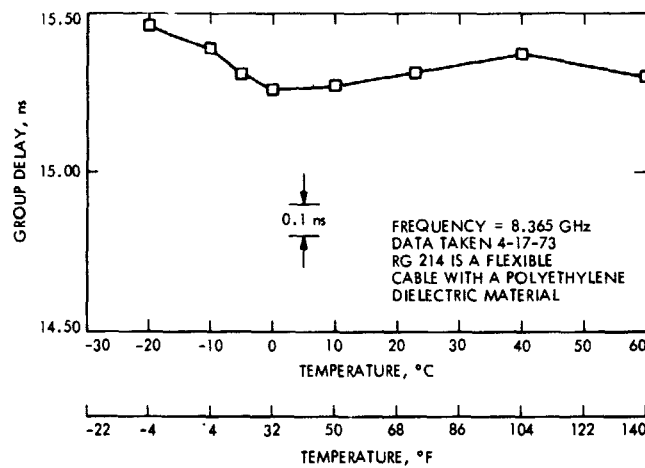
Fig. 9. X-band group delay as a function of temperature for
3.05-m (10-ft) length of RG 214 cable

Characteristics and Simulated Performance of Short Convolutional Codes: Length 7, Rate 1/3

J. W. Layland

Communications Systems Research Section

This article compares the characteristics and performance of two near-optimal constraint-length 7, rate 1/3 convolutional codes. Performance estimates are based upon software simulations for the additive white Gaussian noise channel.

I. Introduction

It is currently expected that in the near future the DSN will be asked to support a series of missions utilizing short-constraint-length convolutional codes. A maximum-likelihood or Viterbi-algorithm decoder will be utilized in the tracking stations. The first application will be the Mariner Jupiter/Saturn 1977 (MJS'77) mission for which a constraint-length 7, rate ½ code has been selected as the baseline design. That particular rate ½ code is generally accepted as being optimal and has been used elsewhere in currently available hardware (Refs. 1, 2). No specific commitment to a rate ⅓ code exists at this time, but it has been shown that if sufficient bandwidth exists, the rate ⅓ codes generally require approximately 0.4 dB less signal-to-noise ratio (SNR) for equivalent perfor-mance than do the rate ½ codes of the same constraint-length (Ref. 3).

Since additionally neither the encoder nor the decoder for a rate ⅓ code is significantly more complex than that for a rate ½ code of the same constraint length, there is considerable motivation for deploying within the DSN a decoder with the multi-mission capability for decoding both rate ⅓ and rate ½ codes of the chosen length (i.e., 7). It is the express purpose of the work described in this article to assist in the selection of the best length 7, rate ⅓ convolutional code. Two codes are discussed in detail here. Of all the 7:⅓ codes which conceptually exist, most are very poor performers, and all are believed to be poorer performers than these two codes.

II. A Good 7:1/3 Code With Weight 14

The first code to be discussed has a generator matrix which may be represented in octal as 7566127. This matrix has weight 14 (14 one's), and hence the code has a maximum free distance of 14. The optimum 7:½ code is embedded within this code. This code has been widely distributed, having been identified by Odenwalder (Ref. 2) as the optimum 7:⅓ code, and later included in LINKABIT (Ref. 4) and Shuttle (Ref. 5) reports. Table 1 lists the lowest weight code words for this code. No code words of odd weight exist. The code is non-transparent so that the 180-deg subcarrier's phase ambiguity must be resolved by the decoder as it is acquiring node-synchronization and before it begins decoding.

III. A Good 7:1/3 Code With Weight 15

The second code of interest has a generator matrix which may be represented in octal as 7576127. The generator matrix of this code is separated by one bit from the generator matrix of the previous code, and it also contains the optimum 7:½ code embedded within it. We were motived to construct this code from the previous one by noting that the upper bound to achievable free-distance is 15 (Ref. 6), and hence that a better code might be available. Table 2 lists the lowest-weight code words for this code. The free-distance bound of 15 is achieved. Hence, at extremely low error probability, where the code performance is almost entirely defined by the free-distance and the code-words at the free distance, this code will have somewhat lower error probability than the weight-14 code. This code is transparent so the 180 deg subcarrier phase ambiguity is not detected by the decoder, but is passed through to the data user.

IV. Comparison by Simulation

Performance of maximum-likelihood decoding of both 7:⅓ codes has been simulated for the additive-white Gaussian Noise Channel. The simulation used 4-bit (16-level) quantization of the input symbols, and a decoder path memory of 64-bits. Decoder bits were taken from the most likely path. The software decoder operates at a relatively unimpressive 6×10^5 bits per hour, thereby limiting practical sample-sizes to about 4×10^6 bits.

Figure 1 shows the simulated bit error probability for the two codes. Data points at 1.6 dB and above represent 4×10^6 bits. The two data points at 1.1 and 1.4 dB represent only 4×10^5 bits. At each value of Eb/N_0 simulated, an identical noise sequence was input to both coders. The noise sequences were distinct for distinct values of Eb/N_0. Because errors in the output of the decoder occur in bursts, rather than independently, confidence intervals for this simulated error probability must be assigned according to the number of bursts, or error events, which occur within the simulation run. The one-sigma confidence intervals were computed on this basis and are listed in Table 3. They are distinct only at 2.4 dB, and they overlap to an ever-increasing extent as Eb/N_0 is lowered.

A three-sigma confidence interval for either code would in all cases include the data point for the other code. Thus while the simulation implies that the weight 15 code performs better by a miniscule 0.02 dB at 10^{-3} bit error rate, it does not provide a statistically significant conclusion. Increasing the sample-size by a factor of 10 or more, as would be needed to achieve a statistically significant differentiation of the two codes, does not seem feasible without a much faster decoder.

Most data transmitted from a spacecraft does not consist of independent bits, but consists instead of instrument data words, each of several bits in duration; e.g., "pixels," or picture elements which have a nominal 8-bit length. As a result, the data user is often interested more in the error clustering characteristics of the coded channel, than in the bit error probability *per se*. Figure 2 shows this clustering characteristic in two forms: the first is the probability that an error burst occurs (typical bursts would be 3-15 bits), and the second is the probability that an 8-bit pixel contains an error. As before, there is no statistically significant difference between the two codes.

V. Conclusion

The comparison between the two convolutional codes with constraint length 7 and rate ⅓ discussed here has shown no significant differences in error performance for bit error probabilities in the neighborhood of 10^{-3}. As a result, the choice between them should be based upon the operational implications of code transparency and the subcarrier phase ambiguity.

References

1. Linkabit Corporation: Sales and Advertising Literature, San Diego, Calif., 1973 and 1974.

2. Odenwalder, *Optimal Decoding of Convolutional Codes*, Ph.D. Thesis, Systems Science Department, University of California, Los Angeles, 1970.

3. Layland, J. W., "Information Systems: Performance of Short Constraint Length Convolutional Codes, and a Heuristic Code-Construction Algorithm," in *The Deep Space Network*, Space Programs Summary 37-64, Vol. II, pp. 41 to 44, Jet Propulsion Laboratory, Pasadena, Calif., Aug. 31, 1970.

4. Gilhousen, K. S., et al., *Coding Systems Study for High Data Rate Telemetry Link*, Linkabit Corp., San Diego, Calif., January 1971.

5. *Shuttle Orbiter/GSFC Communications and Tracking Interface Control Document (Preliminary) ICD-2-0D044*. Lyndon B. Johnson Space Center, Houston, Texas, January 1974.

6. McEliece, R. J., and Layland, J. W., "An Upper Bound to the Free Distance of a Tree Code," in *Supporting Research and Advanced Development*, Space Programs Summary 37-62, Vol. III, pp. 62–64, Jet Propulsion Laboratory, Pasadena, Calif., April 30, 1970.

Table 1. Low-weight code words of 7566127

Weight	Number of 1's at this weight	Code words (information bits)
14	1	1
15	None	
16	2 (20 Total)	1001
	3	10101
	3	1011
	2	11
	3	11001
	3	111
	4	1111
17	None	
18	2 (53 Total)	101
	4	10110001
	3	110001
	5	110010101
	5	1100111
	4	111001
	4	11101
	7	11110111
	8	1111011101
	5	11111
	6	111111
19	None	
20	184 Total	35 distinct sequences
21	None	
22	555 Total	90 distinct sequences

Table 2. Low-weight code words of 7576127

Weight	Number of 1's at this weight	Code words (information bits)
14	None	
15	1 (7 Total)	1
	3	11001
	3	111
16	2 (8 Total)	101
	2	111
	4	111001
17	3 (22 Total)	10101
	3	1011
	5	101111
	3	110001
	5	1100111
	3	1101
18	2 (44 Total)	1001
	4	10110001
	6	1100111001
	6	11001111
	8	1100111111
	4	11011
	4	1110001
	4	1111
	6	111111
19	22 Total	4 distinct sequences
20	94 Total	18 distinct sequences
21	222 Total	35 distinct sequences
22	282 Total	45 distinct sequences

Table 3. One-sigma confidence ranges for estimated bit error probability

Eb/N_0	Code 7566127		Code 7576127	
	Low estimate	High estimate	Low estimate	High estimate
1.6	5.75×10^{-3}	5.95×10^{-3}	5.72×10^{-3}	5.92×10^{-3}
1.8	3.78×10^{-3}	3.94×10^{-3}	3.70×10^{-3}	3.86×10^{-3}
2.0	2.48×10^{-3}	2.58×10^{-3}	2.37×10^{-3}	2.49×10^{-3}
2.2	1.50×10^{-3}	1.58×10^{-3}	1.44×10^{-3}	1.52×10^{-3}
2.4	8.90×10^{-4}	9.55×10^{-4}	8.21×10^{-4}	8.86×10^{-4}
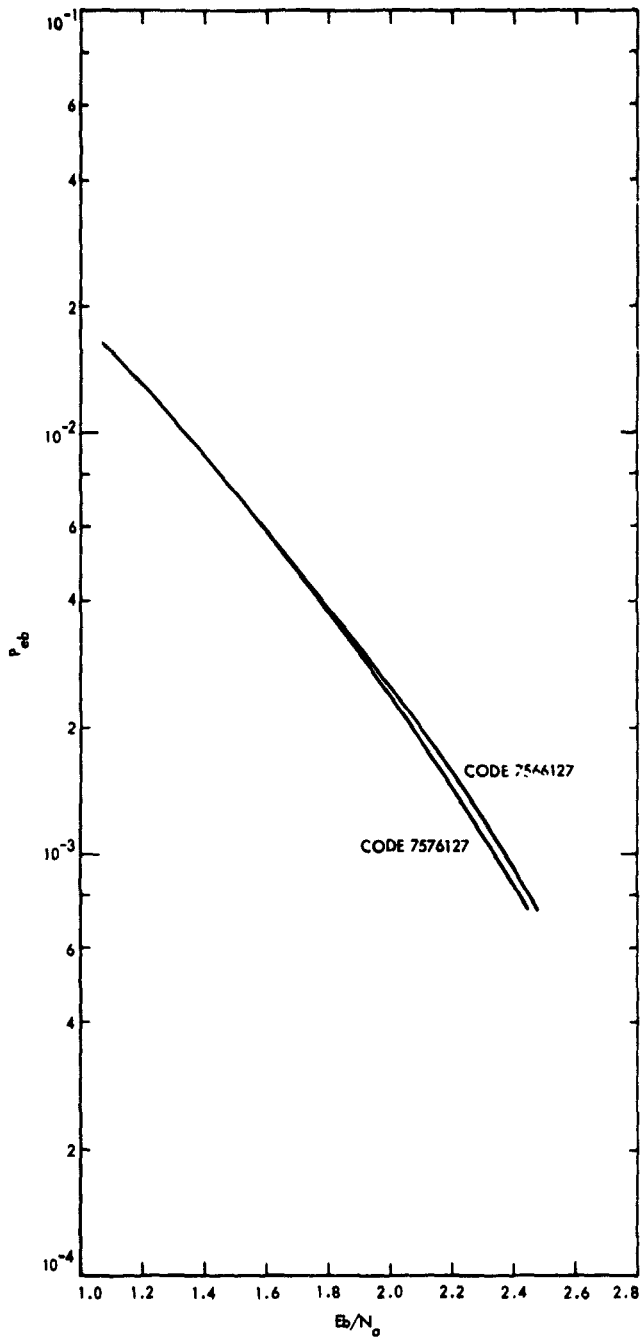
Fig. 1. Simulated bit error probability
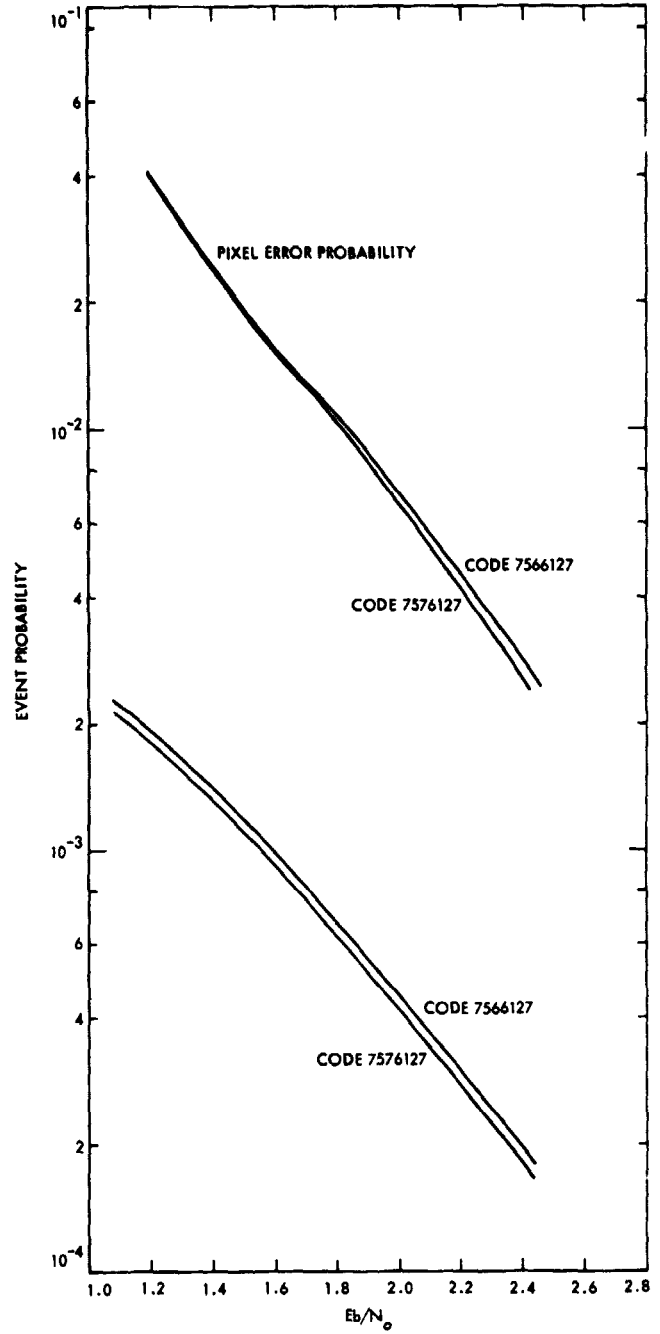
Fig. 2. Simulated pixel error probability and error event probability

Performance Degradation of Uncoded and Sequentially Decoded PSK Systems Due to Log-Normal Fading

B. K. Levitt
Communications Systems Research Section

The 1978 Pioneer Venus (PV'78) orbiter will dispatch several probes into the planet atmosphere. The telemetry from these probes will be transmitted directly to Earth as coherent, binary phase-shift-keyed (PSK) uncoded or convolutionally encoded/sequentially decoded data. These communication links will be subjected to log-normal fading due to turbulence in the atmosphere of Venus. This paper offers a theoretical model for predicting the effects of the channel fading on PV'78 telemetry performance. Because this model considers the effects of a noisy carrier reference on the telemetry performance, it permits the determination of the optimum modulation angle which minimizes the link error rate for a given system. The model predicts that the fading will cause a 1.1 to 1.3 dB increase in the signal-to-noise levels required to achieve a frame deletion rate of 10^{-3} for the PV'78 coded telemetry modes.

I. Introduction

The 1978 Pioneer Venus mission (PV'78) will dispatch several probes into the planet atmosphere. The telemetry from these probes will be transmitted directly to Earth as coherent, binary phase-shift-keyed (PSK) uncoded or convolutionally encoded/sequentially decoded data. Data from the Ru...an spacecraft Venera 4 indicate that these communication links will be subjected to log-normal fading due to turbulence in the atmosphere of Venus (Ref. 1). This paper offers a theoretical model for pre-

dicting the effects of the channel fading on PV'78 telemetry performance.

An earlier article (Ref. 2) analyzed the degradation of PV'78 uncoded telemetry due to log-normal fading; however, this analysis was based on the idealization that the receiver was operating with a strong (noise-free) carrier reference (implying a small modulation angle). Layland has examined the problems of uncoded (Ref. 3) and sequentially decoded (Refs. 4, 5) detection with a noisy carrier reference. This paper extends his noisy reference

models to include the effects of log-normal fading. As in the non-fading case, the noisy reference model illustrates that a given telemetry link has an optimum modulation angle which minimizes the link error rate.

II. Analysis

Signaling errors occur as bit crossovers in the uncoded case, and as frame deletions (buffer overflows) in the sequential decoding case. Conditioned on the effective received signal-to-noise ratio R in the data channel, the error rate is given by

$$P(\epsilon|R) = \begin{cases} Q(\sqrt{2R}); & \text{uncoded case} \\ D(R, N); & \text{sequential decoding case} \end{cases}$$

$$(1)$$

$Q(\cdot)$ is the gaussian error function defined by

$$Q(x) \equiv \frac{1}{\sqrt{2\pi}} \int_x^\infty dy \exp\left(-\frac{y^2}{2}\right) \qquad (2)$$

Layland (Ref. 4, Eq. 3) has determined an approximation for the deletion rate of the form

$$D(R, N) \cong \min\left[1, \exp\left(\sum_{n, r} A_{n, r} R^r (\ln N)^n\right)\right] \qquad (3)$$

where N is the computational capacity of the sequential decoder in computation per bit. The coefficients $\{A_{n, r}\}$ should be determined empirically. Pioneer Venus '78 will use a constraint length 32, rate 1/2 convolutional code, with a 512-bit frame. At the present time, an insufficient amount of PV'78 simulated sequential decoding data exists to determine the $A_{n, r}$'s. Consequently, the analysis below uses the $A_{n, r}$'s of Table 1, determined by Layland (Ref. 5, Table 1) for experimental Helios data. Although Helios uses an 1152 bit frame, its sequential decoding computation distribution should be similar to that for PV'78.

There is, in general, an effective memory duration T_m over which the decoder reaches certain intermediate decisions in its detection procedure. In the uncoded case, the detector makes a single decision based on an integration over a bit time T_B to decode each received bit:

$$T_m = T_B; \quad \text{uncoded case} \qquad (4)$$

For sequential decoding, the value of T_m is more obscure: a hard decision on a received bit may involve many individual searches of different lengths into the code tree. Layland (Ref. 6) has considered this problem at length, and has used a simplified analysis to derive an approximate formula for T_m (Ref. 6, Eq. 6):

$$T_m \cong 2T_B\left[1 - \frac{1}{N}\log_2\left(1 + \frac{N}{2}\right)\right];$$

$$\text{sequential decoding case} \qquad (5)$$

Because of the log-normal fading and the noisy carrier reference, the received signal-to-noise ratio in the data channel is a random process of the form

$$R(t) = \rho[e^{\chi(t)} \cos \phi(t)]^2 \qquad (6)$$

where

$$\rho \equiv \frac{P_T}{N_0} T_B \sin^2 \theta \qquad (7)$$

In the equations above, $e^{\chi(t)}$ is the log-normal fading process (Ref. 2, Eq. 2), $\phi(t)$ is the carrier reference phase error (e.g., Ref. 3, Eq. 1b), P_T/N_0 is the total received signal-to-noise ratio, and θ is the modulation angle. At very high data rates $R_B = 1/T_B, R(t)$ is essentially constant over T_m, and $\chi(t)$ and $\phi(t)$ can be represented by the random variables χ and ϕ. The expected link performance is then characterized by

$$P(\epsilon) = \overline{P(\epsilon|R = \rho e^{2\chi} \cos^2 \phi)}^{\chi, \phi} \qquad (8)$$

For small values of R_B, such that $R(t)$ contains many degrees of freedom over T_m,

$$P(\epsilon) = P\left[\epsilon|R = \rho\left(\overline{e^\chi \cos \phi}^{\chi, \phi}\right)^2\right] \qquad (9)$$

Note in Eq. (9) that the expectation is not over the received signal-to-noise ratio $R = \rho e^{2\chi} \cos^2 \phi$, but rather over $\sqrt{R}$, since it is, in fact, this parameter that characterizes the decoder performance.

The medium rate model is intended to predict the expected error rate for data rates between the two extremes above. A generalization of the approaches used separately for the fading and noisy reference problems (Refs. 2, 3, 5), it is based on the hypothesis that the conditional error rate is given by Eq. (1) with

$$R = \rho \alpha^2 \qquad (10)$$

where

$$\alpha \equiv \frac{1}{T_m} \int_0^{T_m} dt\, e^{\chi(t)} \cos \phi(t) \tag{11}$$

The determination of the statistical behavior of the random variable α is complicated by the dependence of $\phi(t)$ on $\chi(t)$. This problem is examined in Appendices A and B, where it is shown that α has the approximate form

$$\alpha \cong e^\gamma \left(1 - \frac{\sigma_\phi^2 \mu}{2}\right) \tag{12}$$

and expressions are derived for σ_ϕ^2, $p(\gamma)$, and $p(\mu|\gamma)$. Then, numerical integration techniques can be used to compute

$$P(\epsilon) =$$

$$\int_{-\infty}^{\infty} d\gamma\, p(\gamma) \int_0^\infty d\mu\, p(\mu|\gamma)\, P\left[\epsilon\,|\,R = \rho e^{2\gamma}\left(1 - \frac{\sigma_\phi^2 \mu}{2}\right)^2\right] \tag{13}$$

Error rates computed using this model merge smoothly with those of Eqs. (8) and (9) as R_B approaches its extremes.

III. Results

Equation (13) was used to plot $P(\epsilon)$ versus θ, with parameter P_T/N_0, for the PV'78 telemetry modes under consideration. For example, Figs. 1 to 4 compare the non-fading ($\gamma = 0$) and fading cases for uncoded and sequentially decoded systems, for $R_B = 256$ bps. For a given P_T/N_0; it is seen that $P(\epsilon)$ is convex $\cup$ over θ, implying an optimum modulation angle θ_{opt}; because these curves have broad minima, deviations of several degrees from θ_{opt} do not significantly alter system performance. Figures 3 and 4 introduce the computational capacity

$$C \equiv NR_B \text{ computations per sec (cps)} \tag{14}$$

the present DSS capability is $C \sim 25,000$ cps.

Current PV'78 telemetry design objectives are a maximum bit error rate of 10^{-3} in the uncoded case, and a maximum frame deletion rate of 10^{-3} in the coded case. Table 2 compares the minimum values of P_T/N_0 required to achieve these error rates at the corresponding optimum modulation angles θ_{opt} for the four PV'78 data rates R_B. It is shown that θ_{opt} is typically about 10° lower for the sequential decoding modes as compared with the uncoded modes. Also, the model predicts that atmospheric fading will cause a 0.6 to 0.7 dB loss in P_T/N_0 in the uncoded case, and a 1.1 to 1.3 dB loss in the coded case.

IV. Commentary

Although the results above, and Table 2 in particular, have an air of finality, it should be remembered that they are based on a theoretical model, the derivation of which required several approximations. For the moment, these results should be accepted only as rough performance predictions, with further refinements required from telemetry simulation tests.

One particularly weak link in the medium rate model that applies only to the sequential decoding case should be identified. It is generally valid that the instantaneous received signal-to-noise ratio $R(t)$ has the form of Eq. (6) in accounting for the log-normal fading and noisy carrier reference. What may be questionable is the hypothesis that the conditional probability of a frame deletion is characterized by the time average of $\sqrt{R(t)}$ over a *single* interval T_m, as denoted by the random variable α in Eq. (11), despite the fact that many individual decisions over widely varying time intervals are made in decoding a frame of received data. This argument is based on the precedent of Layland's medium rate model for the effects of a noisy carrier reference on sequential decoding performance (Refs. 5 and 6). If we accept the premise that a unique value of T_m exists for which the single time average model yields accurate results, we may still question whether T_m is correctly specified by the theoretical approximation of Eq. (5). When some telemetry simulation data are available, a more accurate model can be produced by discarding Eq. (5) and selecting T_m such that the model conforms to the experimental deletion rate behavior.

Table 1. $\{A_{n,r}\}$ for Helios data

r	n		
	-1	0	1
0	2.397	8.824	-0.9887
1	-0.5331	-6.788	1.569
2	0.02303	0.8848	-0.8543

Table 2. Required P_T/N_0 to achieve $P(\epsilon) = 10^{-3}$ at optimum modulation angle θ_{opt}, assuming no losses other than noisy reference and fading

R_B, bits/s	Uncoded case Bit error rate = 10^{-3} bits/s				Sequential coding Deletion rate = 10^{-3} bits/s			
	No fading		Log-normal fading		No fading		Log-normal fading	
	P_T/N_0, dB	θ_{opt}, deg	P_T/N_0, dB	θ_{opt}, deg	P_T/N_0, dB	θ_{opt}, deg	P_T/N_0, dB	θ_{opt}, deg
16	22.6	52	23.3	52	21.3	42	22.4	45
64	27.3	59	28.0	59	26.1	47	27.2	50
128	29.8	63	30.4	63	28.5	50	29.6	53
256	32.3	67	33.0	67	30.8	53	32.1	57
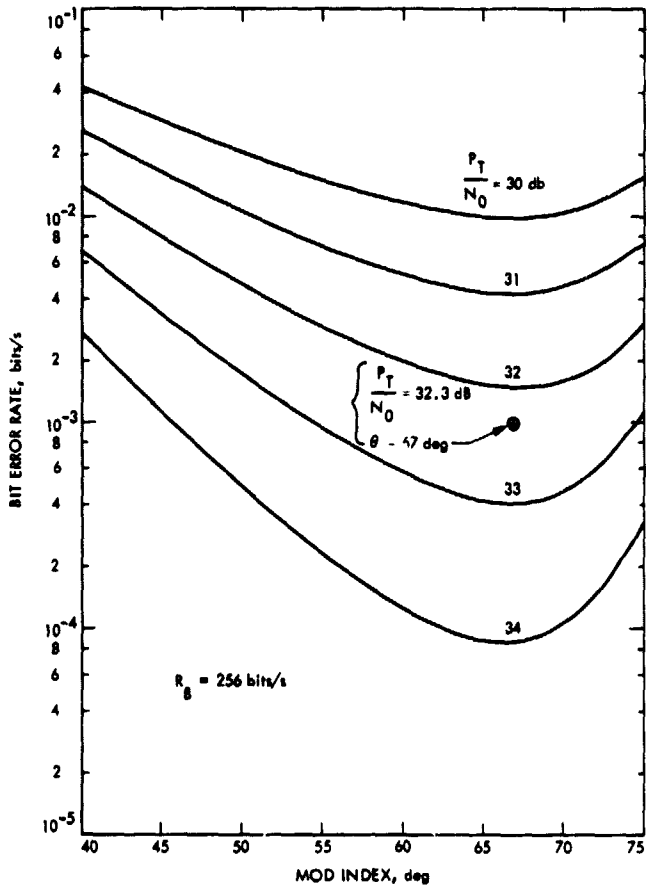
Fig. 1. Uncoded binary PSK, no fading
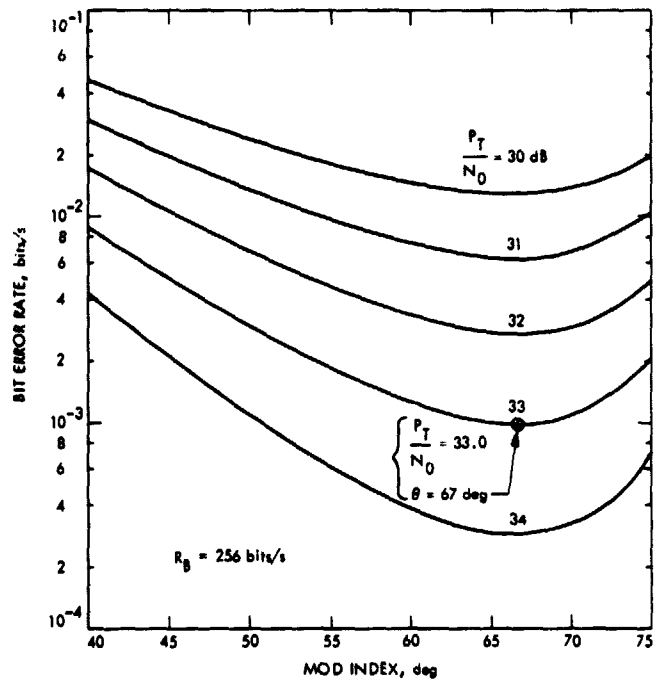
Fig. 2. Uncoded binary PSK, log-normal fading
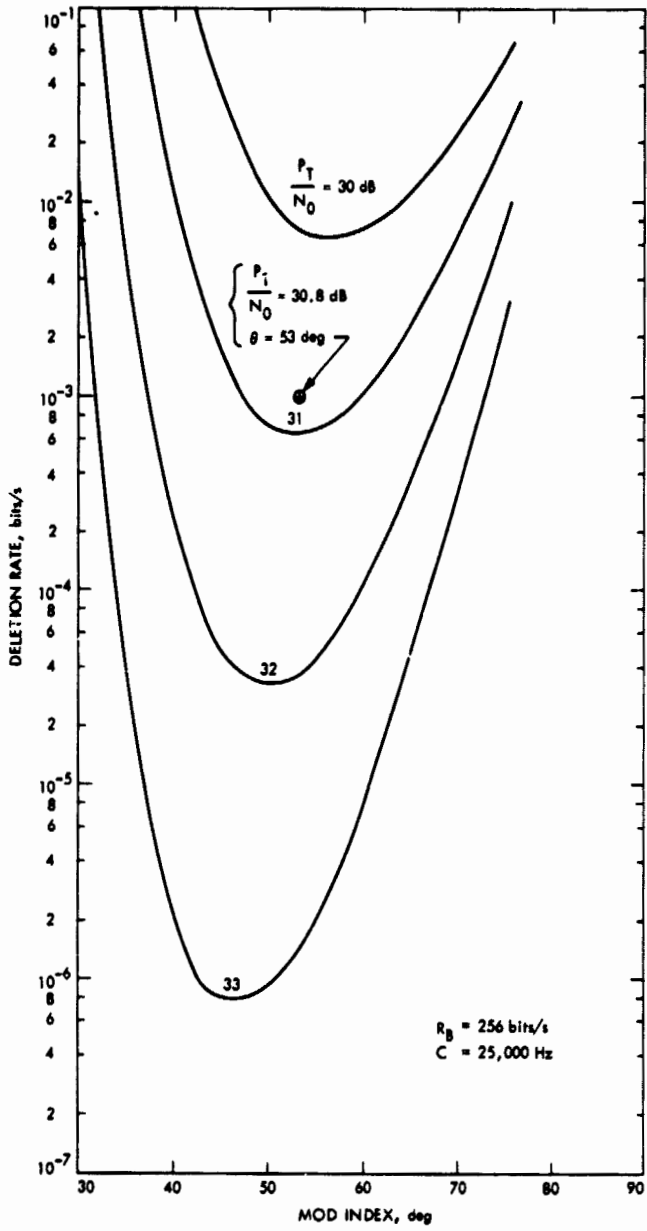
Fig. 3. Sequential decoding, no fading
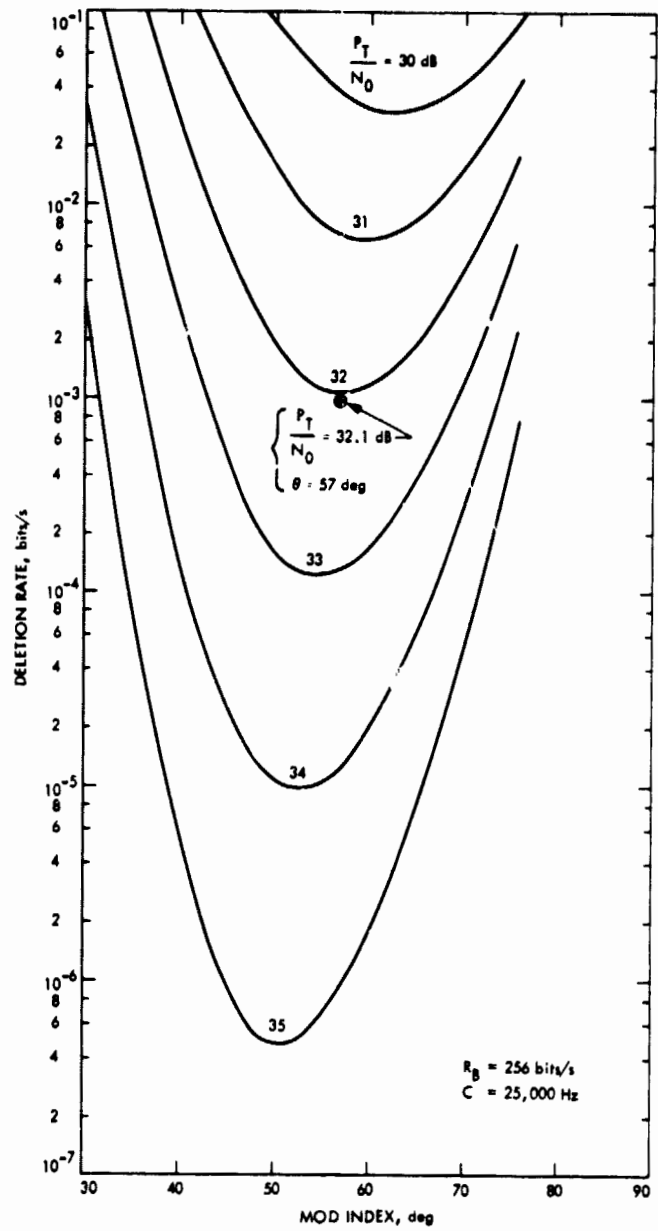
Fig. 4. Sequential decoding, log-normal fading

Appendix A

Linearized 2nd Order Phase-Locked Loop Preceded by a Bandpass Limiter in the Presence of Log-Normal Fading

This section documents approximate expressions used to compute the steady state phase jitter and noise bandwidth of a phase-locked loop receiver with log-normal channel fading.

Initially, suppose there is no fading. Linear phase-locked loop theory shows that the one-sided loop noise bandwidth B_L varies with the received signal-to-noise level (Ref. 7, Eqs. (5-18) and (8-14)):

$$B_L \cong K_1(r + \_) \qquad (A-1)$$

where

$$r \equiv K_2 \alpha_l \qquad (A-2)$$

and K_1 and K_2 are loop constants which need not be defined here. The limiter signal amplitude suppression factor α_l may be approximated by (Ref. 7, Eq. (8-13)):

$$\alpha_l \cong \sqrt{\frac{0.7854\eta_l + 0.4768\eta_l^2}{1 + 1.024\eta_l + 0.4768\eta_l^2}} \qquad (A-3)$$

in terms of the input signal-to-noise ratio

$$\eta_l = \frac{P_c}{N_0 B_l}$$

in the (fixed) limiter bandwidth B_l; P_c is the input power to the tracking loop, and N_0 is the one-sided input noise spectral density.

The tracking loop operating point is often defined in telemetry design control tables by the fictitious signal-to-noise ratio

$$\eta \equiv \frac{P_c}{N_0 2 B_{L_0}} \qquad (A-5)$$

The subscript 0 on B_L above, and on other loop parameters, traditionally denotes the threshold design point, defined to occur when $\eta = 1$:

$$P_{c0} = N_0 2 B_{L0} \qquad (A-6)$$

Using the threshold condition as a reference point, we can write

$$\eta = \frac{P_c}{P_{c0}} = \frac{\eta_l}{\eta_{l0}} \qquad (A-7)$$

$$\frac{B_L}{B_{L0}} = \frac{r_0 \left(\frac{\alpha_l}{\alpha_{l0}}\right) + 1}{r_0 + 1} \qquad (A-8)$$

Typically, B_l is sufficiently large that the tracking loop is operating in the limiter suppression region, $\eta_l \ll 1$. Also, $r_0 = 2$ in a DSS receiver. Then we have

$$B_L \cong \left(\frac{2\sqrt{\eta} + 1}{3}\right) B_{L0} \qquad (A-9)$$

The effective signal-to-noise ratio in the operating loop bandwidth is

$$\rho_L \equiv \frac{P_c}{\Gamma N_0 B_L} \cong \frac{6\eta}{\Gamma(2\sqrt{\eta} + 1)} \qquad (A-10)$$

where Γ is the limiter performance factor, which can be approximated by (Ref. 8, Eq. 21)

$$\Gamma \cong \frac{1 + \eta_l}{0.862 + \eta_l}; \qquad B_l > 10 B_L \qquad (A-11)$$

In the limiter suppression region we can write

$$\rho_L \cong \frac{5.172\eta}{2\sqrt{\eta} + 1} \qquad (A-12)$$

If ρ_L is large, the loop phase error $\phi(t)$ is essentially a zero-mean Gaussian random process with variance $\sigma_\phi^2 = 1/\rho_L$ (Ref. 7, Eq. (8-17)). For intermediate operating levels ($\rho_L > 3$), quasi-linear loop theory yields (Ref. 3, p. 84):

$$\sigma_\phi^2 = \frac{1}{\rho_L} \exp\left(\frac{\sigma_\phi^2}{2}\right) \qquad (A-13)$$

Now consider the effect of perturbing the system with log-normal channel fading. If the phase fading process

is sufficiently narrowband relative to B_L, as is expected for PV'78, it will be tracked by the phase-locked loop receiver. The degradation in the tracking loop performance then results from the lognormal amplitude fading process, $e^{x(t)}$ (Ref. 2, Eq. 2). Equations A-9 and A-12 are applicable to the fading case if η is replaced by the random process $\eta e^{2x(t)}$, wherein η is now regarded as the signal-to-noise ratio in the absence of fading:

$$B_L \cong B_{L0} \left[\frac{2\sqrt{\eta} e^{x(t)} + 1}{3} \right] \qquad \text{(A-14)}$$

$$\rho_L \cong \frac{5.172 \eta \, e^{2x(t)}}{2\sqrt{\eta} e^{x(t)} + 1} \qquad \text{(A-15)}$$

For a communication system employing binary PSK modulation, with modulation angle θ,

$$P_c = P_T \cos^2 \theta \qquad \text{(A-16)}$$

where P_T is the total received power in the modulated carrier. Then Eq. (A-5) is

$$\eta = \frac{P_T \cos^2 \theta}{N_0 \, 2B_{L0}} \qquad \text{(A-17)}$$

Equations (A-13) to (A-15) and (A-17) define the tracking loop performance in terms of the system parameters P_T/N_0, B_{L0}, and θ and the fading process $e^{x(t)}$.

Appendix B

Medium Rate Model

In the main text, it is shown that the effects of log-normal channel fading and a noisy carrier reference depend on the random variable (Eq. 11)

$$\alpha \equiv \frac{1}{T_m} \int_0^{T_m} dt \, e^{\chi(t)} \cos \phi(t) \tag{B-1}$$

The fading term $\chi(t)$ is a stationary Gaussian random process, with mean $m_\chi = -\sigma_\chi^2$ (Ref. 7), and power spectral bandwidth B_χ. For the PV'78 study, Woo established that $\sigma_\chi^2 = 0.014$ (Ref. 8, Eq. 14), and $B_\chi \sim 1$ Hz (Ref. 2, Fig. 3). As discussed in Appendix A, $\phi(t)$ is a non-stationary, zero-mean Gaussian random process, whose variance σ_ϕ^2 and bandwidth B_L depend on $\chi(t)$.

Typically, σ_ϕ^2 is small enough to warrant the approximation $\cos \phi(t) \cong 1 - \phi^2(t)/2$:

$$\alpha \cong \frac{1}{T_m} \int_0^{T_m} dt \, e^{\chi(t)} - \frac{1}{2T_m} \int_0^{T_m} dt \, \phi^2(t) \, e^{\chi(t)} \tag{B-2}$$

The first integral is the time average of $e^{\chi(t)}$ over the effective memory interval $(0, T_m)$, which can be approximated by the log-normal random variable e^γ (Ref. 3):

$$e^\gamma \cong \frac{1}{T_m} \int_0^{T_m} dt \, e^{\chi(t)} \tag{B-3}$$

where γ has the probability density function

$$P(\gamma) = \frac{1}{\sqrt{2\pi\sigma_\gamma^2}} \exp \left(-\frac{(\gamma - m_\gamma)^2}{2\sigma_\gamma^2} \right) \tag{B-4}$$

with

$$\sigma_\gamma^2 = \ln \left\{ 1 + \frac{2\sigma_\chi^2}{\beta_\chi^2} \left[\exp(-\beta_\chi) - 1 + \beta_\chi \right] \right\} \tag{B-5}$$

$$m_\gamma = -\frac{1}{2} (\sigma_\chi^2 + \sigma_\gamma^2) \tag{B-6}$$

$$\beta_\chi \equiv 2\pi B_\chi T_m \tag{B-7}$$

For PV'78, we are concerned with data rates above 16 bps, so that $T_m \gtrsim 1/8$ sec. Therefore, $e^{\chi(t)}$ varies slowly over $(0, T_m)$ such that $\sigma_\gamma^2 \approx \sigma_\chi^2$. On the other hand, if $2B_{L_0} = 12$ Hz and the tracking loop is operating sufficiently above threshold, B_L can be of the order of 50 Hz.

Thus $\phi^2(t)$ varies much more rapidly than $e^{\chi(t)}$. To approximate the second integral in Eq. (B-2), assume $e^{\chi(t)}$ is relatively constant over $(0, T_m)$, having the value of its time average e^γ:

$$\frac{1}{2T_m} \int_0^{T_m} dt \, \phi^2(t) \, e^{\chi(t)} \cong \frac{e^\gamma}{2T_m} \int_0^{T_m} dt \, \phi^2(t) \tag{B-8}$$

Over $(0, T_m)$, conditioned on e^γ, σ_ϕ^2 and B_L are given by

$$\sigma_\phi^2 = \frac{1}{\rho_L} \exp \left(\frac{\sigma_\chi^2}{2} \right) \tag{B-9}$$

$$\rho_L \cong \frac{5.172\eta \, e^{2\gamma}}{2\sqrt{\eta} \, e^\gamma + 1} \tag{B-10}$$

$$B_L \cong B_{L_0} \left(\frac{2\sqrt{\eta} \, e^\gamma + 1}{3} \right) \tag{B-11}$$

Define

$$\mu \equiv \frac{1}{\sigma_\phi^2 T_m} \int_0^{T_m} dt \, \phi^2(t) \tag{B-12}$$

The statistical behavior of the random variable μ has been determined (Ref. 2):

$$p(\mu|\gamma) = \begin{cases} \sqrt{\dfrac{a}{\pi\mu}} \exp \left(-a\mu - \dfrac{b}{\mu} + 2\sqrt{ab} \right); & \mu \geq 0 \\ \\ 0; & \mu < 0 \end{cases} \tag{B-13}$$

$$a = \frac{\beta_\phi}{4} \left(1 + \sqrt{1 + \frac{4}{\beta_\phi}} \right) \tag{B-14}$$

$$b = a + \frac{1}{4a} - 1 \tag{B-15}$$

$$\beta_\phi = \frac{\beta_L}{1 - \dfrac{1}{4\beta_L} [1 - \exp(-4\beta_L)]} \tag{B-16}$$

$$\beta_L \equiv 2B_L T_m \tag{B-17}$$

Now, we have

$$\alpha \cong e^\gamma \left(1 - \frac{\sigma_\phi^2 \mu}{2} \right) \tag{B-18}$$

References

1. Woo, R., et al., *Effects of Turbulence in the Atmosphere of Venus on Pioneer Venus Radio—Phase 1*, Technical Memorandum 33-644, Jet Propulsion Laboratory, Pasadena, Calif., June 30, 1973.

2. Levitt, B. K., and Rhee, M. Y., "Effects of Lognormal Amplitude Fading on Bit Error Probability for Uncoded Binary PSK Signalling," *The Deep Space Network Progress Report 42-21*, pp. 45–54, Jet Propulsion Laboratory, Pasadena, Calif., June 15, 1974.

3. Layland, J. W., *A Note on Noisy Reference Detection*, Technical Report 32-1526, Vol. XVII, pp. 83–88, Jet Propulsion Laboratory, Pasadena, Calif., Oct. 15, 1973.

4. Layland, J. W., "Sequential Decoding with a Noisy Carrier Reference," in *The Deep Space Network*, Technical Report 32-1526, Vol. XII, pp. 167–175, Jet Propulsion Laboratory, Pasadena, Calif., Dec. 15, 1972.

5. Layland, J. W., "A Sequential Decoding Medium Rate Performance Model," in *The Deep Space Network*, Technical Report 32-1526, Vol. XVIII, pp. 29–40, Jet Propulsion Laboratory, Pasadena, Calif., Dec. 15, 1973.

6. Layland, J. W., "A Model for Sequential Decoding Overflow Due to a Noisy Carrier Reference," to be published in the *Proceedings of the International Telemetering Conference* (ITC), held Oct. 15–17, 1974 in Los Angeles, Calif.

7. Tausworthe, R. C., *Theory and Practical Design of Phase-Locked Receivers, Vol. 1*, Technical Report 32-819, Jet Propulsion Laboratory, Pasadena, Calif., Feb. 15, 1966.

8. Tausworthe, R. C., "Information Processing: Limiters in Phase-Locked Loops: Correction to Previous Theory," in *Supporting Research and Advanced Development*, Space Programs Summary 37-54, Vol. III, Jet Propulsion Laboratory, Pasadena, Calif., Dec. 31, 1968.

Data Structure Design Guidelines

R. C. Tausworthe

DSN Data Systems Development Section

Proper modularization of software designs is more than mere segmentation of a program into subfunctions as dictated by control-logic topologies, as might be suggested by classical structured programming, wherein a limited number of program control-logic structures are permitted. Analyzing data connectivity between program segments can be far more complex than analyzing control flow, unless conscientious precautions are taken to avert this possibility. For this reason, data connectivity design should adhere to a discipline which minimizes both data and control-flow connections. This article discusses such considerations within a top-down, hierarchic, structured-programming approach to software design.

I. Introduction

As I shall be dealing with it, design is meant to be that activity which defines program data structures and logical algorithms in response to, and conforming with, a software functional specification. It consists of program organization, data manipulations, input/output (I/O) procedures, and the like, carried to a level of detail sufficient to serve as the working basis for coding and operational implementation. The basic elements required to effect a good program design are an understanding of the function to be served and the mechanisms available to carry out the job.

The data structure design guidelines I shall describe are prompted by what I call "top-down, modular, hierarchic, structured development of software." In doing a top-down, modular, hierarchic, structured design, one starts with an ¹-to-end overall definition of the program and analyzes i . . a number of component parts according to a set of u position rules. In terms of flowcharts, one starts with a single box that represents the entire program at the top hierarchic level, and expands that box into a flowchart at the next level, which displays the component subfunctions as a structured algorithm, in keeping with certain flowchart-topology rules.

Each of the subfunctions is given a precise end-to-end subspecification, some of which will be expanded into separate flowcharts at the next design level, and so on, until the final collection of subspecifications can be coded directly, without functional ambiguity. The American National Standards Institute (ANSI) standard (Ref. 1)

technique for depicting those submodules which are to be expanded by subsequent flowcharts is by "striping" that flowchart symbol on the parent flowchart. I will, therefore, refer to such submodules as striped submodules They are also referred to by others (Ref. 2) as stubs.

Such hierarchic decomposition identifies the programming process as a step-by-step decomposition of mathematical functions into structures of logical connectives and subfunctions which ultimately can be realized directly in the programming language to be used. Such a decomposition tends to channel detail into functional levels which aid human comprehension, and thereby, provides a way to control complexity in a disciplined, systematic way.

Certain flowchart topologies, or logical connectivities of the subfunctions, limited to iterations and nestings of a canonic-structured set (Ref. 2) have been shown (Ref. 3) to produce programs that are readable, understandable, codable, testable, maintainable, modifiable, and manageable. Control branching is entirely standardized so that the flowchart, accompanying narrative, and resultant code can be read from top to bottom without having to trace the branching logic in any intricate, convoluted way.

But proper modularization of software is more than just segmentation of a program into subfunctions as dictated by control-logic topologies. One may conceivably erase all the control flow lines from a flowchart and replace them by lines representing the data accesses instead, as a graphic way to identify operations on the data and to display data interconnectivity between executing modules. Such a chart would undoubtedly be convincing evidence that analyzing data connectivity can be far more complex than analyzing program control flow, unless conscious precautions are taken to avert this possibility.

For this reason, data connectivity design should, from the very first, be made to adhere to a discipline which minimizes module connections and organizes it into understandable units. Such a discipline, when coupled with structured control-logic design methods, offers the possibility of maintaining program clarity and correctness in both data flow and control flow.

II. Information, Data, and Storage Structures

A program operates on data. An information structure is a representation of the elements of a problem or of an applicable solution procedure for the problem; a data structure is a representation of the ordering and accessibility relationships among data items without regard to storage or implementation considerations; and a storage structure is a representation of the logical accessibility between data items as stored in a computer (Ref. 4). For example, in the vector-algebra problem $Ax = b$, the vectors x and b and the matrix A are information structures; when we agree to represent this problem in the form of dimensioned arrays $A(N,N)$, $X(N)$, $B(N)$, then A, B, and X become data structures; when we represent these in computer memory, as for example, by the mapping

$$location(A[I,J]) = location(A[1,1]) + N*(I-1) + J - 1$$

then this becomes the storage structure.

A data structure is generally specified as a set of data items (variables or constants), each typed (a) by a range of values (such as logical, integer, real, complex, double-precision, character, string, or an enumerated set of values) and (b) by a connectivity of items within the structure (such as are implicit in a linear list, stack, queue, deque, orthogonal array, tree, ring, or graph). Perhaps the simplest example of a data structure is a single integer-valued variable.

The data structures which one is apt to use most often depend on the facility with which the programming language to be used accommodates that structure. For example, FORTRAN accommodates integer, real, and complex data types in simple or array data structures. It is certainly possible in FORTRAN to create and manipulate a queue of string records as a data structure; but it is not as easy as it is in, for example, PL/1, where string variables and linked-list data structures are within the language repertoire.

A data structure also possesses another attribute having to do with when and where it is accessed in the program. This is its scope of activity (or merely, its scope). The scope of a structure extends from the earliest point in a program where information appears in that structure, until the latest point that structure is needed, either by the current module, or by another interfacing subsequent module. The structure is active whenever the program is executing within the scope of that structure. The scope need not be continuous. For example, an index variable for an iteration only is active during the iteration, and may be reused by other parts of a program once the iteration has been completed.

III. Data Structure Hierarchies

Dijkstra (Ref. 5) formulated the solution of a programming problem in terms of a set of "levels of abstraction," or concepts capable of being implemented (and interpreted) in many ways, but which were perhaps not fully understood at any particular stage of development. Later stages then provided refinement to each concept until the program was entirely complete. The use of abstractions provided a mechanism for hierarchic refinement by which it was possible to express those details that were known, and relevant at a particular time, and to defer for later refinement, those details which were not.

Hoare (Ref. 6) characterizes an abstract resource, such as a data structure, by three sets of such hierarchics: (1) the representation of the abstract resource, or a set of symbols which one may substitute for the physical aspects of the actual resource; (2) a set of manipulations which provide the transformation rules for representations as a means of predicting the effect of similar manipulations on the physical resources; and (3) a set of axioms which state the relationship and extent to which the physical properties of a resource are shared by their computer representation. The extent to which an abstraction leads to a successful program depends on the extent to which (a) the axioms describe the problem, (b) the axioms model the program behavior, and (c) the choice of a representation, with its manipulations, yields acceptable performance merits.

The way abstractions are formulated also greatly influences the extent and likelihood that a program will need major revision during the development process. This is the case because the nature of the data and the processing they require tend to influence the data structure design significantly. Premature representation of a data structure during design, when the needs of the structure are relatively unknown, leads to errors in judgement that may go undetected until too late for effective removal. The use of abstractions during design can postpone some of the decisions on data representation until a more appropriate time in the development.

IV. Levels of Access

Data structures to be used in a program are particularly well suited (Ref. 6) to being designed into levels of abstraction imposed by the hierarchic decomposition of program specifications. In the top-down method, the top-layer considerations are concerned with the problem, and deeper layers traverse the span to programming language.

The specification hierarchy for a data structure will thus begin with one fitting the needs of the problem and wind up with detail at the programming language level.

For example, suppose, in the upper layers of the design, that a module function may recognize the need for a "stack" to hold certain data. No more information is supplied at that level, not even the name, because no other interfaces appear. However, at some eventual hierarchic detailing of the module, the name will become important, as well as perhaps those functions which fetch and store data in the stack. Upon hierarchic expansion of these functions, more detail is needed about the stack, such as its size and the pointer to its top element. Eventually, the entire detail of the stack, down to the bit-by-bit machine configuration, will be specified in one form or another.

The hierarchy of definition thus describes the data structure in *levels of access*. At the top, the only access is through a vague notion of the data to be held; at deeper levels, the structure is accessed by name, then by increasingly more detailed operations, until, at the final level, the individual components are accessible. A level of access for a set of resources is defined as an interface through which all accesses to any constituent part of a resource must pass, except for those at deeper levels within the hierarchy.

Extending the example above, let us suppose that data at some level can be accessed in a stack by way of operations PUSH and PULL. Then let all accesses to the stack in the rest of the program, except for accesses within the access functions themselves, be made only via this level of access. Accesses to stack components within the PUSH-PULL functions have a deeper, more detailed level of access to the data structure. Then the access functions *own* the structure at each level of access.

The concept may be extended; suppose functions PUSH(*stack*) and PULL(*stack*) represent a level of access for a set of stack structures whose names can be substituted for the syntactic variable *stack* above. Again, the access functions own the set of stacks exclusively at that level of access in the sense that modules outside PUSH and PULL wishing to access a stack *must* do so only through these functions.

The general idea here is that a data structure (and, indeed, any resource) may be characterized by its levels of access as well as by the function it serves. Levels of access, then, can provide a conceptual framework for

achieving a clear and logical design. At the lowest level are the access functions for individual resource units, such as arithmetic registers, memory cells, file elements, etc. File elements are built into records by defining functions to process groups of file elements as a unit; records are built into files by defining functions to process groups of records as a unit; and so on, up the hierarchy. Each level supports an important abstraction of the hierarchic buildup of the resource.

Each access level consists of one or more externally accessible functions which share commonly owned resources. The connections in control and data among the various access modules induced by the top-down hierarchy are then limited in a natural way. Every resource used by a program will eventually be represented in a hierarchy whose levels map the needs of the problem into characteristics of the resource.

V. Data Design

As was indicated earlier, data-flow analysis is a natural tool for specifying what a program function is in terms of transformations of input data to the output wanted. In a design, which specifies how the computer is to implement these, it is useful to identify module interfaces to show the precedence of data creation and use among modules, and to promote understanding of the program interactions. For example, if data created in modules A and B are going to be further processed by module C, then the execution of A and B must precede C; if A and B do not share data, either may be executed first.

Data-flow diagrams depict the activity of a program module as reading certain input data structures and writing other output data structures according to predefined rules. Such diagrams can be every bit as useful as flowcharts, because they provide a means of attacking a problem in which questions of control, which at the early stages of design only tend to obscure the solution anyway, are secondary. They further provide a means to identify, and then to minimize, data-connections and side-effects among modules. They fit in with the top-down, hierarchic, modular, structured design discipline. They are eminently suitable as documentation to communicate the overall program organization. They identify the elements most important to the program mainstream, so that priorities and alternate operational modes can be established. In summary, data connectivity diagrams (data-flow charts), with their accompanying explanatory narrative, form another effective tool for the designer's bag.

Probably the most effective use of data-connection analysis will occur at the highest levels of the design. Then, as design progresses, data interconnectivity becomes more firmly established in the mind of the designer (and any reviewers), so graphic aids diminish in value. This is just the opposite of flowcharting, where the control at the top levels tends to be rather non-contributory to understanding, but becomes exceedingly more important at the deeper levels.

The data-connection guideline is the following: Design the control logic of a module so as to be independent of the way the data are structured whenever practicable, and modularize accesses to data structures so that if data are restructured at a later time (e.g., for more efficiency), only the access functions need be altered; organize submodules to minimize data interfaces whenever possible.

VI. Data Structure Design

Data structuring is primarily concerned with selection of type. Each programming language has certain elementary (unstructured) types, such as integers and reals, which form the basis of more extended, or structured, types. Then each new data structure typed is defined in terms of previously defined types, and there is a corresponding set of operations valid on that type.

The fundamental aspects of data structure design are: (1) deciding when to save data rather than regenerate them from the input, and (2) deciding how to store them when they are to be saved. Such decisions not only depend on the input data (type) but on the amount (e.g., to store in files versus core), their characteristics (e.g., sparse versus dense within the information structure), and the uses to which such data are to be put (e.g., predominance of comparisons versus updates). One important decision is the degree of packing to save space versus the lack of packing to save execution time. Other decisions have to be made concerning whether the data accesses are to be direct (i.e., accessed directly within the structure) or indirect (i.e., accessed indirectly through a surrogate structure of pointers).

The principal key to making such decisions is experience. No generalized guidelines can relate what data structure best fits the needs of specific problem. However, hierarchic abstraction does provide a generalized procedure for linking experience and expertise to the needs of the problem.

VII. Documentation of Data Structure Design

Another key toward effecting a good data-structure design, as well as promoting correctness in programming, is worthwhile documentation of the data structure. Such documentation can be organized in the same hierarchic levels of detail as emerged naturally in the design process. In fact, if the designer sets down the data design in this form from the beginning and maintains it throughout during the design process, then the documentation forms the vehicle for design.

Such documentation keeps track of the current state of the program requirements and all assumptions concerning its data structures, their levels of access, etc., up to the current phase. Moreover, programmers should be encouraged to make this hierarchic, top-down, concurrent documentation record not only the formal, definitive aspects of a structure, such as how the structure is formed and what its levels of access are, but also the more informal descriptive aspects of the problem, such as the rationale why the structure is defined the way it is.

The rationale of a program and its data structures is for the benefit of humans, not the computer. If this rationale is based on the hierarchic structuring of detail into increasingly refined levels of access, then humans can comprehend program complexity at each level by regarding the next lower level as a functional subunit.

Documentation also forms the basis for the assessment of program correctness, whether it be by formal proof, informal desk-checking, or testing the running program. In the next Section, I give guidelines relating to the level and content of documentation for data structures.

VIII. Data Structure Documentation Guidelines

The overall guideline which has governed the remainder of this section is the following: Documentation of each program submodule should exist to a sufficient degree that correctness can be assessed rigorously on the basis of its control logic and auditably for functional completeness.

To this end, I shall assume that the control logic for a given submodule has been specified completely (as structured programming does), so that module control is explicit, and therefore fulfills the guideline. For all decisions to be explicit and determinable within an individual submodule with no other aid than references to

preceding levels of the design, the unstriped (non-stub) subfunctions must give explicit settings to all control flag assignments. A striped (stub) subfunction at the current level which is specified to alter a control flag at a later level, but used at the current or prior level, must be accompanied by documentation which details explicit flag settings and the rationale for the setting.

Data structures accessed by unstriped submodules must be declared as to specific type attributes necessary for the intended programming language to access that structure without any ambiguity. Internal data structures accessed by striped modules, not pertinent to control logic or functional correctness, as specified above, may be detailed in later levels in the design. Further expansions of striped boxes successively provide more and more detail about the data structures and requirements involved. Specifically, each further detailing of a data structure definition must be made consistent with every previous assumption concerning its use as a minimum. The final, explicit form of a data structure definition should contain: (i) the structure name; (ii) its mnemonic derivation; (iii) type attributes (e.g., real, string/array variable, simple variable, etc.); (iv) range of values; (v) scope of activity (i.e., over what portions of the program the structure is not available for reassignment or reuse by other parts of the program); (vi) description of the use of the data structure in the program; and (vii) a list of any data structures which share storage with this structure.

Declaration, or declaration and initialization of a *new* data structure may appear as an entry requirement of the current submodule, to be performed in specified, previously defined modules. Such actions are documented by annotations to the flowchart and code for the current module; the actual declaration/initialization code is located within the specified modules (striped or unstriped), indented (if permitted by the programming language) to show that it is a later addition to that module (not contributing to nor detracting from the previous assessment of correctness) and annotated to indicate the later module which requires this initialization.

Data Structures may be referenced by striped modules in generic terms when not related to control-logic correctness. Assumptions made in such references must be consistent with the current state of the data structure definition. For example, a striped module may state that a set of characters is "put in the name table," whereas the unstriped submodule which implements that function must be specific, as "NPTR = NPTR + 1, NAME(NPTR) = N$",

in which NPTR, NAME, and N$ appear as appropriate detailed declarations in a Data Structure Definition Table.

A data structure referred to in generic terms, or any other way other than by its specific name, should have an entry in the software design document glossary, which then gives the actual structure name.

The current state of every data structure definition should be maintained in a Data Structure Definition Table in the software design document. This table either contains the definition or gives an explicit reference to defining material elsewhere in the design document. This table can be listed in alphabetic order for ease in locating structures referred to.

For readability, it is useful to provide the mnemonic derivation of all data-structure names used in a submodule unless such names have previously occurred in a direct ancestrial module. Names appearing in "cousin" sub-modules, unreferenced in their common ancestor should repeat the mnemonic derivation for ease in reading.

IX. Summary

The guidelines for data structure design are very highly influenced by the control-logic design and other design aspects of a program. I have indicated in this paper how the top-down, hierarchic, modular, structured-program approach is particularly well suited to effective data structure design because it permits the postponement of data-structure decisions until the requirements for a particular data representation are more concrete, when more is known about the program behavior and the characteristics of the data. Errors in judgement tend thus to be averted and easier to correct when detected.

References

1. *American National Standard Flowchart Symbols and Their Usage in Information Processing,* ANSI X3.5-1970, American National Standards Institute, Inc., Sept. 1, 1970.

2. Mills, H. D., *Mathematical Foundations of Structured Programming,* IBM Document FSC72-6012, Federal Systems Division, IBM Corp., Gaithersburg, Md., February 1972.

3. Baker, F. T., and Mills, H. D., "Chief Programmer Teams," *Datamation,* Vol. 19, No. 12, pp. 38–61, December 1973.

4. Robert, D. C., "File Organization Techniques," *Advances in Computers,* Vol. 12, Academic Press, Inc., New York, 1972.

5. Dijkstra, E. W., "Notes on Structured Programming," in *Structured Programming,* pp. 1–82, Academic Press, Inc., New York, 1972.

6. Hoare, C. A. R., "Notes on Data Structuring," in *Structured Programming,* pp. 83–174, Academic Press, Inc., New York, 1972.

High-Speed Data Throughput

J. P. McClure
DSN Data Systems Development Section

A study of inbound high-speed data (HSD) over a 25-week period shows an overall throughput of 99.46% from the DSSs. Of the faulty blocks, 19% contained bit errors and the remaining 81% were either not received or were not recognizable. Throughput performance is plotted on a weekly basis for each station.

As previously reported, the performance of the high-speed data circuits from the DSS to the JPL central communications terminal is continuously monitored by the GCF. The JPL Communications Processor (CP) records the monitor data and produces a weekly report detailing inbound HSD circuit performance for each tracking pass. These CP reports have been analyzed to determine HSD throughput. Throughput is defined as the percentage of transmitted blocks which are delivered error-free. The remaining blocks are either delivered with bit errors in them or are not delivered at all.

The period analyzed covers 25 weeks, February 18 through August 11, 1973. During this interval the DSN was principally engaged in the routine tracking of Pioneer 10 and the launch and tracking of Pioneer 11. All passes were tallied; hence the results presented herein represent normal GCF HSD performance.

The results of the analysis are shown in Table 1. The "Good" column is a count of error-free blocks delivered to the user. The "Error" column reflects blocks containing errors which were delivered. (The number of bit errors in each block is not known.) The "Out-of-lock" count occurred when a circuit failed between the DSS and JPL (the most prevalent cause) or when blocks could not be synchronized due to heavy errors. The performance of each station is shown, as well as the Ames-to-JPL circuits. The "All DSS" entry indicates the combined performance of all the DSSs shown.

Throughput for all of the DSSs was 99.465%. If DSS 51, the worst station from a transmission standpoint, is omitted the throughput increases to 99.607%.

The Goldstone stations, which are geographically close, have better than average throughputs, as one would expect. However, they are not much better. Goldstone's percentage of error blocks is much lower than the other stations. Combining these two characteristics leads to a recognized point—Goldstone has low block error rates. However, their circuit reliability is not markedly better. The Ames circuits, which are heavily used and fairly short, are generally comparable to the DSS circuits.

The tabulated data do not reflect the wide throughput variations which occur even on a weekly basis. Plots of throughputs for several stations are illustrated in Figs. 1 and 2. Significant drops in throughput are usually the result of a single extended outage during the week.

Table 1. HSD throughput, February–June 1973
(4800 bps, 1200 bit blocks, 203 data sets)

Location	Block count			Circuit hours	Throughput, %
	Good	Error	Out of lock		
DSS 11	7,979,318	1686	30,256	556	99.580
DSS 12	13,963,142	3553	31,227	972	99.752
DSS 14	13,466,668	2635	22,368	937	99.815
DSS 42	22,469,582	29,895	91,397	1569	99.463
DSS 43	9,830,033	13,882	26,184	685	99.594
DSS 44	5,568,608	10,280	24,166	398	99.385
DSS 51	19,222,892	35,339	203,600	1351	98.772
DSS 61	8,026,117	4212	14,859	559	99.762
DSS 62	12,283,789	13,719	52,342	857	99.465
DSS 71	1,347,357	942	1182	94	99.842
Ames	82,369,397	66,195	170,873	5737	99.713
All DSS	114,157,506	116,143	497,581	7978	99.465
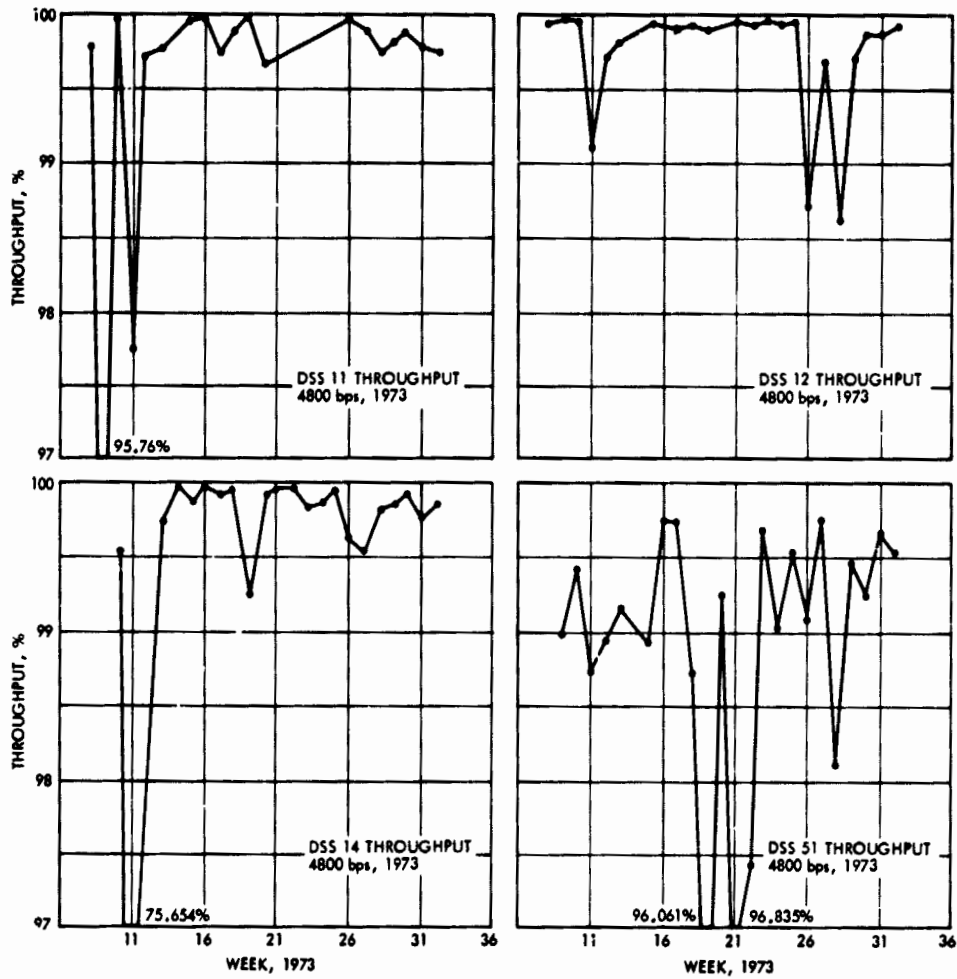
Fig. 1. High-speed data block throughput, at 4800 bps, 1200-bit blocks
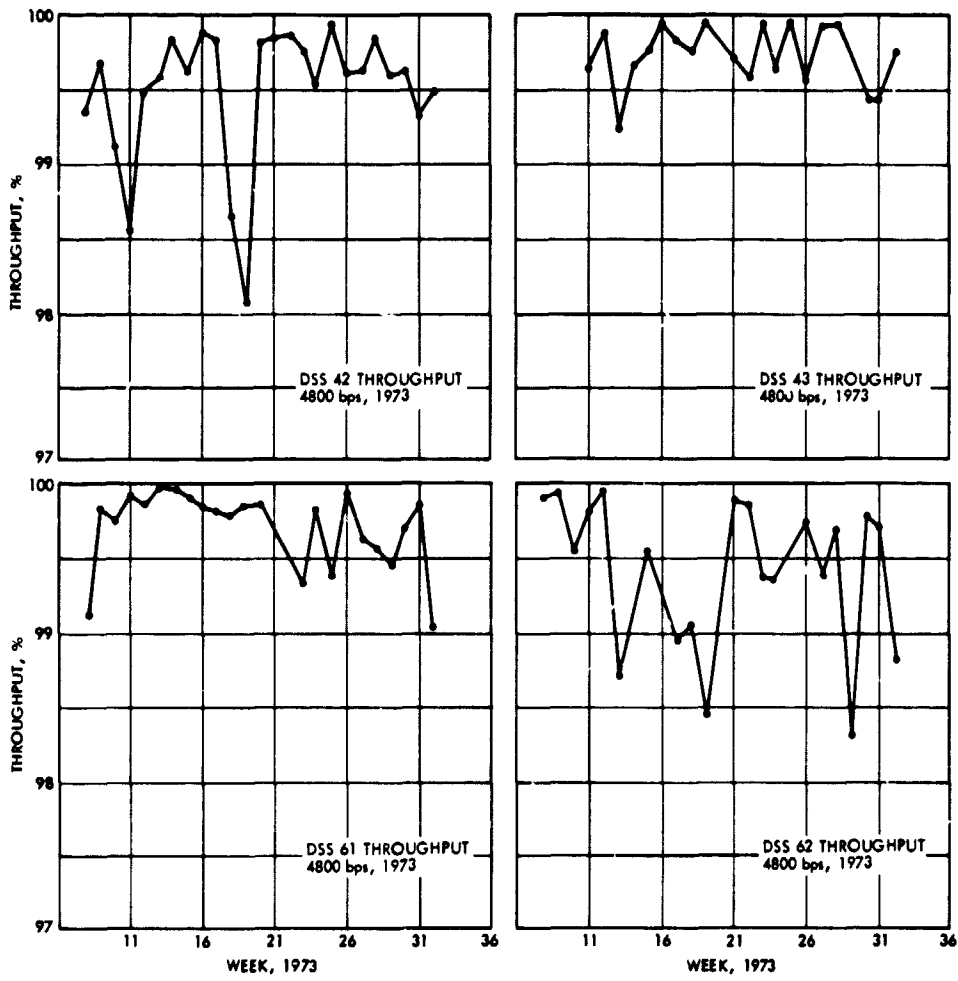
Fig. 1 (contd)

"Tutorial Input"—Standardizing the Computer/Human Interface

A. I. Zygielbaum
Communications Systems Research Section

This article describes a new technique for implementing a human/computer interface for computer-based subsystems for the DSN. Known as "tutorial input," this technique provides convenient short input procedures for the experienced operator and a helping hand for the novice. From the programmer's viewpoint, the technique is implemented in a compact, modular, easily modified table-driven structure. The technique has been successfully used through two generations of R&D ranging m. ..ines.

I. Motivation

Though much time is spent by programmers in producing efficient, clean, and ego-pleasing code, very little time is spent in developing an efficient, reliable human/computer interface. From an operational standpoint, this interface is the most important and least understood in DSN subsystem programming. With a view toward minimizing operator error and increasing subsystem efficiency, this article will present the technique for human/computer communication successfully used in two generations of R&D ranging systems.

In a typical subsystem program, the operator must provide operating parameters, critical times and perhaps limits to the software. Two interface techniques are generally used. With the first technique the operator may be queried on an input-by-input basis. For instance,[1]

---

[1] Computer typeouts are underlined.

ENTER T1: >
26

ENTER T2: >
15

ENTER T3: >
15

A second technique is the preset format wherein the operator must enter numbers in accordance with some specified template. An analogous entry to the one given above could be

*/26/15/15$

The first technique has the advantage that a format need not be memorized or followed. Given the parameters, an operator just follows directions. The disadvantage is that at the 10 characters per second of the usual tele-

typewriter, the questions sometimes waste an unacceptable amount of time. The second technique is clearly faster but requires a thorough a priori knowledge of the format. This leads to increased training time and a greater chance of operator error from misplaced fields.

Overriding the problems and tradeoffs inherent in these techniques is the multitude of programs involved in a typical DSN operation. An operator may have to communicate with a variety of programs, each designed with a different input philosophy and format. This situation naturally leads to an increased probability of human error.

In a real-time mission environment, an incorrect program entry can be just as disastrous as an equipment malfunction. A specific example occurred to ranging during the Mariner Mars 1971 (MM'71) mission. The software for command and telemetry running on the XDS 920 Telemetry and Command Processors (TCPs) used a dollar sign for a line terminator, whereas the software for the Mu ranging system used a carriage return. On at least two occasions, range data were lost because the operator typed a dollar sign at the end of an input line and walked away thinking his task complete. The ranging software waited the time-out period and then cancelled the necessary input. A simple modification to the software to allow it to recognize both a dollar sign and carriage return as a terminator saved a significant amount of data.

II. Proposal

Usually the subsystem operator is treated as a button-pusher who is taught to run specific software and devices. This view was believed incorrect, and software to support both the Mu-I and Mu-II ranging systems was developed with the direct cooperation and interaction of the operators. The input routine devised in this effort has been shown to be easy to learn as well as easy to operate. It uses a table-driven structure which makes it highly visible to the programmer who must implement it and relatively easy to modify and enlarge. This algorithm, known as "tutorial input," is presented here.

III. Tutorial Input as Viewed by an Operator

There are basically two parts to an input using the "tutorial" technique. First, a command is typed to designate the type of entry; second, the parameter or parameters are entered. For clarity, consider the commands used with the Mu-II system given in Table 1. (Parameter definitions are given in Table 2 for completeness.)

To input commands and data, the operator first notifies the PDP 11/20 that command input is desired by pressing an interrupt button (this could be a breakpoint on the XDS 9-series machines). When the machine responds with a pound sign (#) he types an input line terminated with a carriage return. The first field is a command followed by a slash (/). If the command is acceptable, the software looks to see if anything else is in the input line. If more characters have been typed, they are used. If not, the operator is queried by a specific message for the appropriate parameter of the now-active command. This is true every time a field containing a command or parameter has been used. If more characters are in the input line, they are processed; if not, and more parameters are required, the operator is queried.

The field delimiters used are a slash between a command and parameters and commas between multiple parameters. Note that the whole line is used. This allows commands to be entered contiguously.

The following are equivalent ways to initialize all ranging parameters:

Example 1:

   #A/ ⟩

   TOF ⟩

   #1200 ⟩

   SYN FREQ: ⟩

   # 44.01234 ⟩

   T1,T2,T3,TC: ⟩

   # 20,20,20,12 ⟩

   C1,C2,CN: ⟩

   # 4,19,3 ⟩

   MODE: ⟩

   # - ⟩

Example 2:

   #A/1200,44.01234,20,20,20,12,4,19,3,- ⟩

Example 3:

   #A/1200,44.01234,20,20,20 ⟩

   TC: ⟩

   #12,4,19 ⟩

   CN: ⟩

   #3,- ⟩

Example 1 shows how the operator can be led through the input parameters. In Example 2, an experienced operator has entered all parameters without software prompting. The operator in example 3, after losing his place, has let the computer request the remaining required numbers.

Multiple commands may be entered on a single line. In order to change the mode and number of components, for instance, one could enter

#M/124,C/3,10,50 ⟩

or

#M/124,C/ ⟩
C1,C2,CN: ⟩
#3,*,50 ⟩

The asterisk (*) entered for C2 causes the previous value of C2 to remain unchanged.

A further provision to ease the operator's task is error correction. Input cancellation (control R—R^c) results in immediately exiting the input routine. Character deletion (C^c) causes the program to type ← and results in the deletion of the last character entered into the string. Character deletion may be used more than once, e.g., to delete the last three characters so that they can be retyped. Line deletion (E^c) deletes the line, upspaces, types →, and allows the whole line to be retyped. Error correction can also be accomplished by use of the command to change a particular parameter.

IV. Tutorial Input as Viewed by a Programmer

Although written in machine language for a PDP-11/20, via the SAPDP Xerox Sigma 5 cross assembler (Ref. 1) the routine is amenable to coding in another machine language or in a higher level language such as BASIC or FORTRAN. In this discussion the interaction of the input rou...ne with other real-time processors will not be covered. The Mu-II software required interfaces to a teletype output routine and to a real-time scheduler. These topics will be documented in a forthcoming article on the Mu-II system software.

Though perhaps not meeting the letter of structured programming, which is difficult, if not impossible, in a real-time environment, tutorial input does realize all advantages normally claimed for structured programming. Through the use of a table-driven technique, the input

sequencing and programming is straightforward, easily modified, and simply documented.

The technique involves two tables. The first table is the command list. Each entry in the list takes three words in the Mu-II realization. There is one entry for each command. The first word has the two characters of the command, e.g., "A/" or "TF," the second a pointer to a word in the second table, and the third word a number equal to the number of parameters to be entered with the particular command.

The second table is the parameter list. Each entry in this list takes four words. There is one entry for each parameter. The first word of the entry contains the number of characters in the message associated with each parameter, while the second contains the message location. (The messages are the queries shown earlier, e.g., TOF: ⟩.) The third word gives the location of the decoding subroutine (integer, floating point, etc.) to convert the parameter's ASCII character string to binary. The fourth and final word contains the location of the destination for the binary number. Figure 1 contains a listing of the two tables in the Mu-II software.

The algorithm which interprets these tables is described structurally in Fig. 2 and in a detailed flow chart in Fig. 3.

As an example of the algorithm, let us consider that a command "T/" has been input and follow the algorithm operation. Scanning the command list (Fig. 1), a match is found (line 334) giving the parameter table location as SCT1 and the number of parameters to be input as four. The program looks to see if there are any more characters in the input string. If not, the message TMSG, containing 14 characters, is typed as shown by the SCT1 entry in the parameter list. If input already exists, the message is skipped. In either case, the input parameter is processed by INGR which is the integer decoding subroutine and the result stored in IT1.

Thus far, one parameter has been processed and three more are left. The program proceeds directly to the SCT2 entry in the parameter table and repeats the input process. This continues until all parameters are entered.

Once again the algorithm checks to see if there are more characters in the input stack. If there are none, the routine exits. If there are more, the first field is used to search the command stack as the program assumes that another command is in the input string. The process goes on until an error occurs or until the input line is exhausted.

The input logic flow is readily observable by following the driving tables. The tables are also a simple documentation of the input sequences. The ease with which commands and entries can be modified or deleted is shown by a program change that occurred during the Mariner Venus/Mercury 1973 (MVM'73) mission.

As originally written, an operator could modify any parameter or set of parameters individually except for time of flight (TOF). The only way to change this parameter was through the "enter all parameters" A/ command. As the mission proceeded, the TOF changed by several seconds each day. It was obvious that going through the entire initial ation sequence to change TOF was a waste of time The decision was made to add the TF/ command so that TOF could be changed individually.

Because of the table-driven structure, only three cells were actually needed. These were, from Fig. 1, lines 346–348:

"TF"	Command
SCTOF	Parameter Table Pointer
1	Number of parameters to be entered.

This simple modification changed a tedious operation into a trivial one.

V. Summation

Data will continue to be lost due to incompatibilities, indeed contradictions, between input formats in various DSN software systems. This coupled with the trend toward smaller station operational crews, automation, and the continued proliferation of minicomputers in the DSN makes standardization increasingly important. The algorithm presented herein is a candidate to aid in that task.

A final comment, tutorial input has been used in ranging software throughout the MVM'73 mission. It has shown itself to be an easy-to-use as well as an easy-to-learn input technique. The extra time taken to interact with experienced ranging operators during its development has been paid back many fold through simplified training and the low probability of human error. This programming effort clearly shows the value of bringing the system operators into the software design process at a very early stage. Many times the operators were able to point out features which were not helpful and could be discarded as well as request features which would simplify their task. The success of the Mu-II system programming is largely due to this cooperation between the programmer and the system operators.

Reference

1. Erickson, D. E., "The SAPDP Program Set for Sigma 5 Assembly," in *The Deep Space Network Progress Report*, Technical Report 32-1526, Vol. VII, pp. 91–96, Jet Propulsion Laboratory, Pasadena, Calif., Feb. 15, 1972.

Table 1. Mu-II commands

Command	Parameter to be entered
A/	All operational parameters: TOF, SYN FREQ, T1,T2,T3,TC,C1,C2,CN,MODE
TF/	TOF
C/	C1,C2,CN
T/	T1,T2,T3,TC
S/	SYN FREQ
M/	MODE
Z/	Requested TØ time
Y/	Typewriter printout ON/OFF: i.e., Y/ON Y/OFF

Table 2. Parameter definitions

Abbreviation	Meaning
TOF	Round-trip light time
SYN FREQ	Exciter synthesizer frequency
T1	First component integration time
T2	Lower-frequency components integration time
T3	Post-acquisition DRVID integration time
TC	10-MHz calibration integration time
C1	Highest-frequency component
C2	Lowest-frequency component
CN	Number of post-acquisition DRVID points before automatic reacquisition
MODE	Select configuration (i.e., Block III or IV receiver phasing, reacquisition with or without coder sync, etc.) "-" results in standard configuration
TØ	Coder synchronization time

```
326*                                         PAGE
327*                                    *COMMAND LIST
328*    01 00782 2   C1         A    CONSCAN BYTE    8:301:,8:257:   A/
        01 00782 3   AF         A
329*    01 00783     1EFA       N            WORD   SCTOF
330*    01 00783 2   000A       A            WORD   10
331*    01 00784     C3         A            BYTE   8:303:,8:257:   C/
        01 00784 1   AF         A
332*    01 00784 2   1F2A       N            WORD   SCC1
333*    01 00785     0003       A            WORD   3
334*    01 00786 2   D4         A            BYTE   8:384:,8:257:   T/
        01 00785 3   AF         A
335*    01 00786     1F0A       N            WORD   SCT1
336*    01 00786 2   0004       A            WORD   4
337*    01 00787     D3         A            BYTE   8:323:,8:257:   S/
        01 00787 1   AF         A
338*    01 00787 2   1F02       N            WORD   SCSYNF
339*    01 00788     0001       A            WORD   1
340*    01 00788 2   DA         A            BYTE   8:332:,8:257:   Z/
        01 00788 3   AF         A
341*    01 00789     1F4A       N            WORD   SCTO
342*    01 00789 2   0001       A            WORD   1
343*    01 0078A     _D         A            BYTE   8:315:,8:257:   N/
        01 0078A 1   AF         A
344*    01 0078A 2   1F42       N            WORD   SCMOE
345*    01 0078B     0001       A            WORD   1
346*    01 0078B 2   D4         A            BYTE   8:324:,8:306:   TF
        01 0078B 3   C6         A
347*    01 0078C     1EFA       N            WORD   SCTOF
348*    01 0078C 2   0001       A            WORD   1
349*    01 0078D     D9         A    CONEND  BYTE   8:331:,8:257:   Y/
        01 0078D 1   AF         A
350*    C1 0078D 2   1F52       N            WORD   TYCMD
351*    01 0078E     0001       A            WORD   1
352*                                         PAGE
353*                                   *PARAMETER LIST
354*    01 0078E 2   0006       A    SCTOF   WORD   6
355*    01 0078F     1F5A       N            WORD   TOFMSG
356*    01 0078F 2   1BF0       N            WORD   INGR
357*    01 007C0     2872       N            WORD   ITOF
358*    01 007C0 2   030E       A    SCSYNF  WORD   14
359*    01 007C1     1F60       N            WORD   SYNFMSG
360*    01 007C1 2   1C3E       N            WORD   INDPFP
361*    01 007C2     2874       N            WORD   ISYNF
362*    01 007C2 2   000E       A    SCT1    WORD   14
363*    01 007C3     1F6E       N            WORD   TMSG
364*    01 007C3 2   1BFC       N            WORD   INGR
365*    01 007C4     2864       N            WORD   IT1
366*    01 007C4 2   0006       A    SCT2    WORD   6
367*    01 007C5     1FB0       N            WORD   T2MSG
368*    01 007C5 2   1BF0       N            WORD   INGR
369*    01 007C6     2866       N            WORD   IT2
370*    01 007C6 2   0006       A    SCY3    WORD   6
371*    01 007C7     1FB6       N            WORD   T3MSG
372*    01 007C7 2   1BF0       N            WORD   INGR
373*    01 007C8     2868       N            WORD   IT3
374*    01 007C8 2   0006       A    SCTC    WORD   6
375*    01 007C9     1FBC       N            WORD   TCMSG
376*    01 007C9 2   1BF0       N            WORD   INGR
377*    01 007CA     286A       N            WORD   ITC
378*    01 007CA 2   000E       A    SCC1    WORD   14
379*    01 007CB     1F7C       N            WORD   CMSG
380*    01 007CB 2   1BF0       N            WORD   INGR
381*    01 007CC     286C       N            WORD   IC1
382*    01 007CC 2   0006       A    SCC2    WORD   6
383*    01 007CD     1FC2       N            WORD   C2MSG
384*    01 007CD 2   1BF0       N            WORD   INGR
385*    01 007CE     2862       N            WORD   IC2
386*    01 007CE 2   000C       A    SCCN    WORD   6
387*    01 007CF     1FC8       N            WORD   CNMSG
388*    01 007CF 2   1BF0       N            WORD   INGR
389*    01 007D0     286E       N            WORD   ICN
390*    01 007D0 2   000A       A    SCMDE   WORD   10
391*    01 007D1     1F8A       N            WORD   MMSG
392*    01 007D1 2   1CC0       N            WORD   INMDE
393*    01 007D2     2870       N            WORD   IMDE
394*    01 007D2 2   000E       A    SCTO    WORD   14
395*    01 007D3     1F94       N            WORD   TOMSG
396*    01 007D3 2   1D6C       N            WORD   INTO
397*    01 007D4     288C       N            WORD   ITO
398*    01 007D4 2   000E       A    TYCMD   WORD   14
399*    01 007D5     1FA2       N            WORD   TVMSG
400*    01 007D5 2   1C92       N            WORD   CNTRL
401*    01 007D6     287C       N            WORD   ITYSWT
```

Fig. 1. Mu-II software listing

```
Command, IF command request DO.

        Save current parameters.

        Input line.

        DO UNTIL input stack empty.

                Separate next input field.

                Search command table for match.

                IF NOT match.

                        Notify operator.

                        EXIT command.

                ELSE.

                        Location — command table (match +1).

                        Count — comn...nd table (match +2).

            Parameter, DO UNTIL count = 0.

                If input stack NOT EMPTY.

                        Separate next input field.

                ELSE

                        Print parameter table (location) characters from
                            string addressed by parameter table (location +1).

                        Input line.

                Location — location +2.

                DO SUBROUTINE addressed by parameter table (location).

                Location — location +1.

                Store result in parameter addressed by parameter table (location)

                Location — location +1.

                Count — count −1

            END

        END

END
```

Fig. 2. Structured representation
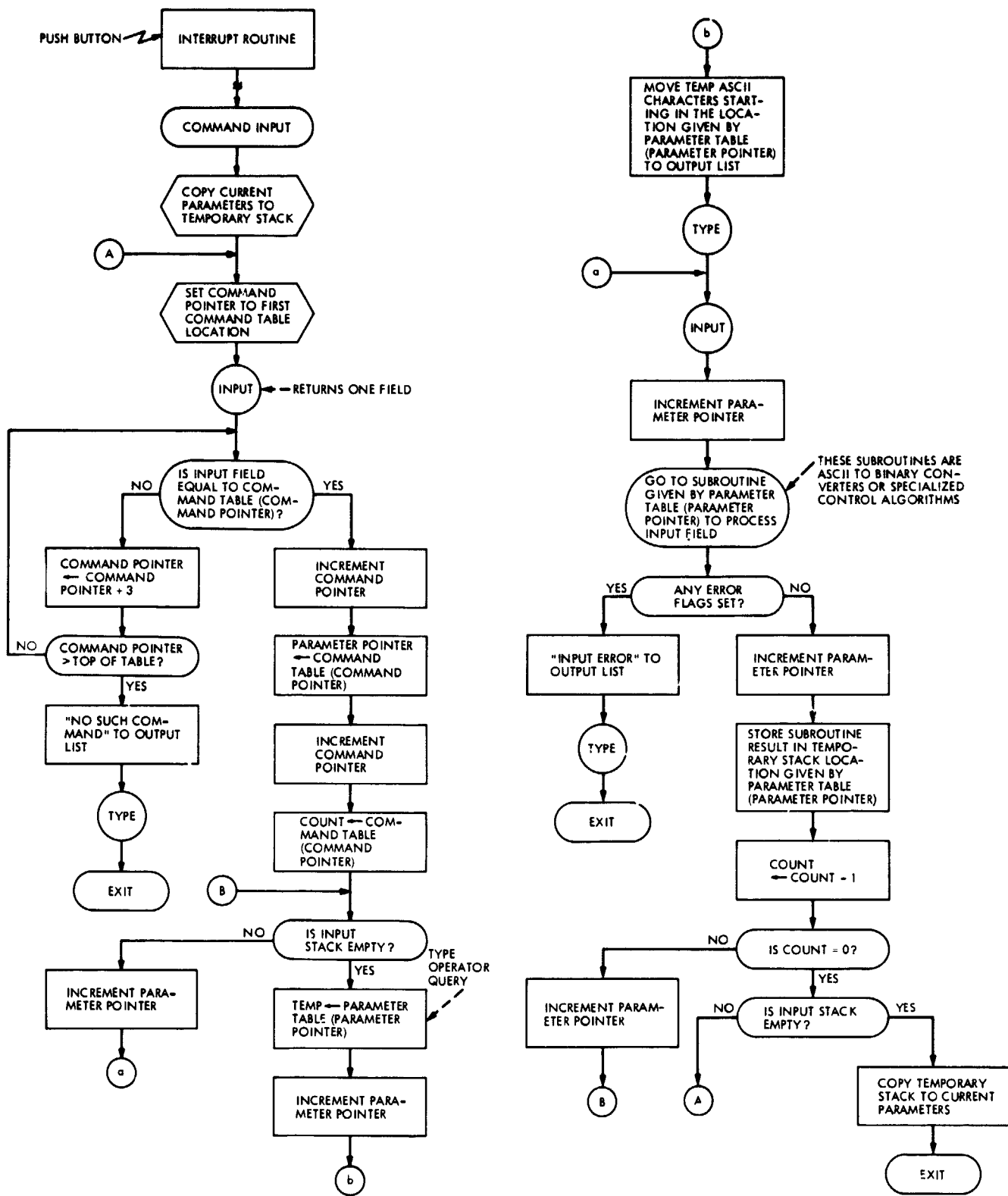
Fig. 3. Tutorial input schematic flowchart (Mu-II realization)
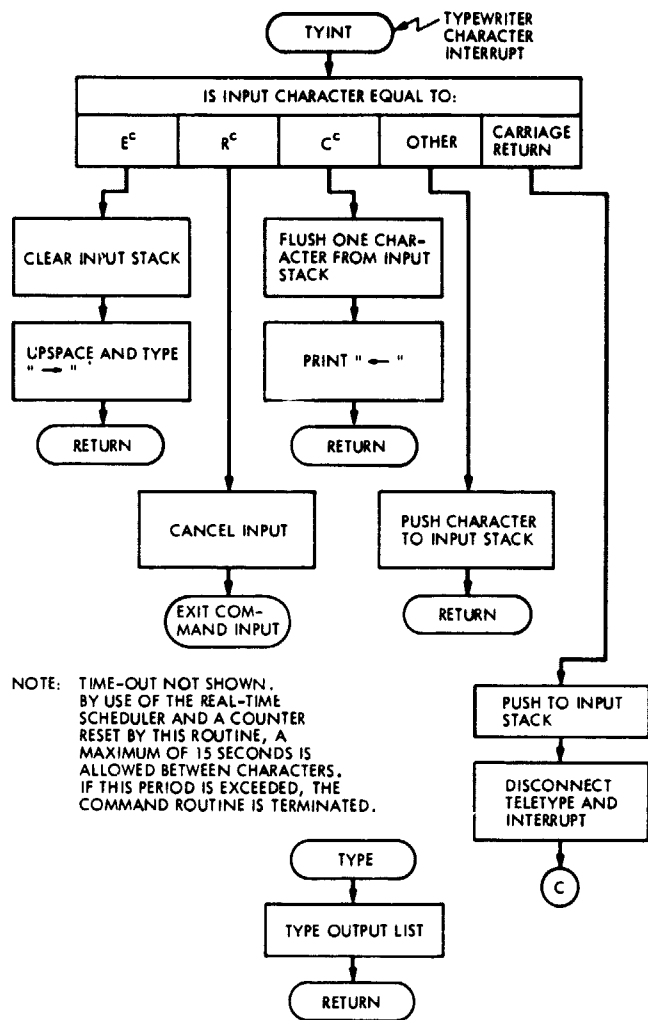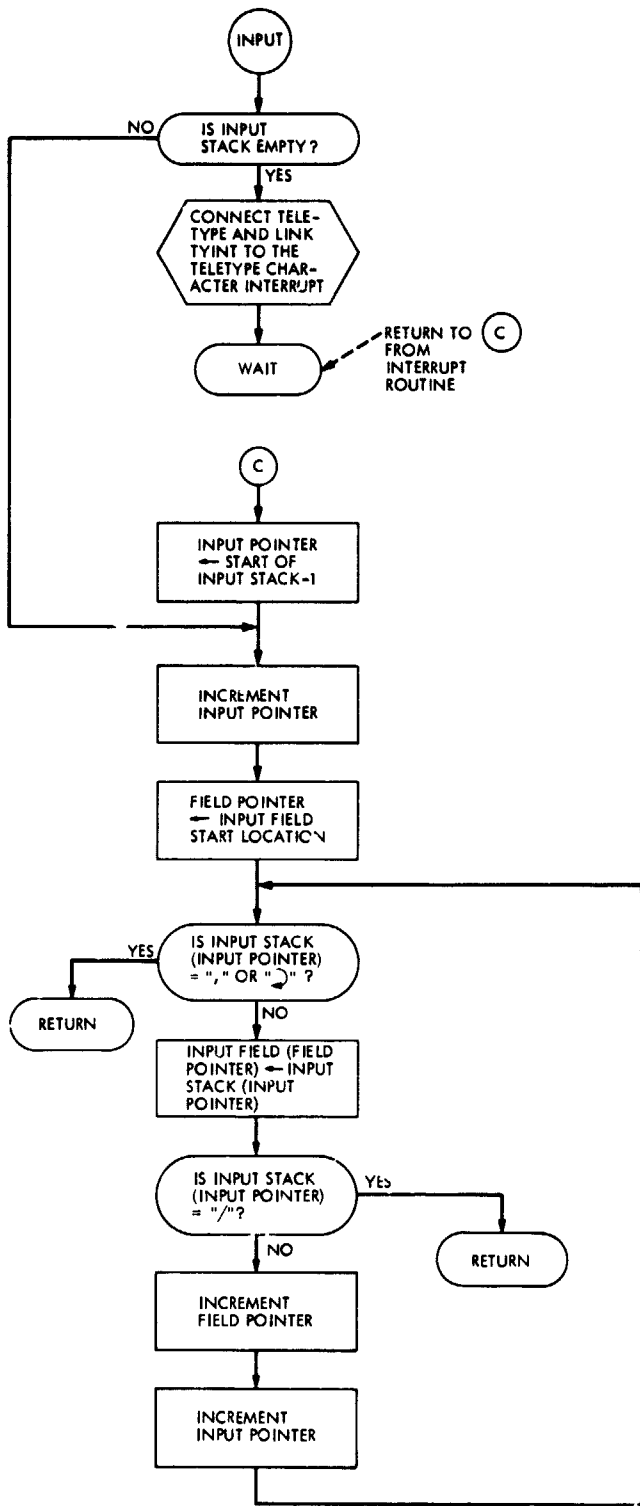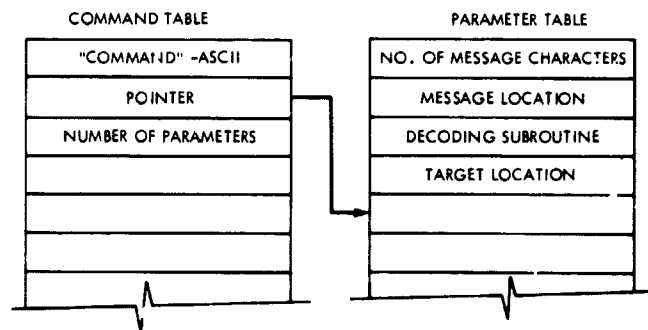
Fig. 3 (contd)

Helios Spin-Modulation Doppler Effects

N. C. Ham

DSN Engineering Section

It is predicted that the spin-stabilized Helios spacecraft when communicating via its low-gain antenna to the deep space stations of the Deep Space Network will affect the observed radio frequency doppler signal which is normally only a function of the spacecraft-to-Earth radial velocity. The effect is due largely to the spin modulation created by the spacecraft rotation and the right-circularly-polarized element of the spacecraft antenna system that is physically offset several radio frequency wavelengths from the rotational axis. The discussion develops the expected effects to the general doppler equation, and expressions for the resultant one-way uplink and downlink and two-way coherent doppler frequency cases are presented.

I. Introduction

The effects on the doppler frequency induced from the spin modulation generated by the Helios spacecraft rotating low-gain antenna (LGA) will be discussed, and equations expressing the resultant effects will be developed for the one-way, uplink and downlink, and two-way coherent doppler cases.

A spacecraft traveling at a radial velocity v_R away from the ground transmitter will receive the transmitted RF signal changed by this velocity (Fig. 1). If D is the instantaneous distance between the transmitter and spacecraft, the total number of RF wavelengths λ contained in this one-way uplink path is $n_\lambda = D/\lambda$, and since there are 2π radians angular excursions of the phase angle γ per wavelength, the total number of these angular excursions made by the transmitted wave is $\gamma = 2\pi D/\lambda$.

With the spacecraft in motion, D and the phase γ are changing, and the change in γ with respect to time is frequency and is the doppler angular frequency ω'_D given by

$$\omega'_D = 2\pi f'_D = \frac{d\gamma}{dt} = \frac{2\pi \, dD/dt}{\lambda} = \frac{2\pi v_R}{\lambda}$$

(1)

II. Rotating Spacecraft With Offset LGA for Uplink Case

Consider now the case of a spacecraft rotating at an angular rate ω_r (approximately 1 revolution per second) containing a right-circularly-polarized (RCP) horn antenna displaced physically approximately 6λ from the spin axis z, as is the Helios spacecraft (Fig. 2). The effect of the

uniformly rotating offset antenna is equivalent to varying a distance cyclically about D, or $D + \Delta D$, where ΔD varies sinusoidally along the velocity path; thus $D = D' - (\sin \psi \, 6\lambda) \cos \omega_r t$, where ψ is the aspect angle formed by the spacecraft–Earth line and the spacecraft spin axis, and D' is the mean distance. Equation (1) now becomes:

$$\omega_D = \frac{2\pi}{\lambda} \frac{d}{dt} [D' - (\sin \psi \, 6\lambda_{RCV}) \cos \omega_r t]$$

$$= \frac{2\pi}{\lambda} \left[\frac{dD'}{dt} + (\sin \psi \, \omega_r \, 6\lambda_{RCV}) \sin \omega_r t \right]$$

where $6\lambda_{RCV}$ is the displaced value of the horn antenna in wavelengths, at the spacecraft receive frequency, or

$$\omega_D = \frac{2\pi}{\lambda} \left[v_R + (\sin \psi \, \omega_r \, 6\lambda_{RCV}) \sin \omega_r t \right], \text{rad/s} \tag{2}$$

The doppler angular frequency, related to the ground transmitted RF angular frequency $\omega_{T, GRD}$, is

$$\omega_D = \omega_{T, GRD} \left[\frac{v_R + (\sin \psi \, \omega_r \, 3\lambda_{RCV}) \sin \omega_r t}{C} \right] \tag{3}$$

where $\lambda = C/f$, and C is the velocity of propagation.

An additional factor results from the rotating RCP horn antenna when receiving the transmitted wave. The orientation of the antenna E plane vector rotates through 360 deg at the rotational rate ω_r and results in an additional angular frequency component of approximately 1 rad/s, adding to or subtracting from the carrier angular frequency depending upon the rotational sense of the spacecraft (Ref. 1). For the Helios case, the resultant carrier is less by the value of ω_r. If the transmitted wave were left-circular-polarized, the transmission efficiency would be low, and the received signal level would be greatly attenuated (Ref. 2) relative to RCP, with the rotational component now appearing additive.

Therefore, the resultant spacecraft received angular frequency is comprised of three components which modify the ground transmitted frequency: the doppler angular frequency related to spacecraft–Earth radial velocity, a bias angular frequency equal to the spacecraft angular rate due to the rotating RCP antenna, and a cyclic deviating angular frequency (about the resultant of two above components) also occurring at the spacecraft angular rate with the deviation magnitude related to the antenna displacement and aspect angle.

The spacecraft received signal, considering all of the components becomes

$$\omega_{R, S/C} = \omega_{T, GRD} \left[1 + \frac{v_R + (\sin \psi \, \omega_r \, 6\lambda_{RCV}) \sin \omega_r t}{C} \right]$$

$$- \omega_r, \text{rad/s} \tag{4}$$

which is the resultant received one-way uplink case, and these doppler components are illustrated in Fig. 3.

III. Downlink Received Signal

By reciprocity, similar results are observed at the ground receiver when receiving a signal transmitted by the spacecraft in a one-way downlink configuration, i.e.,

$$\omega_{R, GRD} = \omega_{T, S/C} \left[1 + \frac{v_R + (\sin \psi \, \omega_r \, \frac{240}{221} \, 6\lambda_{RCV}) \sin \omega_r t}{C} \right]$$

$$- \omega_r, \text{rad/s} \tag{5}$$

where the physical horn antenna displacement in wavelengths is approximately greater by 240/221 at this frequency.

IV. Two-Way Coherent Doppler

The next configuration to consider is that of the two-way coherent mode. The physical rotation of the spacecraft with a displaced RCP antenna can be considered as an equivalent angular frequency generator additive circuit to the transmitted carrier angular frequency. The generator frequencies are the angular rate of the spacecraft, which frequency deviates the carrier at a deviation proportional to the horn displacement and aspect angle, the bias signal proportional to the spacecraft angular rate, and the doppler angular frequency component proportional to the radial velocity and transmitted frequency.

The transponder functions to coherently transform the resultant spacecraft received angular frequency by a constant factor 240/221 and transmit this signal through the same rotating RCP horn antenna to the ground receiving system. However, in addition, a delay ζ occurs in the transponding process. This delay is to the carrier frequency (phase delay ζ_γ) and the modulation (or group delay ζ_g) which can be influenced by the spacecraft thermal temperature, received signal level and resultant signal-to-noise ratio.

The carrier phase delay variation is assumed to be small during a normal DSS tracking period such that $d\zeta_\gamma/dt << d\gamma/dt$ and should not alter the doppler frequency, as expressed by Eq. (1).

The group delay ζ_g is a factor only if it becomes a significant value, since this would have the effect of effectively shifting the horn antenna for the downlink signal to a lagging angle relative to the actual horn antenna location receiving the uplink signal.

Equation (4) is the expression for the received signal appearing at point A of Fig. 4, and the transpond ratio and group delay ζ_g modifying this to give the expression at point B as,

$$\omega_{T,s/c} \cdot \frac{240}{221}\left(\omega_{T,GRD}\left[1 + \frac{v_R + (\sin\psi\,\omega_r\,6\lambda_{RCV})\sin(\omega_r + \zeta_g)t}{C}\right] - \omega_r\right), \text{rad/s} \tag{6}$$

The result of a signif::ant apparent lag angle is that the frequency deviation component cyclic zero crossing (Fig. 3) as a function of time would be the vector sum of the contributing uplink and downlink angular modulating signals. Fortunately, the group delay at 1 Hz will probably be very low through the transponder circuits so that the effective horn location for downlink will be coincident with the uplink horn location and preserve any reference to the spacecraft frame structure.

Progressing further through the system configuration, the rotating offset horn antenna has the effect of varying ΔD about the mean distance D to the downlink signal with effects similar to those of the uplink signal.

A study of Eqs. (4) and (5) for the uplink and downlink received signals reveals that the values of the velocity, frequency deviation, and bias components are not dependent upon the signal amplitude, or the characteristics of the antenna gain patterns, for either link case. Specifically the coefficient to the frequency deviation components is proportional to the sine function of the aspect angle. Thus, in this two-way coherent mode, dissimilarity in the antenna gain patterns at a given aspect angle is incidental to the value of this component.

The overall doppler signal $\omega_{D,TOTAL}$ can be found by the comparison of the ground transmitted signal to the ground received signal. The general equation for this overall two-way doppler condition is expressed as

$$\omega_{D,TOTAL} = \frac{240}{221}\omega_{T,GRD} - \frac{240}{221}\omega_{T,GRD}\left(1 + \frac{2v_R'}{C}\right) - \frac{240}{221}\omega_r\left(1 + \frac{v_R'}{C}\right) - \omega,$$

where the ground system functionally multiplies the transmitter frequency by 240/221 during the doppler extraction process as shown in Fig. 4.

Or

$$\omega_{D,TOTAL} = \frac{240}{221}\omega_{T,GRD}\left(\frac{2v_R'}{C}\right) - \frac{461}{221}\omega_r - \frac{240}{221}\omega_r\left(\frac{v_R'}{C}\right) \tag{7}$$

where v_R' is the velocity factor which is a function of the change in distance D.

The factor for the rotating offset horn antenna was developed in Eq. (2) and is applicable here; thus, the final overall doppler expression is

$$\omega_{D,TOT\,AL} = \frac{\left(\frac{240}{221}\omega_{T,GRD}\right)2(v_R + (\sin\psi\,\omega_r\,6\lambda_{RCV})\sin\omega_r t)}{C}$$
$$- \frac{461}{221}\omega,$$
$$- \frac{\frac{240}{221}\omega_r(v_R + (\sin\psi\,\omega_r\,6\lambda_{RCi})\sin\omega_r t)}{C}, \text{rad/s} \tag{8}$$

or expressed in terms of frequency as

$$f_{D,TOTAL} = \frac{\left(\frac{240}{221}F_{T,GRD}\right)2(v_R + (\sin\psi f_r\,12\pi)\sin 2\pi f_r t)}{C}$$
$$- \left(\frac{461}{221}f_r + \frac{\frac{240}{221}f_r(v_R + (\sin\psi f_r\,12\pi)\sin 2\pi f_r t)}{C}\right), \text{Hz} \tag{9}$$

where f_r is the spacecraft rotational frequency.

Thus, in this two-way coherent mode it can be seen that the doppler velocity component has increased by a factor of 2 relative to the one-way, downlink mode; and similarly, the deviation frequency component value has doubled. However, the bias frequency component has been modified by the factor

$$-\left(\frac{461}{221}\omega_r + \frac{\frac{240}{221}\omega_r(v_R + (\sin\psi_\omega, 6\lambda_{Rr})\sin\omega_r t)}{C}\right)$$

V. Doppler With Ground System Antenna Linear Polarization

The complete spacecraft LGA is comprised of the RCP horn antenna and a vertical-linear-polarized dicone antenna. The vertical-linear component of the horn element combines with the dicone antenna element to create interferometry effects at aspect angles in the vicinity of $\psi \simeq 42 \rightarrow 50$ deg (Ref. 3).

A mode to lessen these effects would be to utilize a horizontal-linear polarization on the ground transmitter/receiver system to operate only with the horizontal-linear component of the RCP horn LGA. This mode essentially reduces the influence of the dicone antenna and caters largely to the horn LGA over the aspect angles of $0 \rightarrow 40$ deg.

Owing to the fact that the spacecraft horn antenna is still rotating, and physically the E-plane vector is also rotating, the same equations stated for the ground system RCP mode are applicable to this linear polarization mode. The signal level, however, would be attenuated approximately -3 dB because of receiving only the linear component of the RCP wave (Ref. 2).

VI. Polarization Definition

The bias angular frequency component due to the rotating E-plane vector shift direction as discussed above is based on the standardized convention of the Institute of Radio Engineers (IRE) and the spacecraft rotation sense.

The direction of the spacecraft rotation is such that, after the spin axis has been properly pointed so that it is approximately normal to the ecliptic plane, the spin is counterclockwise as viewed from the northern ecliptic pole (Ref. 4) and is illustrated in Fig. 2 as seen by the ground stations.

The uplink radiated wave to the spacecraft is similarly rotating clockwise (clockwise wave receding) as adopted by the discussion of paragraph 2 following the IRE standard for a RCP wave (Ref. 1), which is opposite to the classical physics usage. Hence, the net resultant spacecraft received signal appears as a longer wavelength, or a shift to a lower frequency, as shown in Fig. 3.

References

1. Kraus, J. D., *Antennas*, McGraw-Hill, New York, 1950, pp. 471 and 484.

2. Jasik, H., *Antenna Engineering Handbook*, McGraw-Hill, New York, p. 17-8.

3. Ham, N. C., "Helios Spacecraft Low-Gain Antenna Model," in *The Deep Space Network Progress Report*, Technical Report 32-1526, Vol. XVIII, pp. 147–162, Jet Propulsion Laboratory, Pasadena, Calif., Dec. 15, 1973.

4. "Deep Space Network/Helios Spacecraft Telecommunications Interface Definition," Document 613-6, Rev. A, Change 1, Jet Propulsion Laboratory, Pasadena, Calif., Mar. 1, 1974 (an internal document).
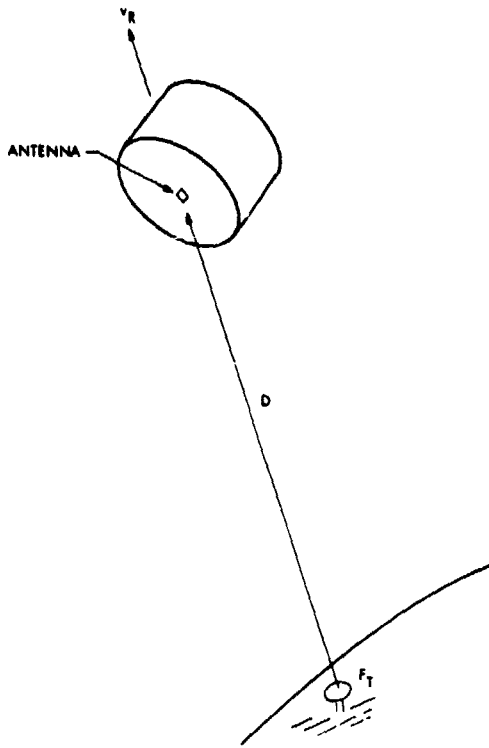
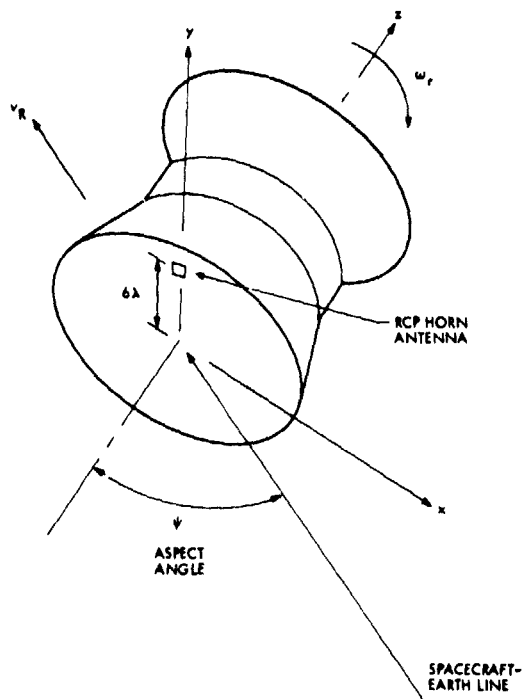Fig. 1. Typical ground transmitter and
spacecraft geometry

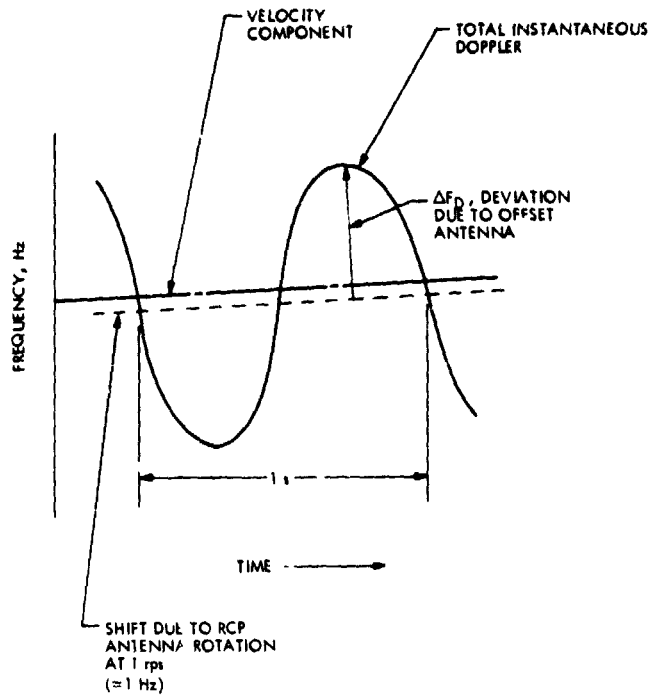Fig. 2. Rotating spacecraft with displaced
antenna configuration

Fig. 3. Instantaneous doppler components of spacecraft
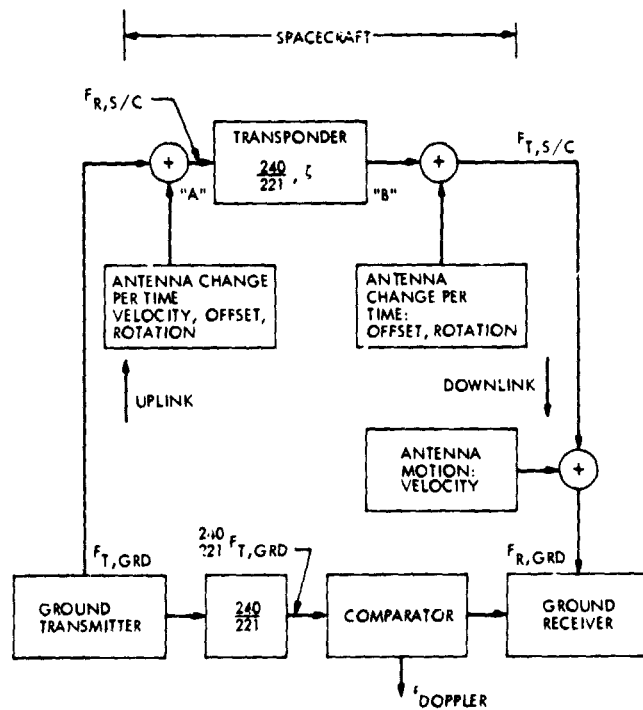received RF signal

Fig. 4. Coherent two-way doppler model for spacecraft
with rotating offset antenna

A Proposed Method of Reducing the Gravity Distortions of the 64-Meter Antenna Main Reflector

M. S. Katow

DSN Engineering Section

The surface panels of the 64-m main reflector are presently set to a prescribed paraboloid at 45 deg elevation angle. Rotation about the elevation axis to the horizon or zenith attitude introduces additional root-mean-square (rms) distortions due to the change in the direction of the gravity vector with respect to the symmetric axis. This article proposes a method of reducing the humps or bumps over the unyielding "hard" portions of the elevation wheel assembly supporting the reflector structure, thus reducing the rms distortions due to gravity for the structure. The bumps can be effectively removed by controlling the height of the panels above the reflector structure by means of mechanical leverage connections to the elevation motion, thus maintaining the simplicity and reliability of the reflector system. A table of overall rms distortions resulting from the summations of various options is included.

I. Introduction

From the initial outputs of the contour maps describing the normal distortions to the best fit paraboloid (Ref. 1), two humps or bumps existed over the elevation bearings for the gravity "off to on" loading case with the reflector at the zenith attitude or look. In the studies for a larger reflector structure, an upgraded 64-m model with deleted bumps was used as a basis for dimensional analysis with the expectation that it would be feasible.

This article describes a proposed method for actuating the surface panels to effectively reduce the bumps to almost zero. The improvements in the rms distortion values were computed as vector distortions, using the NASTRAN structural analysis program, and evaluated by the rms program which best fits a paraboloid and outputs SC4020 contour plots of the residuals and the rms of the $\frac{1}{2}$ RF pathlength errors (Ref. 2).

II. Analysis Discussion

The primary outputs of the structural analysis are the distortion (3-dimensional) vectors from the two loadings as follows:

(1) Gravity "off to on" loading in the symmetric axis direction.

(2) Gravity "off to on" loading in the antisymmetric direction.

For any particular elevation angle, the relations of the unit gravity vector and its component values along the symmetric and antisymmetric directions are pictured in Fig. 1.

Since the symmetric axis gravity component value Z is equal to the cosine of the elevation angle multiplied by the unit value, it follows that an eccentric crank arrangement rotating 90 deg produces an offset S equal to the cosine of the angle multiplied by the eccentric radius R. If the eccentric radius R is selected to equal the maximum correction required at the surface panel support as shown by the contour maps, this support will be fully corrected throughout the elevation angle range.

The analysis method also revealed that an overcorrection is actually necessary since the best fit paraboloid adjusts for the corrections in a Z lateral motion in the next iteration of best fitting. At first, only the bumps from the symmetric loading case were removed; but with the large percentage change resulting from the analysis, two bumps of smaller area were removed from the antisymmetric loading case for study.

Figures 2, 3, and 4 show half views (the reflector assembly at Goldstone, California, is symmetric about the center vertical plane) of the contour maps describing the residuals after the paraboloid best fitting of the computed distortion vectors as "before" and "after" corrections. Figure 2 shows the change for the symmetric gravity loading case and Fig. 3 shows the change at horizon look with the panels set at 45 deg with only the symmetric bumps removed. Figure 4 shows the differences for the antisymmetric loading case. Here, the bumps were over the top and bottom trusses of the rectangular girder where strong and rigid connections with the elevation wheel assembly occur.

III. Results

Table 1 details the analytically computed rms performance values in ½ RF pathlength errors for the various options noted. Included also are rms values for available surface panels and a figure for the subreflector surface attained for the multiple panel assembly for the symmetric hyperboloid. It should be pointed out that an unsolved problem at this time is the manufacture of the subreflector symmetric about one plane as required for the shaped cassegrain optics arrangement.

References

1. Katow, M. S., "Primary Reflector Analysis," in *Supporting Research and Advanced Development*, Space Programs Summary 37-52, Vol. II, pp. 86–92. Jet Propulsion Laboratory, Pasadena, Calif., July 1, 1968.

2. Katow, M. S., and Schmele, L. W., "Antenna Structures: Evaluation Techniques of Reflector Distortions," in *Supporting Research and Advanced Development*, Space Programs Summary 37-40, Vol. IV, pp. 73–76. Jet Propulsion Laboratory, Pasadena, Calif., Sept. 30, 1968.

Table 1. Half-pathlength error, rms, distortion from gravity loadings, mm (in.)

Antenna attitude	Reflector structure				Plus surface panels[a] and subreflectors			
	Normal	Bump removed			Normal	Bump removed		
		Zenith only	Horizon only	Both		Zenith only	Horizon only	Both
Zenith look, set 45 deg	0.50 (0.020)	0.45 (0.018)	0.40 (0.016)	0.33 (0.013)	0.81 (0.032)	0.79 (0.031)	0.76 (0.030)	0.74 (0.029)
45 deg elevation, panels set	0.25 (0.010)[b]	–	–	–	0.64 (0.025)	0.64 (0.025)	0.64 (0.025)	0.64(0.025)
Horizon look, set 45 deg	0.63 (0.025)	0.34 (0.013)	0.62 (0.024)	0.31 (0.012)	0.91 (0.036)	0.74 (0.029)	0.89 (0.035)	0.71 (0.028)
Zenith look, gravity off/on	0.86 (0.034)	0.43 (0.017)	–	–				
Horizon look, gravity off/on	0.63 (0.025)	–	0.46 (0.018)	–				

[a]Optimum manufacturing surface panel distortion rms = 0.51 mm (0.020 in.).
  Optimum subreflector distortion rms = 0.31 mm (0.012 in.).
[b]Optimum surface panels setting error rms = 0.25 mm (0.010 in.).

Root-mean-square sum $= \sqrt{\Sigma\ rms_i^2}$; no rms distortion due to lateral offsets at the primary focus accounted; perfect pointing assumed (CONSCAN use equivalent to rms = 0.5 mm (0.020 in.) = 0.1 dB at X-band).
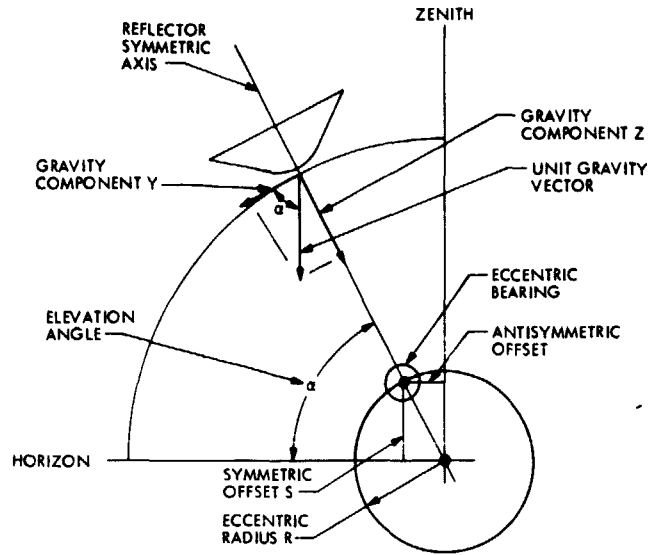
Fig. 1. Relations of the gravity vector components
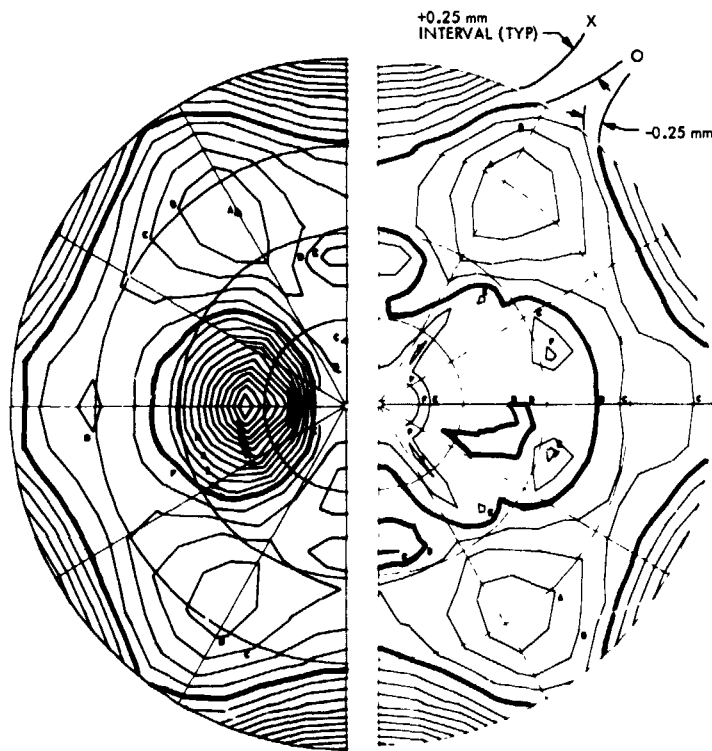
(a) NORMAL

RMS = 0.86 mm (0.034 in.)
FOCAL LENGTH = 27.13312 m (1068.233 in.)

(b) AFTER BUMP REMOVAL

RMS = 0.43 mm (0.017 in.)
FOCAL LENGTH = 27.12999 m (1068.110 in.)

Fig. 2. Contour maps of the distortions measured normal to the surface of the best fit paraboloid. Loading: gravity off to on, zenith altitude
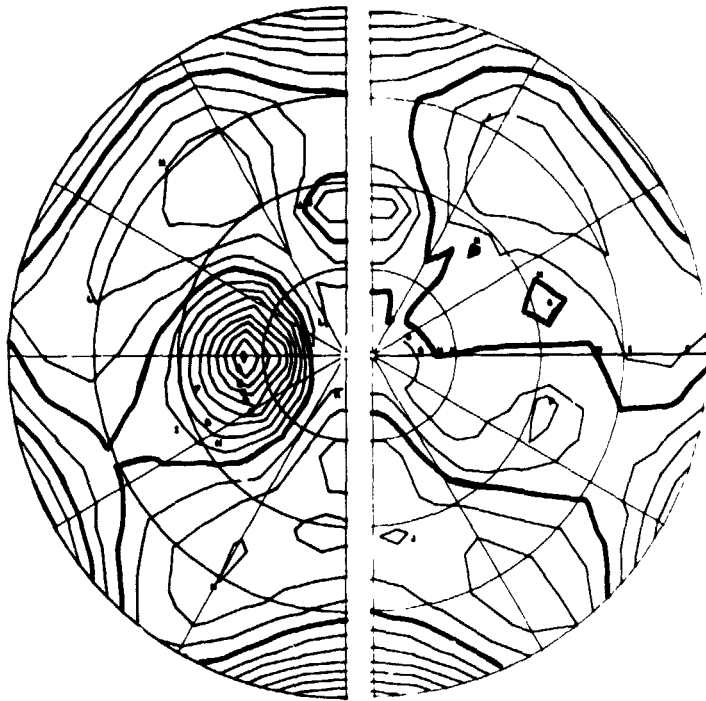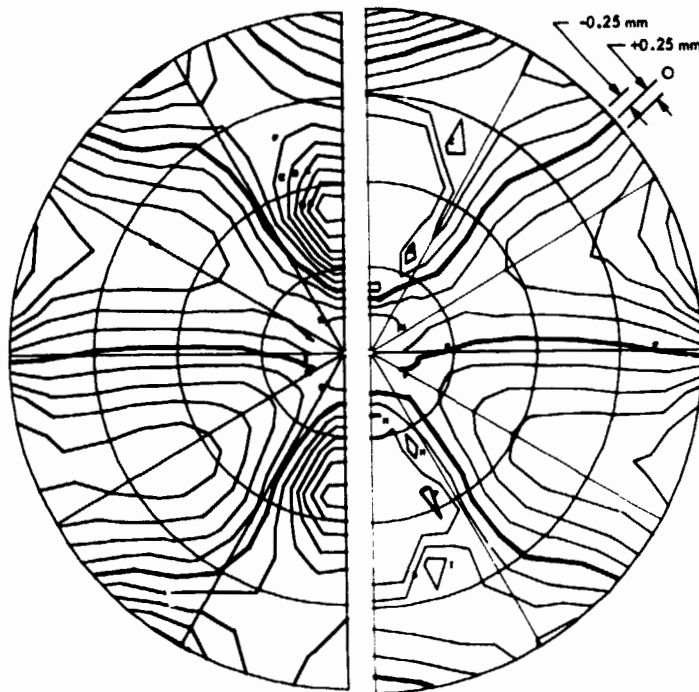
(a) NORMAL
RMS = 0.63 mm (0.025 in.)
FOCAL LENGTH = 27.09276 m (1066.644 in.)

(b) AFTER ZENITH BUMP REMOVAL
RMS = 0.34 mm (0.013 in.)
FOCAL LENGTH = 27.09497 m (1066.731 in.)

Fig. 3. Contour maps of distortions measured normal to the surface of the best fit paraboloid. Loading: gravity, horizon look, panels set at 45 deg

(a) NORMAL

(b) AFTER BUMP REMOVAL

RMS = 0.62 mm (0.025 in.)
FOCAL LENGTH = 27.11041 m (1067.339 in.)

RMS = 0.46 mm (0.018 in.)
FOCAL LENGTH = 27.11046 m (1067.341 in.)

Fig. 4. Contour maps of distortions measured normal to the surface of the best fit paraboloid. Loading: gravity off to on, horizon altitude

Three-Spacecraft Simulation for Viking 1975

M. M. Whang
DSN Data Systems Development Section

A telemetry simulation capability is provided at each Deep Space Station, by way of the Simulation Conversion Assembly (SCA), for testing station equipment and training of operations personnel prior to each mission. The simulation equipment provided to the DSN for support of the Viking 1975 mission has been substantially more complex than that provided for previous missions. No single station in the DSN has had the requirement to track three spacecraft simultaneously for any past flight project. Deep Space Stations will be required to support the equivalent of four spacecraft (two orbiters and two landers) for the Viking 1975 mission.

However, any single station will have a view angle of the equivalent of only three spacecraft maximum at any given time (two orbiters and one lander). Since each spacecraft has two telemetry channels (one science and one engineering channel), the Deep Space Stations must be prepared to process six channels of telemetry data and hence a six-channel simulation capability must be provided. This entails the generation of an additional two channels of simulated telemetry data over the present four-channel capability of the Simulation Conversion Assembly. This article describes the SCA modification necessary to prepare for the Viking 1975 mission.

I. Introduction

The Simulation Conversion Assembly (SCA) provides a mission-independent source of simulated data for use in the checkout and test of telemetry data handling equipment at a Deep Space Station (DSS). The SCA is also a serial element of the DSN Simulation System with the DSS Telemetry and Command Data Handling Subsystem to process data generated at the Mission Control and Computing Center (MCCC) and distribute the data to the various equipment throughout the DSS, including the Subcarrier Demodulator Assembly (SDA), Symbol Synchronizer Assembly (SSA), Telemetry and Command Processor (TCP), Block Decoder Assembly (BDA), Digital Decoder Assembly (DDA), and the test transmitter assemblies. At present, all of the SCAs have been updated to support MVM'73. For the Viking 1975 mission, the SCAs at the 64-m stations (DSS 14, 43, and 63), and temporarily at CTA 21, will be updated to support mission requirements. At the 26-m stations, the SCA hardware will remain unchanged; however, new software capabilities are provided to support the project.

II. Viking 1975 Simulation Requirements

The simulation requirements imposed on the SCA by Viking 1975 are defined in detail in Ref. 1. The following paragraphs briefly describe these requirements as they specifically pertain to the SCA; for further information refer to Ref. 1.

The SCAs at the 64-m DSSs will be required to simulate high-rate (science) and low-rate (engineering) data for each of two orbiters and one lander spacecraft. The two orbiter high-rate channels will be required to provide block coded data at a maximum rate of 16.0 kbps and uncoded data up to 4 kbps. The orbiter low-rate channels will provide uncoded data at a maximum rate of 33-⅓ bps. The lander high-rate channel will be required to provide block coded data at a maximum rate of 1 kbps; the low-rate channel will provide uncoded data up to 8-⅓ bps.

Each of the six telemetry channels (channels 1 through 6—5 and 6 are new) will require biphase modulation. The orbiter high-rate channels will be modulated by a subcarrier frequency of 240 kHz, the low rate at 24 kHz. The lander high-rate channel will be modulated by a subcarrier frequency of 72 kHz, the low rate at 12.0 kHz.

The 64-m DSSs will also require a third test translator with associated modulator, mixer, and modulation index control to provide for new channels. The test translator RF carrier will be 2.11 GHz.

The SCAs at the 26-m DSSs will require a four-channel (existing channels 1 through 4) simulation only. The data rates, formats (uncoded or block coded), and subcarrier frequencies are the same as for the 64-m DSSs. These stations will be required to simulate high- and low-rate data for each of two orbiters (four channels) or high and low rate for one orbiter and one lander.

The existing SCA software, DOI-5089-TP-C (DROP C), will require updating to become DOI-5089-TP-F (DROP F). The new software will provide for maximum control of the hardware at the 64-m DSSs. The same software will also provide for control at the 26-m DSSs. In addition to hardware control and high-speed data line (HSDL) (bit stream) data routing, the software will be required to simulate the following fixed data outputs (maximum capabilities):

(1) Two orbiters:

(a) Visual Imaging Science (VIS) data (high-rate data with incrementing line and picture counts);

capabilities provided on telemetry channels 1, 2, 5, and 6; capabilities exist at 26-m (channels 1 and 2 only) and 64-m DSSs.

(b) Viking Orbiter Science (VOS) data (high-rate, fixed data); channels 5 and 6 only; capabilities exist at 64-m DSSs only.

(c) Viking Orbiter Engineering Launch (VOEL) data (low-rate, fixed data); channel 4 only; capabilities exist at 26- and 64-m DSSs.

(d) Viking Orbiter Engineering Cruise (VOEC) data (low-rate, fixed data); channel 3 only; capabilities exist at 26- and 64-m DSSs.

(2) One lander:

(a) Visual Imaging Lander (VIL) data (with incrementing line and picture counts); capabilities provided on telemetry channels 1 and 2 only (26- and 64-m DSSs).

(b) Viking Lander Engineering Format 4 (VLE4) and SSCA (surface sampler) low-rate, fixed data; channel 1 only (26- and 64-m DSSs).

(c) Viking Lander Engineering Format 5 (VLE5) (low-rate, fixed data); channel 2 only (26- and 64-m DSSs).

III. Existing SCA Capabilities

At present, the SCA is capable of simulating four channels (channels 1 through 4) of telemetry data. Two of the channels (channels 1 and 2) have block coding, high- and low-rate capabilities. The other two channels provide uncoded low-rate data only. Each of the four channels can be biphase (BI-ϕ) or interplex-modulated.

The SCA also provides a computer-controlled data selection matrix which provides for modulation control, modulation index setting, and test signal routing to various DSS equipment.

The existing software provides for control of the SCA hardware, input and processing of HSDL inputs from MCCC, and MVM'73 fixed data simulation of Imaging 1 (IM-1) at 117.6 kbps. The IM-1 data were embedded in the MVM'73 SCA software.

For purpose of Viking 1975, the 26-m stations will retain the existing hardware capabilities; however, new software will provide for the required fixed data simulations described in Section II.

IV. New SCA Capabilities Required

In addition to the existing capabilities described in Section III, the 64-m DSSs will be required to provide two new telemetry channels (for a total of six), with associated block coders and variable data-rate capabilities.

Two new modulators are required to provide two additional biphase outputs. These modulators will be identical to the four existing modulators and will also be capable of providing interplex modulation. A new mixer, with associated modulation index setting capabilities, and a power amplifier will be required to provide for a third transmitter test signal. The SCA data selection capabilities will be expanded to provide for routing of the two new channels, and for increased test signal outputs to an increased number of DSS equipments.

In addition to the new hardware required, a new software SCA Data Routing Operational Program (DROP) is required to provide for control of the new hardware and also to provide two additional telemetry channel outputs and simulation of the fixed data described in Section II. This program must be compatible for use at both the 26- and the 64-m DSSs.

V. Implementation of New Capabilities

The SCAs at the 64-m DSSs will be updated to meet the requirements of Viking 1975. These modified SCAs will be redesignated to become the SCA II. At present, the SCAs at CTA 21 and DSS 14 have been updated and are in use. The SCAs at DSSs 43 and 63 will be updated in the near future.

The SCA II is basically an add-on and expansion of the existing SCA configuration. The requirement for a six-channel simulation is satisfied by adding two new telemetry channels (5 and 6) to the existing four-channel configuration. The two new channels are capable of providing high or low rate, block coded or uncoded data outputs.

Since three channels of high-rate data and three channels of low-rate data must be simulated, the SCA II will provide expanded bit rate capabilities. This was accomplished by adding one new bit sync generator and a frequency divider network. The bit sync generator provides the basic timing clock for the new telemetry channel 5. The frequency divider provides for selection of either low rates, or bit sync generator rates, for existing telemetry channels 1 and 2. Channel 3 and 4 bit rates are also selectable and are obtained from an existing fixed-rate generator (low rates) or from a bit sync generator. Telemetry channel 6 receives a bit rate input from existing bit sync generator 2 (BSG 2).

Four new video conditioner modulators, with biphase and interplex modulation features, will be added to provide a total of eight video conditioner outputs. New video conditioners 5 and 6 will provide for modulated or unmodulated outputs of the two additional telemetry channels. Video conditioners 5 and 6 are also interconnected to provide for interplexed data outputs. These two video conditioners provide outputs and modulation index setting for a third test transmitter signal.

Video conditioners 5 and 6 receive subcarrier frequency inputs from the new frequency divider network. A new, fourth, subcarrier frequency generator (SFG) is provided for a basic frequency input to the frequency divider, and for subcarrier input to video conditioner 7. The three SFGs contained in the existing SCA configuration provide for SFG inputs to video conditioners 1, 2, 3, 4, and 8.

New video conditioners 7 and 8 will be installed at DSSs 43 and 63 only, and will provide test signal inputs to eight SDAs.

The SCA II contains expanded data selection capabilities to provide for six-channel routing, modulation control, and modulation index control. The new capabilities also provide further test signal inputs to more DSS interfacing equipment. This is accomplished by expanding the basic design of the existing data select drawer to provide a new drawer. The new drawer will provide for routing any one or all or any combination of the six telemetry channels, data types nonreturn-to-zero level (NRZL) or nonreturn-to-zero mark (NRZM), to the following units, as the test data described:

(1) Bit error rate (BER) outputs to a maximum of five SSAs (NRZL only) and three TCPs.

(2) Word error rate (WER) (channels 1, 2, 5, and 6 only, with block coding capabilities) outputs to a maximum of five Data Decoder Assemblies (DDAs) and three Block Decoder Assemblies (BDAs).

(3) Convolutional error rate (CER) (channel 1 only) outputs to a maximum of five DDAs.

(4) Bit sync (BS) outputs to three TCPs.

The data select drawer also provides for modulation control of the video conditioners and for control of the modulation index attenuators contained within the video conditioners. These capabilities will provide for biphase or interplex modulation of test signal outputs to a maximum of eight SDAs (four new), nonmodulated data outputs to a maximum of five SSAs, and nonmodulated outputs to provide for integrated, low-rate inputs to eight TCPs. Eight modulation index attenuators can be controlled to provide settings for pairs \ inputs (1 and 3, 2 and 4, 5 and 6; 7 and 8 are not used) to associated mixers for test signals to three transmitters.

The existing SCA hardware configuration consists of two standard buffer assemblies and a two-cabinet XDS 910 computer. This configuration will remain unchanged at the 26-m DSSs. At the 64-m DSSs a third buffer assembly with associated interfacing cables will be added to provide the hardware for the new capabilities required.

The third cabinet will receive EOM/POT inputs directly from the computer via a PIN/POT expansion chassis added to the computer memory cabinet. A photograph of the new cabinet, buffer cabinet 3, is shown in Fig. 1, and the front and rear physical layouts are shown in Fig. 2. The SCA II installation at CTA 21 is shown in Fig. 3. Note that the SCA II consists of, from left to right, the new buffer cabinet 3, existing buffer cabinets 1 and 2, and two XDS 910 computer buffer cabinets.

The new DROP program is compatible for operation at both the 26- and 64-m DSSs. At the 64-m DSSs the program provides for control of the maximum hardware control capabilities and the fixed data outputs described in Section II. Throughout the design and development of the SCA II, the software development presented the most problems. In order to accomplish all of the software requirements, some of the software functions were incorporated into the SCA II hardware.

Reference

1. Davis, E. K., and Mudgway, D. J., *Deep Space Network Support Plan for the Viking '75 Project*, Project Document 614-19 (Change 2), Jet Propulsion Laboratory, Pasadena, Calif., Aug. 15, 1973 (an internal document).
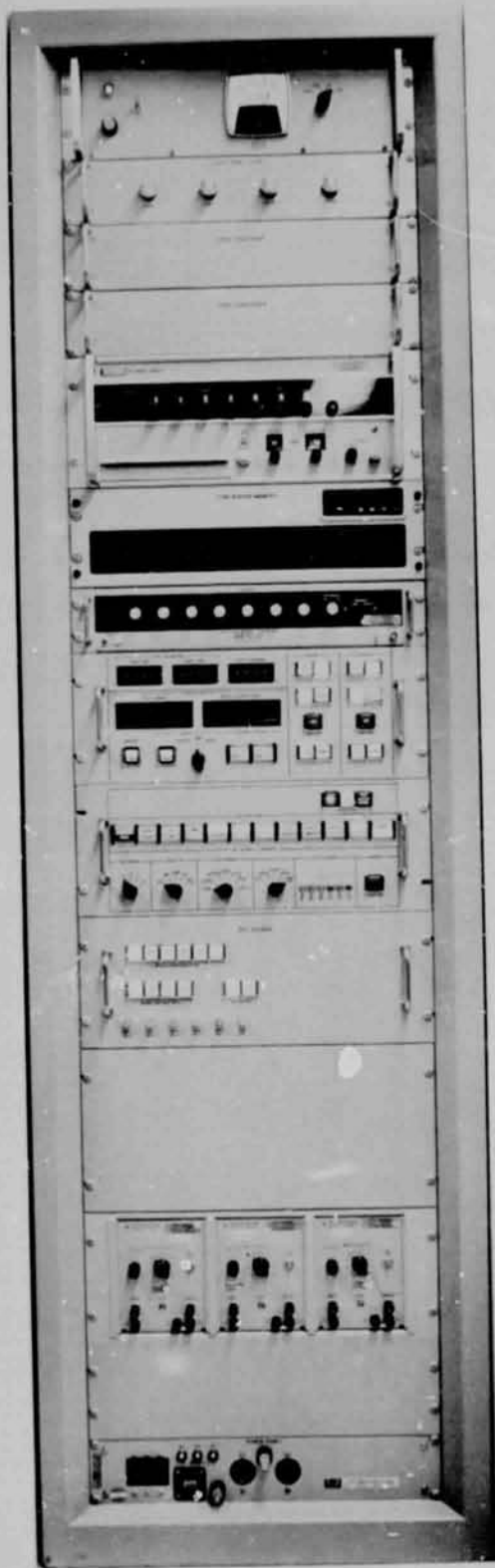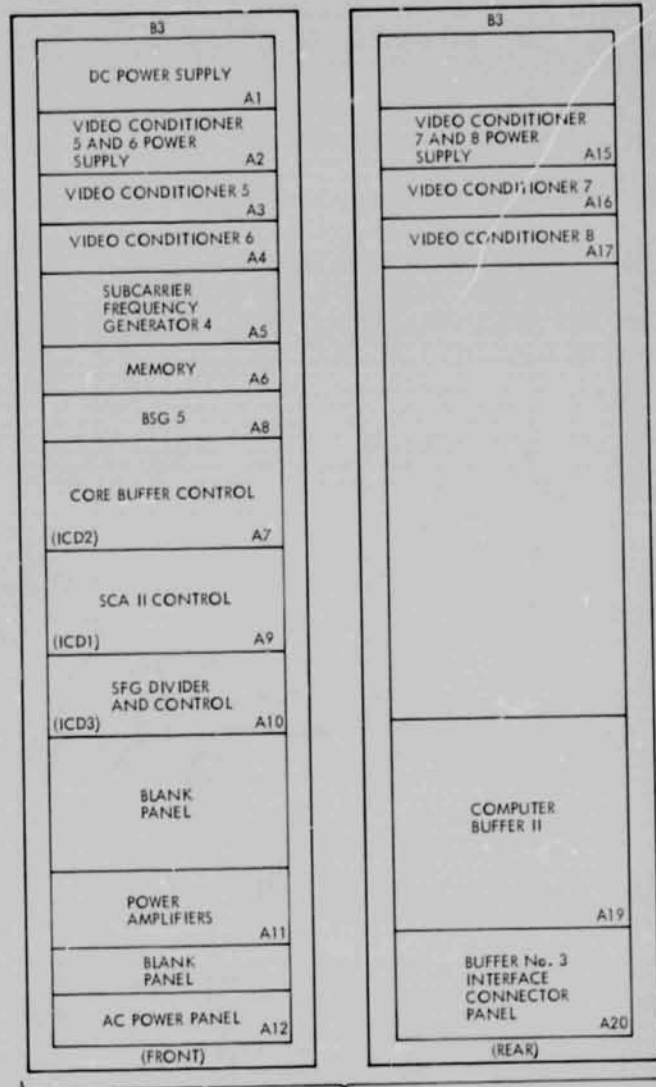
Fig. 1. SCA II buffer cabinet 3, front view

BUFFER CABINET 3 TCD-102

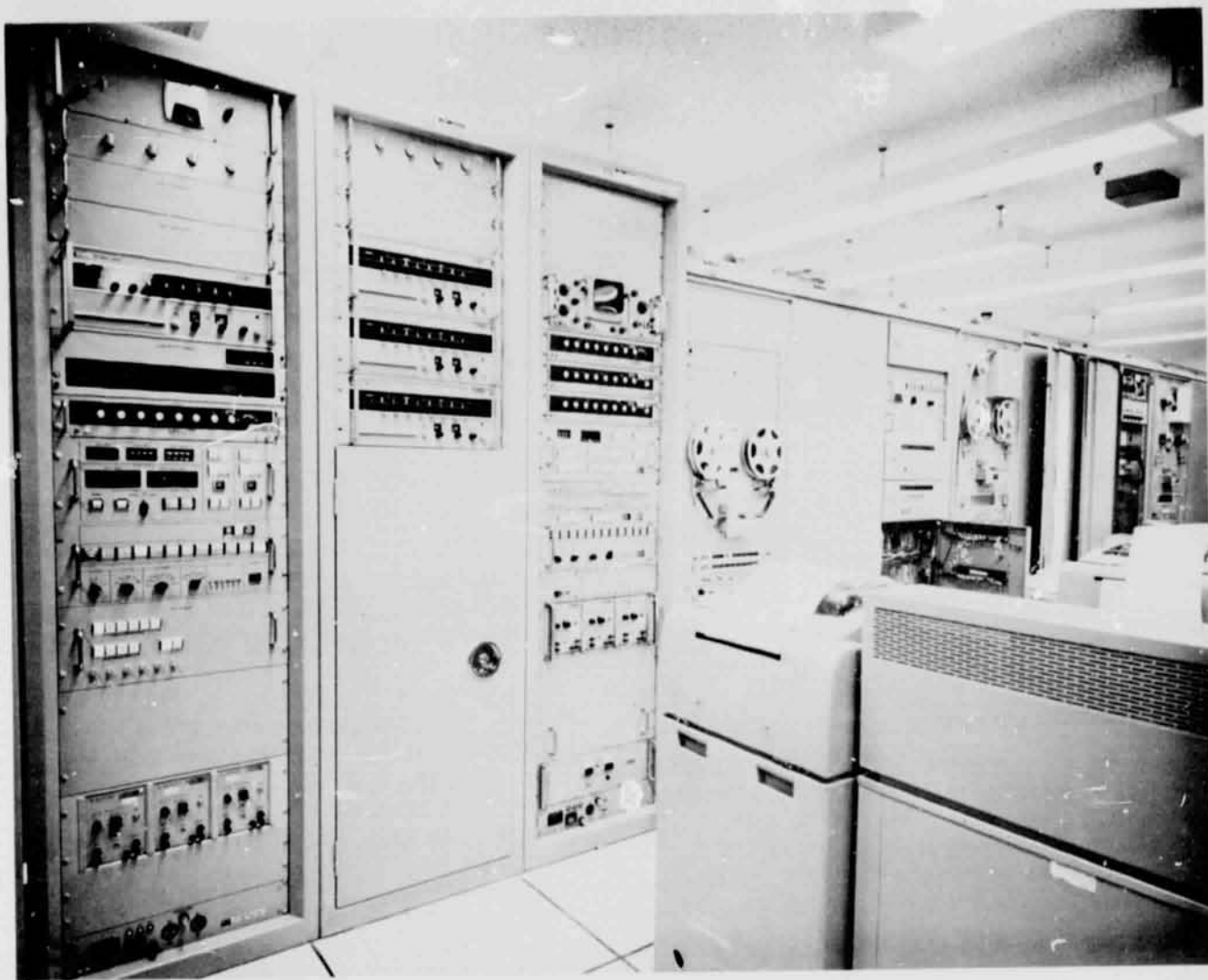Fig. 2. SCA II buffer cabinet 3, physical layout

Fig. 3. SCA II installation at CTA 21

AGC Calibration Accuracy

G. L. Stevens

Network Operations

Currently, measurement of received signal power at the DSN stations is performed by calibrating the automatic gain control voltage as an indicator of received signal power level. Errors in the AGC voltage vs sig   *wer level calibration ore identified and the overall AGC calibration acc   estimated.*

I. Introduction

At present, DSN Standard Test Procedure No. 853-51 4A-07 Rev B is used to calibrate the receiver automatic gain control (AGC) voltage vs the received carrier power so that the Digital Instrumentation Subsystem (DIS), the Telemetry and Command Processor (TCP), and the voice report all yield an accurate estimation of the received spacecraft carrier power. Fifteen AGC voltage/signal level pairs covering a 30-dB range are used in the calibration. The test transmitter output signal level is adjusted to the desired calibration levels using the Y-factor technique of power ratio measurements.

The AGC voltage/signal level pairs are used by the DIS to generate a third-degree polynomial curve fit. The TCP performs a seven-point best fit straight line approximation to the calibration data. Received spacecraft signal power estimation is performed independently by the DIS and TCP. The DIS samples the receiver AGC voltage and calculates the coi   onding carrier power using the third-degree polynomial established in the AGC calibration. Similarly, the TCP samples the AGC voltage and estimates the received signal power using its linear approximation of the AGC voltage/signal power relationship.

This report presents a discussion of the theoretical aspects a:.! limitations of the AGC voltage vs received CW signal power calibration prucedure.

II. Procedure

The signal level calibration consists of four major steps. Each of these major steps will be examined, and those items which appear to limit the accuracy of the calibration will be identified. An attempt will be made to place a bound on each of these discrete error contributions and to estimate the overall AGC calibration accuracy.

A. Step 1: Y-Factor Calculations

In order to calculate the Y-factors that are required to input the desired test transmitter signal levels, it is first necessary to obtain measured values for:

T_{op} effective system noise temperature, K

B uncorrected bandwidth of the 10-kHz bandpass filter in the Y-factor detector assembly

G gain factor of the Y-factor detector assembly

These parameters, along with the desired input carrier power levels from the test transmitter, are used by the Y-factor computer program DOI-5343-SP-B to calculate the Y-factors used in the AGC calibration. The formula used by the DIS to calculate the Y-factors is:

$$Y_{dB} = 10 \log \left\{ 1 + \text{antilog} \left[\frac{pad + P_c + 198.6 - G}{10} \right. \right.$$

$$\left. \left. - \log (T_{op} \cdot B) \right] \right\} \qquad (1)$$

where

pad = test transmitter reference step attenuator calibrated value, dB.

P_c = test transmitter carrier power, dBm.

198.6 = Boltzman's constant

In order to evaluate the accuracy of the calculated Y-factors, it is first necessary to define the errors in the measured system parameters. These errors are:

$\triangle T$ = the error in the measured value of system operating temperature, K

$\triangle B$ = the error in the measured value of the 10-kHz crystal filter bandwidth in the Y-factor detector assembly

$\triangle G$ = the error in the measured value of the gain factor, dB

$\triangle pad$ = the error in the calibrated value of the test transmitter reference step attenuator

The error $\triangle Y$ in the calculated value of Y can now be expressed as

$$\triangle Y = \frac{\partial Y}{\partial (pad)} \triangle pad + \frac{\partial Y}{\partial G} \triangle G + \frac{\partial Y}{\partial T_{op}} \triangle T_{op} + \frac{\partial Y}{\partial B} \triangle B$$

$$(2)$$

where

$\frac{\partial Y}{\partial (pad)}$ = the sensitivity of the Y-factor calculation to an error in the *pad* value

$$= \frac{10^x}{1 + 10^x} \qquad (3)$$

$\frac{\partial Y}{\partial G}$ = the sensitivity of the Y-factor calculation to an error in the gain factor

$$= - \frac{10^x}{1 + 10^x} \qquad (4)$$

$\frac{\partial Y}{\partial T_{op}}$ = the sensitivity of the Y-factor calculation to an error in the measured value of system noise temperature

$$= - \frac{4.34 \cdot 10^x}{(1 + 10^x) T_{op}} \qquad (5)$$

$\frac{\partial Y}{\partial B}$ = the sensitivity of the Y-factor calculation to an error in the measured value of the 10-kHz filter bandwidth.

$$= - \frac{4.34 \cdot 10^x}{(1 + 10^x) B} \qquad (6)$$

where

$$X = \frac{pad + P_c + 198.6 - G}{10} - \log (T_{op} \cdot B) \qquad (7)$$

The error $\triangle Y$, in the calculated value of each Y-factor will result in an error in the setup value of carrier power of $\triangle P_c$. Solving Eq. (1) for P_c yields

$$P_c = 10 \log (10^{Y/10} - 1) + 10 \log T_{op}$$

$$+ 10 \log B - pad - 198.6 + G \qquad (8)$$

The sensitivity of the setup value of carrier power to the error in the calculated Y-factors is obtained by taking the derivative of P_c with respect to Y. We obtain

$$\frac{\partial P_c}{\partial Y} = \frac{10^{Y/10}}{10^{Y/10} - 1} \qquad (9)$$

Therefore, the error in the setup signal level due to the Y-factor errors is given by

$$\triangle P_c = \frac{\partial P_c}{\partial Y} \triangle Y \qquad (10)$$

or

$$\triangle P_c = \frac{10^{Y/10}}{10^{Y/10} - 1} \triangle Y \qquad (11)$$

In order to evaluate the calibration signal level error contributions discussed so far, it is necessary to assign values to $\triangle T_{op}$, $\triangle B$, $\triangle G$, and $\triangle pad$. These four values are given below:

(1) The measured value of T_{op} has a worst case (3σ) error of 1.3 K (Ref. 1).

(2) The accuracy of the measured value of bandwidth is limited primarily by the accuracy of the Airborne Instrument Laboratories (AIL) precision attenuator. The precision attenuator is used to calibrate the filter attenuation as a function of frequency. The accuracy of the precision attenuator over the range used for this calibration is 0.06 dB (Ref. 2), corresponding to a bandwidth error of 140 Hz.

(3) The gain factor accuracy is limited by the precision attenuator and is approximately 0.03 dB.

(4) The capability exists to calibrate the test transmitter step attenuators to an accuracy of 0.05 dB. This is the accuracy of the reference step attenuator (*pad*) value.

The AGC calibration errors introduced by the Y-factor calculations are summarized in Table 1.

B. Step 2: Calibration Signal Level Adjustments

The second major step in the AGC calibration is to set up precise test transmitter signal levels using the Y-factor equipment. Three major factors which limit the accuracy of the calibration signal level settings are:

(1) The resetability and nonlinearity of the precision attenuator. For Y-factors such that 4 dB $\leq$ Y $\leq$ 16 dB, the precision attenuator accuracy is approximately 0.04 dB.

(2) The operator's ability to "eyeball average" the strip chart recorder trace and to duplicate that average by adjusting the test transmitter output level. The inherent limitations of this technique result in an additional worst case error contribution of 0.05 dB.

(3) The procedure of using the test transmitter step attenuator to decrease the signal power in two 10-dB steps to provide three calibration points for each of the five calculated and set up Y-factors. This procedure results in calibration signal power errors (in 10 of the 15 calibration points) of not more than 0.05 dB.

These three error sources and their net worst case error contribution to the signal level adjustments are summarized in Table 2.

C. Step 3: AGC Voltage Measurements

The third phase of the calibration is the measurement of the noisy AGC voltage. The AGC voltage is averaged over a 100-s interval by the 2401C integrating voltmeter and is then displayed. The principal sources of error to be considered include:

(1) The CW power stability of the test transmitter (Ref. 3). The published specification of 0.5 dB is not representative of actual performance over the five short periods (7 to 10 min each) during which the calibration signal level must remain constant. It is assumed that the power stability of the test transmitter over these short time periods is 0.05 dB.

(2) The maser gain stability over the period of time (approximately 1 h) that it is used during the AGC calibration and the accuracy to which its gain can be set. The short-term fixed position gain stability is 0.05 dB/10 s and the long-term gain stability is 0.5 dB/12 h (Ref. 4). The total calibration error due to the maser gain adjustment and gain variation is assumed to be not greater than 0.15 dB.

(3) The receiver gain stability. The receiver gain stability during the AGC calibration is assumed to be 0.05 dB.

(4) The variance of the 100-s averages taken by the integrating voltmeter due to the variance of the AGC voltage. The variance of the AGC voltage can be calculated by using the results of Chapters 7 and 8 of Tausworthe (Ref. 5). It has been shown by Lesh (Ref. 6) that the variance of the 100-s averages is related to the variance of the AGC voltage by:

$$\sigma_A^2 = \sigma_{AGC}^2 \left[\frac{2\tau}{T} + \frac{2\tau^2}{T^2} \left(e^{-\frac{T}{\tau}} - 1 \right) \right]$$

$$\approx \frac{2\sigma_{AGC}^2 \tau}{T} \tag{12}$$

for T/τ large, where

$\sigma_A^2 =$ the variance of the 100-s sample

$\sigma_{AGC}^2 =$ the variance of the AGC voltage

$T =$ the integration time (100 s)

τ = the closed loop AGC time constants

$$\tau = \begin{cases} 2.69\text{ s (narrow)} \\ 0.241\text{ s (medium)} \\ 0.283\text{ s (wide)} \end{cases}$$

The accuracy of Step 3 of the AGC calibration is plotted as a function of signal level in Fig. 1.

D. Step 4: Manual Gain Control (MGC) Sampling and Curve Fitting

The fourth major step in the AGC calibration is the process of adjusting the MGC voltage to the value obtained in Step 3, sampling these voltages with the DIS and TCP, and performing the seven-point best fit (TCP) and the third-degree least squares curve fit (DIS). The three parts of this phase of the calibration will be considered separately:

(1) The MGC voltage stability and setability will create an error not exceeding 0.002 V or 0.02 dB.

(2) Gain stability, zero offset and linearity specifications for the AGC isolation amplifier (Ref. 7) indicate a maximum error contribution by this component of 0.1 dB. If the digital voltmeter is used to check the zero offset, gain, and linearity while the amplifier adjustments are made, this maximum error can be reduced to approximately 0.02 dB.

The error contributions of the TCP analog multiplexers will not be greater than 0.0025 V (Ref. 8), and the accuracy of the TCP analog-to-digital converter (ADC) is 0.0035 V (Ref. 9). These two errors result in an additional TCP worst-case calibration error of 0.06 dB. Similarly, the DIS analog multiplexer (Ref. 10) and analog-to-digital converter (Ref. 11) errors result in an additional DIS calibration error of approximately 0.04 dB.

(3) The AGC voltage/signal level pairs are used by the DIS to generate the third-degree polynomial curve fit. The TCP performs a seven-point best fit straight line approximation to these data. A study by Lesh (Ref. 12) of a similar calibration technique indicates that the calibration error contribution by the DIS curve fitting process is less than 0.01 dB. Similarly, the TCP calibration error introduced by the straight-line approximation does not exceed 0.02 dB.

A tabulation of the MGC sampling and curve fitting errors is given in Table 3.

IV. Total AGC Calibration Accuracy

The total worst case AGC calibration error is obtained by combining the results of Tables 1 through 3 with Fig. 1. Figure 2 is a plot of the total AGC calibration error vs signal level. A probable error scale is included by making the assumption that the worst-case error is a 3σ value of the calibration error. It should be noted that there is no significant difference between the DIS and TCP accuracies, since most of the calibration errors result from sources that are common to the DIS and TCP.

V. Summary

This step-by-step view of the AGC calibration procedure has hopefully identified the principal sources of calibration errors. The calibration errors associated with each of the four calibration phases have been estimated. It has been shown that the AGC calibration accuracy is largely a function of two factors:

(1) Calibration of all hardware associated with the AGC calibration including:

   Test transmitter.
   Maser.
   Receiver.
   50-MHz AIL precision attenuator.
   Y-factor detector assembly (10-kHz bandpass filter).
   AGC isolation amplifier.
   TCP and DIS analog multiplexers and ADCs.

(2) The accuracy to which system measurements and adjustments are made by the operator.

It is important to note that this report is concerned with only the calibration accuracy of the receiver AGC voltage as an indicator of the CW power level at the receiver input reference plane. The AGC calibration accuracy (Fig. 2) should not be confused with the overall accuracy of spacecraft signal level reporting. Many other factors are involved, including:

(1) DSS antenna gain variations and pointing errors.

(2) Maser gain variation as a function of antenna pointing angle.

(3) Uncertainties in path loss.

(4) Long-term equipment stabilities.

These would have to be considered in a study of the overall spacecraft signal-level reporting accuracy.

References

1. Stelzried, C. T., Reid, M. S., and Nixon, D., *Precision Power Measurements of Spacecraft CW Signal Power with Microwave Noise Standards*, Technical Report 32-1066, pg. 13, Jet Propulsion Laboratory, Pasadena, Calif., June 15, 1972.

2. *Instruction Manual for Type 32 Precision IF Attenuator*, p. 2, Airborne Instruments Laboratory, Deer Park, L. I., N. Y.

3. "DSIF Test Transmitter," Technical Manual TM00101, pp. 1–2, Jet Propulsion Laboratory, Pasadena, Calif. (an internal document).

4. "Traveling Wave Maser Group Block III," Technical Manual TM00714, p. 1-16, Jet Propulsion Laboratory, Pasadena, Calif. (an internal document).

5. Tausworthe, R. C., *Theory and Practical Design of Phase Locked Receivers*, Vol. I, Technical Report 32-819, Jet Propulsion Laboratory, Pasadena, Calif., Feb. 1968.

6. Lesh, J. R., "Correlated Sampling with Applications to Carrier Power Estimation Accuracy," in *The Deep Space Network Progress Report*, Technical Report 32-1526, Vol. VII, Jet Propulsion Laboratory, Pasadena, Calif., Feb. 15, 1972.

7. "Dynamics Amplifier," Technical Manual TM10116, pp. 1.1—1.2, Jet Propulsion Laboratory, Pasadena, Calif. (an internal document).

8. "MU65-2 Analog Multiplexer," Technical Manual TM10580, Jet Propulsion Laboratory, Pasadena, Calif. (an internal document).

9. "AD30-12 Analog to Digital Converter," Technical Manual TM10582, Jet Propulsion Laboratory, Pasadena, Calif. (an internal document).

10. "MU3204 Analog Multiplexer," Technical Manual TM15087, Jet Propulsion Laboratory, Pasadena, Calif. (an internal document).

11. "AD20-14 Analog to Digital Converter," Technical Manual TM10522, Jet Propulsion Laboratory, Pasadena, Calif. (an internal document).

12. Lesh, J. R., "Carrier Power Estimation Accuracy," in the *Deep Space Network Progress Report*, Technical Report 32-1526, Vol. IX, pp. 207–217, Jet Propulsion Laboratory, Pasadena, Calif., June 15, 1972.

Table 1. Y-factor calculation errors

Error source	Value	Worst-case error contribution, dB
ΔT = system temperature error	1.3° K	0.18
ΔB = bandwidth error	140 Hz	0.06
ΔG = gain factor error	0.03 dB	0.03
Δpad = pad value error	0.05 dB	0.05
Y-factor calculation worst-case error total		0.32

Table 2. Signal level adjustment errors

Error source	Value, dB
Precision attenuator	0.04
Test transmitter adjustments	0.05
Test transmitter step attenuator	0.05
Calibration signal level error (worst case)	0.14

Table 3. MGC Sampling and curve fitting errors

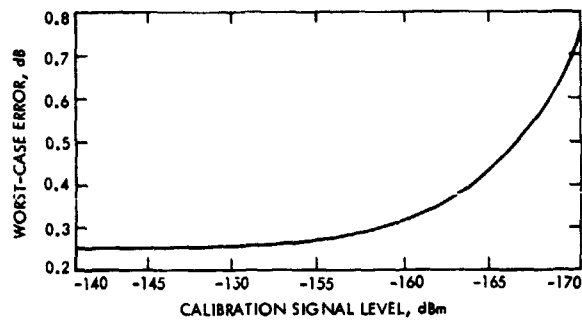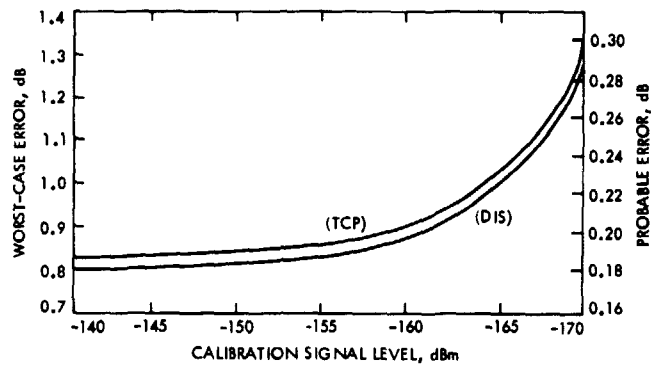| Error source	Value, dB	
MGC voltage adjustments	0.02	
AGC isolation amplifier	0.02	
Analog multiplexers and A/D's	(TCP) 0.06	(DIS) 0.04
Curve fitting	(TCP) 0.02	(DIS) 0.01
Worst-case total	(TCP) 0.12	(DIS) 0.09

Fig. 1. AGC voltage measurement error

Fig. 2. Total AGC calibration accuracy

Sequential Decoding in the Presence
of a Noisy Carrier Reference

J. R. Lesh
Network Operations

A new model for predicting the computational performance of a sequential decoder operating in a noisy carrier reference environment is described. The major difference between this model and previous models is that the new model characterizes the number of computations per frame as the sum of the computations resulting from a number of independent searches. This number of independent searches can then be considered as an effective frame length. When this computational model is averaged over noisy reference phase errors using a medium-rate interpolation scheme, the results are found to agree quite favorably with experimental measurements.

I. Introduction

Characterizing the computational behavior of a sequential decoder in the presence of a noisy carrier reference has long been recognized as a difficult problem. The first difficulty one encounters when undertaking such a study is to characterize the computational behavior of an ideal (noiseless carrier reference case) decoder. It was conjectured by Savage (Ref. 1) and subsequently verified many times experimentally that the number of computations required to decode one bit (or branch) behaves as a Pareto random variable. However, when using sequential decoding one must necessarily group the incoming data into blocks or frames, in which case the random variable of interest is the number of computations per frame rather than the number of computations per bit. Unfortunately, no satisfactory model for the distribution of computations per frame has been proposed to date. Some progress has been reported by Layland (Refs. 2 and 3) using curve fitting techniques of data produced by simulations. Such a technique has the obvious disadvantage of being valid only when the simulation conditions are reproduced, and furthermore, one often loses the insight afforded by more analytical models. In this paper we develop directly a model for the distribution of computations per frame which is based not on simulations but on convolutions of Pareto distributions (Section II). In Section III, we compare the results of this model to experimental data and link the two by considering a quantity called the effective frame length.

In Section IV we attack the second major difficulty associated with actual decoder performance modeling: i.e., the effects of a noisy carrier reference. We consider both high- and low-rate phase error effects upon the ideal decoder model developed previously. The final "real" decoder model results using a medium-rate technique developed by Tausworthe (Ref. 4). This final model is compared with experimental data in Section V, followed by conclusions in Section VI.

II. Convolutions of Pareto Distributions

Let C_1 represent the number of computations required for the decoder to decode (or advance) one bit. As previously stated, it is well known that the random variable C_1 approximately obeys the Pareto law; i.e.,

$$P_r\{ C_1 > L\} \approx L^{-\alpha} \tag{1}$$

where α is the Pareto exponent determined by

$$E_0(\alpha) = \alpha R_X \tag{2}$$

where $E_0(\alpha)$ is the random coding bound exponent function (Ref. 5) which depends implicitly on the signal-to-noise ratio and R_X is the code rate in bits per channel symbol. It is customary to plot computational distributions on log-log paper, in which case Eq. (1) represents a straight line with slope $-\alpha$. Now let C_F denote the number of computations required to decode a frame of F bits. Two models for the frame computational distribution which have been proposed in the past are

$$P_r\{C_F \geq L\} = FL^{-\alpha} \tag{3}$$

and

$$P_r\{ C_F \geq L\} = \left(\frac{L}{F}\right)^{-\alpha} \tag{4}$$

Equation (3) assumes that the accumulation of L computations occurs from a single long search, whereas Eq. (4) assumes that every bit requires exactly the same number of computations. Both of these expressions are clearly wrong since $P_r\{C_F \geq F\}$ is incorrectly predicted by Eq. (3) (except when $F = 1$ or $\alpha = 1$), and the assumption for Eq. (4) is clearly invalid. However, it is important to note that Eq. (3) represents a vertical shift of Eq. (1) by $\log F$ (on log-log paper), whereas Eq. 4 represents a horizontal shift of $\log F$. Both of these observations will become useful later.

With this background, let us consider the following construction. We assume that the computational distribution per bit is given by Eq. (1) (with equality). That is to say:

$$P_r\{C_1 = L\} = L^{-\alpha} - (L + 1)^{-\alpha} \tag{5}$$

Now, let us assume that the number of computations required to decode a frame of F_e bits (C_{F_e}) is given by the sum of F_e independent and identically distributed (i.i.d.) random variables each distributed according to Eq. (5). (This assumption will be modified later.) Then it is well known that the probability density function of C_{F_e} is given by the $(F_e - 1)$ fold convolution sum of Eq. (5). Figure 1 illustrates the results of such convolutions when the Pareto exponent $\alpha = 1.5$ and for various values of F_e. It is interesting to note that as the frame length F_e increases, the "Pareto-like" characteristic of C_{F_e} rapidly disappears with the appearance of a low end knee. Such a knee has been observed in experimentally determined distributions of computations per frame. Also of significance is the fact that all of the curves tend asymptotically to the result given in Eq. (3), with F replaced by F_e. Such behavior was predicted earlier by Sussman (Ref. 6). Figure 2 illustrates the behavior of the distribution of C_{F_e} as α varies (i.e., signal-to-noise ratio (SNR) varies) for $F_e = 192$.

In order to utilize these results, it is necessary to characterize the distribution of C_{F_e} without having to perform the convolutions each time. For the purpose of characterizing these distributions, a large number of Pareto distribution convolutions were performed at different values of α and F_e and the results studied. It soon became apparent that a pattern was emerging. In particular, it was noticed (at least for reasonably large F_e) that if one fixed the value of α and varied F_e, the point on each C_{F_e} distribution which had a tangent line parallel to the original Pareto distribution occurred at a value of L which was a constant multiple of F_e. In other words, given α and F_e sufficiently large, there exists a constant $K(\alpha)$ such that the tangent line to the distribution C_{F_e} at $L = K(\alpha)F_e$ has slope $-\alpha$. This point appears to be quite useful since it is quite close to the value of L for which the distribution of C_{F_e} begins to rapidly drop. Several values of $K(\alpha)$ are shown in Fig. 3. We note that $K(\alpha)$ can be well approximated by

$$K(\alpha) \exp \frac{1.54}{\alpha^{2.1}} \tag{6}$$

This approximation is also shown in Fig. 3.

Let us now consider the following model for the distribution of C_{F_e}. Given α and F_e let $P_r \{C_{F_e} \geq K(\alpha) \cdot F_e\} = 1$. At $K(\alpha) \cdot F_e$ let the model distribution begin dropping in a straight-line manner which best describes the rapid descent region of the convolved Pareto distribution. This amounts to letting the distribution be characterized as behaving initially as a Pareto distribution with exponent (say) α'. At the point where this straight-line distribution crosses the asymptotic distribution given by Eq. (3) we begin following the asymptotic distribution. By performing such constructions, we again find that the value of α' is also reasonably independent of F_e (for sufficiently large F_e). Several values of α' are shown in Fig. 4 along with an approximation given by

$$\alpha' \approx \alpha + \frac{3\,\alpha^{2.91}}{4} \qquad (7)$$

Combining these results we obtain the model for the distribution of C_{F_e} given by

$$P_r \{C_{F_e} \geq L\} = \begin{cases} 1 \; ; \; L < K(\alpha)F_e \\[2mm] \left[\dfrac{L}{K(\alpha)F_e}\right]^{-\alpha'} \; ; \; K(\alpha)F_e \leq L < L^* \\[2mm] F_e\,L^{-\alpha} \; ; \; L^* \leq L \end{cases} \qquad (8)$$

where

$$L^* = exp\left\{\frac{\alpha'\ln[K(\alpha)F_e] - \ln F_e}{(\alpha' - \alpha)}\right\} \qquad (9)$$

Figure 5 compares the results of the model with the corresponding Pareto distribution convolutions for $F_e = 64$ and $\alpha = 1.0$ and $\alpha = 1.5$. It is interesting to note that a similar type of model (i.e., Pareto distribution with discontinuous α) has been used in the past by Berger and Mandelbrot (Ref. 7) for characterizing the distribution of sequences of intererror gaps in telephone lines.

We will find it useful to scale the results of our model by the frame length F_e. In particular we let

$$N = \frac{L}{F_e} \qquad (10)$$

represent the average number of computations per bit (when a frame of F_e is decoded using L computations). It should be noted that N is quite different from the ensemble average of the random variable representing the number of computations per bit. For example, for any values of L and F_e, N is defined as their ratio. On the other hand, the average of the number of computations per bit is a fixed number and may be either finite or infinite depending on the value of α. In terms of N, our model for the distribution of C_{F_e} becomes

$$P_r \{C_{F_e} \geq N \cdot F_e\} = \begin{cases} 1 \; ; \; N < K(\alpha) \\[2mm] \left[\dfrac{N}{K(\alpha)}\right]^{-\alpha'} \; ; \; K(\alpha) \leq N < N^* \\[2mm] F_e^{1-\alpha}\,N^{-\alpha} \; ; \; N^* \leq N \end{cases} \qquad (11)$$

where

$$N^* = exp\left\{\frac{\alpha'\ln K(\alpha) + (\alpha-1)\ln F_e}{\alpha' - \alpha}\right\} \qquad (12)$$

III. The Concept of Effective Frame Length

Now that we have a model for the distribution of C_{F_e} let us see if it can be used to predict sequential decoder performance. To accomplish this, the model in Eq. (11) was compared with experimentally determined frame computation distributions provided by Layland (Ref. 8). Figure 6 illustrates this comparison where we notice immediately that the value of F_e for which the model approximates the experimental result is very much smaller than the frame length F used in the experiment. In fact, it appears in Fig. 6 (as well as in essentially all other comparisons made but not included in this paper) that the value of F_e that one should use is

$$F_e \approx \frac{F}{50} \qquad (13)$$

Indeed, this result appears to have been a significant factor in improving the accuracy of the model.

Let us reflect upon what Eq. (13) is telling us. Recall that in Section II F_e was used to determine the number of convolutions which we performed. Consequently, F_e, which we shall interpret as the "effective frame length," represents the number of independent searches made by the decoder. Recall also that a characteristic of the Pareto distribution is that a single long search of length L is more likely than two searches of length $L/2$. However, a single

long search covering the entire distance L is also very unlikely. Consequently, one would expect that within a frame of reasonable length there should be several long searches. Equation (13) tells us that, within a frame, approximately 2% of the bits in the frame result in long searches.

It can be argued that F_r should depend on α. Indeed this surely seems plausible and certainly a model for F_r showing this dependence would be an improvement. However, there are certain factors which make the exact selection of F_r less critical. At large α there is a good separation between lines of different F_r, and consequently Eq. (13) can be visually justified. As α approaches unity, all of the lines of F_r collapse into the same line. Consequently, any value of F_r will work in this region. In the interval $0 < \alpha < 1$, the different F_r curves again separate, except this time with the larger values of F_r on top. However, probabilities are always constrained to be not more than one, so that there is a limit to the separation that can occur for this region of α's. Furthermor peration of decoders at these values of α usually occurs n relatively small probability, so that if one is interesteu in average performance, the error contributions resulting from the region $0 < \alpha < 1$ are usually quite small.

IV. The Effects of a Noisy Carrier Reference

When sequential decoders are used in data links involving phase-coherent carrier tracking, one must not only determine the operating characteristics of the decoder but must also determine the effect that the carrier tracking loop has on the decoder as well. There are two cases where these effects can be quite easily determined. The first of these, called the low-rate model, occurs when the data rate is so small relative to the carrier tracking loop bandwidth W_L (two-sided) that one can consider that the tracking loop phase error process $\phi(t)$ varies very rapidly over a sequential decoder bit (branch). In this case, cne can compute the effective or degraded symbol energy to noise ratio $\overline{R}$ from

$$\overline{R} = R\,[\,E\,\{\cos\phi\,(t)\}\,]^2 \tag{14}$$

where R is the input symbol SNR. Lindsey (Ref. 9) has shown that Eq. (14) can be expressed as

$$\overline{R} = R\left[\frac{I_1\,(\rho_L)}{I_0\,(\rho_L)}\right]^2 \tag{15}$$

where $I_v(\cdot)$ is the vth order modified Bessel function and ρ_L is the carrier loop signal to noise ratio. Now, using $\overline{R}$ one can determine the appropriate random coding error exponent function $E_0(\cdot)$, and then from Eq. (2) the value of the Pareto exponent can be determined. Since we recognize that α depends on the signal-to-noise ratio we shall designate the low-rate Pareto exponent as $\alpha\,(\overline{R})$. Finally, the low-rate model is obtained by using Eq. (11) with α replaced by $\alpha\,(\overline{R})$.

At the opposite extreme, consider the case where the data rate is so high relative to W_L that one can consider the phase error process $\phi(t)$ as being constant over the entire sequential decoder frame. In this case one creates a high-rate model by computing $\alpha(R\cos^2\phi)$, where ϕ is a random variable distributed as $\phi(t)$. Viterbi (Ref. 10) has shown that this ϕ has a density function given by

$$p(\phi) = \frac{\exp(\rho_L\cos\phi)}{2\,\pi\,I_0(\rho_L)} \tag{16}$$

Thus, the high-rate model becomes

$$P_r(C_F \geq N \cdot F) = \int_{-\pi}^{\pi} P_r\{C_F \geq N \cdot F | \phi\}\,P(\phi)\,d\phi \tag{17}$$

Unfortunately, in many cases the data rate is such that neither the high or low rate assumptions are justified. When this situation occurs one uses some type of interpolation scheme to interpolate between the high- and low-rate models. The one we shall use is the method developed by Tausworthe (Ref. 4).

The usual problem one encounters when attempting to use this method or any other interpolation model originally developed for uncoded or block coded data, is determining the effective integration time T_M of the sequential decoder. It appears that a great deal of insight into the characterization of T_M can be gained by using the effective frame length developed in the previous section. To understand this, recall that L represents the total number of computations required to decode a frame of length F. Furthermore, we assume that there are F_r long (and independent) searches. For the remaining $(F - F_r)$ bits in the frame let us assume that each bit is decoded using only one computation. Thus, for these $(F - F_r)$ bits the effective integration time T_M, is simply the time per bit T_b. If this is true, then the F_r long searches must accumulate

a total of $L - F + F_e$ computations. Thus, for the bits in this group there is an average number of computations per bit (N') given by

$$N' = \frac{L - F + F_e}{F_e} \qquad (18)$$

In order to convert N' to a time we will use the "full tree" assumption suggested by Layland (Ref. 3). This assumption essentially says that if a long search occurs, the search pattern is more likely to look like a full tree search rather than a long search along a single wrong path. Since the average branch depth in a full binary tree containing N' branches is $\log_2 (1 + N'/2)$ the average integration time T_{M_2} for the long search bits is

$$T_{M_2} = T_b \log_2 \left(\frac{L - F + 3F_e}{2F_e} \right) \qquad (19)$$

Let us now apply the Tausworthe interpolation separately to the short and long searches. Toward this end let P_L and P_H represent the results computed from the low- and high-rate models respectively. Then we have

$$P_i(C_F \geq N \cdot F) = (1 - a_i) P_L + a_i P_H, i = 1,2 \qquad (20)$$

where

$$a_i = \frac{\delta_i}{4} \left[1 - \frac{\delta_i}{8} \left(1 - e^{-\frac{8}{\delta_i}} \right) \right] \qquad (21)$$

$$\delta_i = \frac{2}{W_L T_{M_i}} \qquad (22)$$

and where $P_i (C_F \geq N \cdot F)$, $i = 1,2$ represent the medium-rate estimates of the computations distribution for the short and long search bits respectively. Then, if we average $P_i (C_F \geq N \cdot F)$, $i = 1,2$ over the times during which each result applies we obtain the final estimate $\hat{P}(C_F \geq L)$ given by

$$\hat{P}(C_F \geq L) = \left(\frac{F - F_e}{L} \right) [P_1 (C_F \geq L) - P_2 (C_F \geq L)]$$
$$+ P_2 (C_F \geq L) \qquad (23)$$

V. Comparison of Predicted and Experimental Results

The real test of a model is its ability to predict performance under real decoding conditions. In order to

make such a comparison, data from DSS 71 (Ref. 11) as well as data from DSN System Performance Tests (SPTs), were compared with our model. Actually, a slightly more complex version of the model was used. In particular, the independent search computations distribution model given by Eq. (11), which is a two-straight-line model, was replaced by a three-line model constructed from the two-line result. The construction procedure is illustrated in Fig. 7 and results in a model given by

$$P_r \{ C_{F_e} \geq N \cdot F_e \} = \begin{cases} 1 ; N < N_0 \\ \left(\dfrac{N}{N_0} \right)^{-\alpha_1} ; N_0 \leq N < N_1 \\ \left[\dfrac{N^*}{K(\alpha)} \right]^{-\frac{\alpha'}{2}} \left(\dfrac{N}{N_1} \right)^{-\alpha_2} ; N_1 \leq N < N_2 \\ F_e^{1-\alpha} N^{-\alpha} ; N_2 \leq N \end{cases} \qquad (24)$$

where

$$N_0 = \sqrt{K(\alpha)} \qquad (25)$$

$$N_1 = \sqrt{K(\alpha) N^*} \qquad (26)$$

$$N_2 = \left[\frac{(N^*)^3}{K(\alpha)} \right]^{1/4} \qquad (27)$$

$$\alpha_1 = \frac{\alpha' \log \left[\dfrac{N^*}{K(\alpha)} \right]}{\log N^*} \qquad (28)$$

and

$$\alpha_2 = \frac{-\log [F_e^{1-\alpha} (N^*)^{-\alpha}]}{\log \left[\dfrac{N^*}{K(\alpha)} \right]} + \frac{\alpha - \alpha'}{2} \qquad (29)$$

However, the use of Eq. (24) produces only slight differences in the predictions relative to the two-line model.

Whenever comparing theoretical predictions with data taken in the DSN, one must be careful to separate the loss or degradation resulting from the carrier tracking loop from those occurring in the rest of the system (specifically the subcarrier tracking loop and symbol tracking loop). To accomplish this, a telemetry analysis computer program created by Dunn (Ref. 12) was used to determine system and subsystem losses. Those losses which did not

occur as a result of the carrier tracking loop were considered as degradations on the symbol energy-to-noise ratio.

Figure 8 illustrates the closeness of the predicted values to data provided from Ref. 11. These data were obtained using the Helios frame length of 1152, and each curve is characterized by the bit rate, modulation index and total-power-to-noise-density ratio P_T/N_0. In Fig. 9 we see the comparison of our model with data provided by the SPTs, also for a frame length of 1152. In this figure, the separate curves are characterized by the bit rate, modulation index and the symbol error rate (SER). It is believed that the separate curves can be more accurately characterized by using the SER since this quantity is directly measurable.

In Fig. 10 we see the comparison of the predicted result with experimental results for the Pioneer frame length of 192. Here we see a reasonable separation between the theoretical and experimental values. It is believed that this difference is a result of characterizing the distribution of C_{r_e}. Recall that if we use the 2% figure to relate the actual and effective frame lengths, then for Pioneer we are using an effective frame length of less than 4. However, it was stated that Eq. (11) (or, equivalently, Eq. 24) was a good approximation only for sufficiently large F_e. It is therefore believed that a more accurate model for the distribution of C_{r_e} is needed at the Pioneer effective frame lengths if one is to perform better estimates than are indicated in Fig. 10.

VI. Conclusions

We have seen that the performance of an ideal sequential decoder can be quite accurately predicted by considering a number of convolutions of Pareto distributions. We then found that the number of such convolutions could be interpreted as an effective frame length. The effective frame length proved not only useful in characterizing the ideal decoder but also provided much insight into determination of the medium-rate interpolation parameters used in characterizing real decoders operating in a noisy carrier reference environment. Although predictions for Pioneer frame lengths were found to be somewhat in error, the accuracy at longer frame lengths appears to be quite satisfactory.

Acknowledgment

The author wishes to express his appreciation for the comments, advice and experimental data provided by J. W. Layland.

References

1. Savage, J. E., "Sequential Decoding – The Computational Problem," *Bell System Tech. J.*, Vol. 45, pp. 149–174, 1966.

2. Layland, J. W., "Sequential Decoding with a Noisy Carrier Reference," in *The Deep Space Network Progress Report*, Technical Report 32-1526, Vol. XII, pp. 167–175, Jet Propulsion Laboratory, Pasadena, Calif., Dec. 15, 1972.

3. Layland, J. W., "A Sequential Decoding Medium Rate Performance Model," in *The Deep Space Network Progress Report*, Technical Report 32-1526, Vol. XVIII, pp. 29–40, Jet Propulsion Laboratory, Pasadena, Calif., Dec. 15, 1973.

4. Tausworthe, R. C., "Communications Systems Development: Efficiency of Noisy Reference Detection," in *The Deep Space Network*, Space Programs Summary 37-54, Vol. III, pp. 195–201, Jet Propulsion Laboratory, Pasadena, Calif., Dec. 15, 1968.

5. Gallager, R. G., *Information Theory and Reliable Communication*, John Wiley, New York, 1968.

6. Sussman, S. M., "Analysis of the Pareto Model for Error Statistics on Telephone Circuits," *IEEE Trans. Comm. Systems*, pp. 213–221, June 1963.

7. Berger, J. M., and Mandelbrot, B., "A New Model for Error Clustering in Telephone Circuits," IBM J. Res. Dev., Vol. 7, pp. 224–236, July 1963.

8. Layland, J. W., "Performance of an Optimum Buffer Management Strategy for Sequential Decoding," in *The Deep Space Network Progress Report*, Technical Report 32-1526, Vol. IX, pp. 88–96, Jet Propulsion Laboratory, Pasadena, Calif., June 15, 1972.

9. Lindsey, W. C., "Performance of Phase-Coherent Receivers Preceded by Bandpass Limiters," *IEEE Trans. Comm. Tech.*, Vol. Comm-16, No. 2, April 1968, pp. 245–251.

10. Viterbi, A. J., *Principles of Coherent Communication*, McGraw Hill, New York, 1966.

11. Layland, J. W., "DSS Tests of Sequential Decoding Performance," in *The Deep Space Network Progress Report 42-20*, pp. 69–77, Jet Propulsion Laboratory, Pasadena, California, April 15, 1974.

12. Dunn, G. L., "Conversational Telemetry Analysis Program," IOM 421E-74-108, May 1974 (JPL internal document).
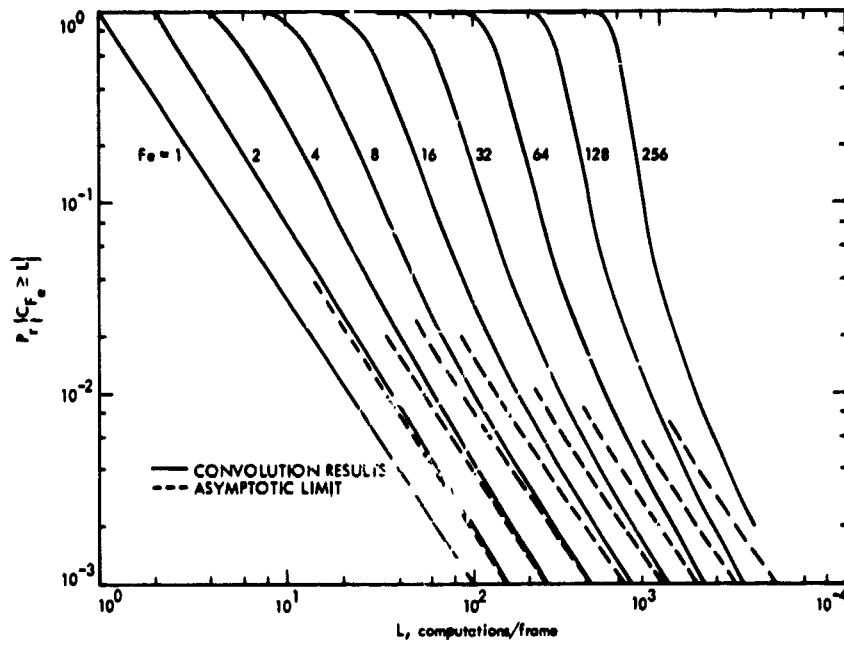
Fig. 1. Distribution of computations resulting from $(F_e\text{-}1)$ convolutions of Pareto distribution $\alpha = 1.5$ (dashed lines indicate asymptotic result of Eq. 3)

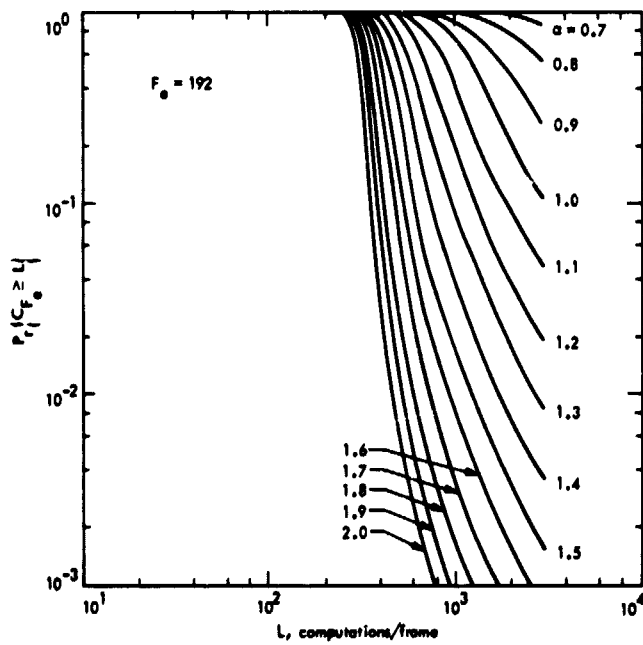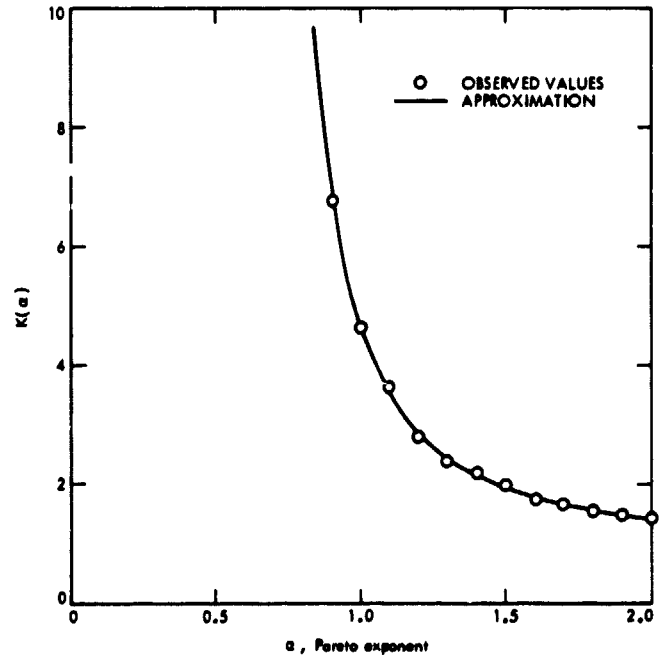Fig. 2. Distribution of computations for independent searches, $F_e = 192$
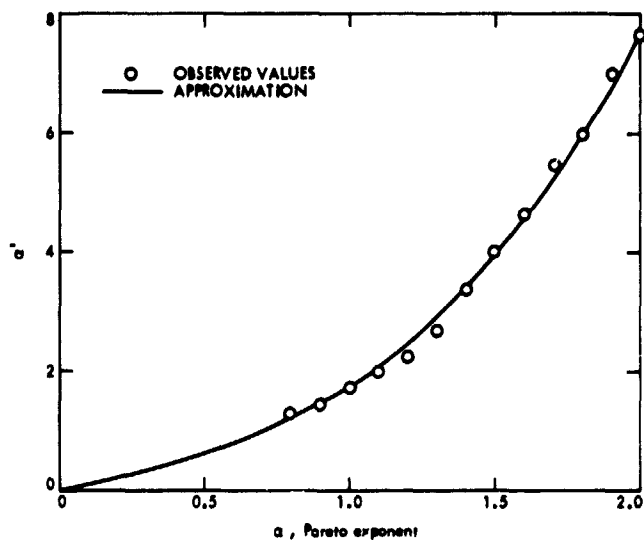

Fig. 3 Characterization of $K(\alpha)$
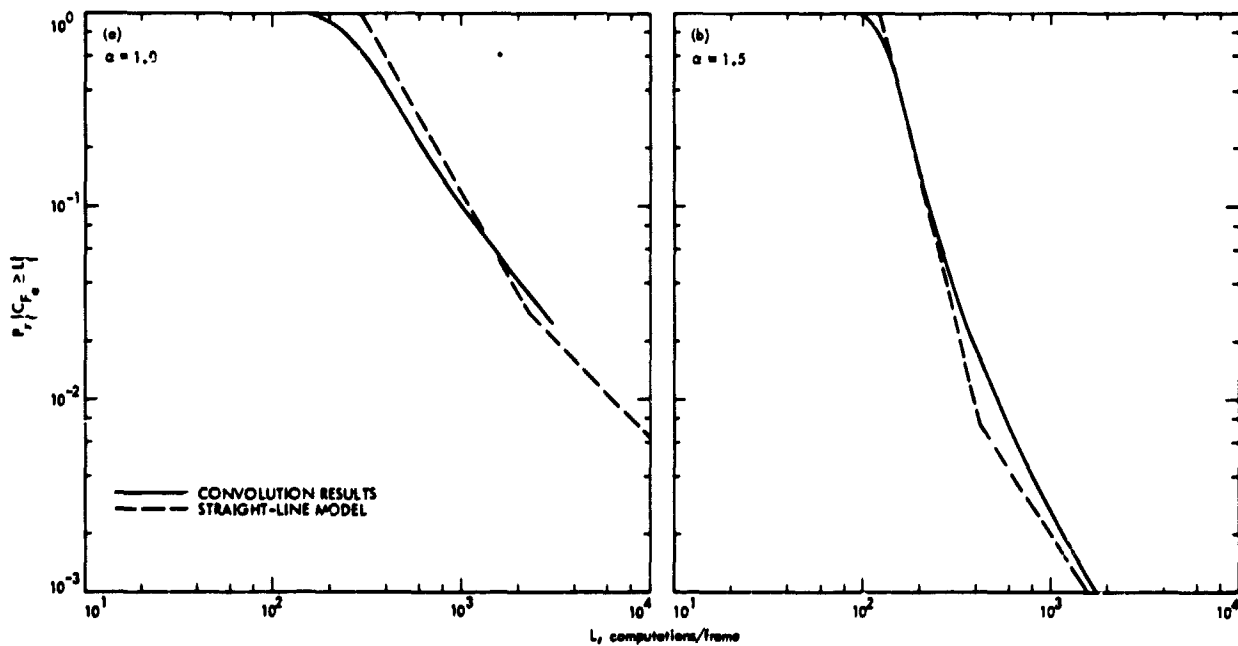
Fig. 4. Characterization of α'

Fig. 5. Comparison of Pareto convolutions and straight-line model for $F_e = 64$ and (a) $\alpha = 1.0$, (b) $\alpha = 1.5$
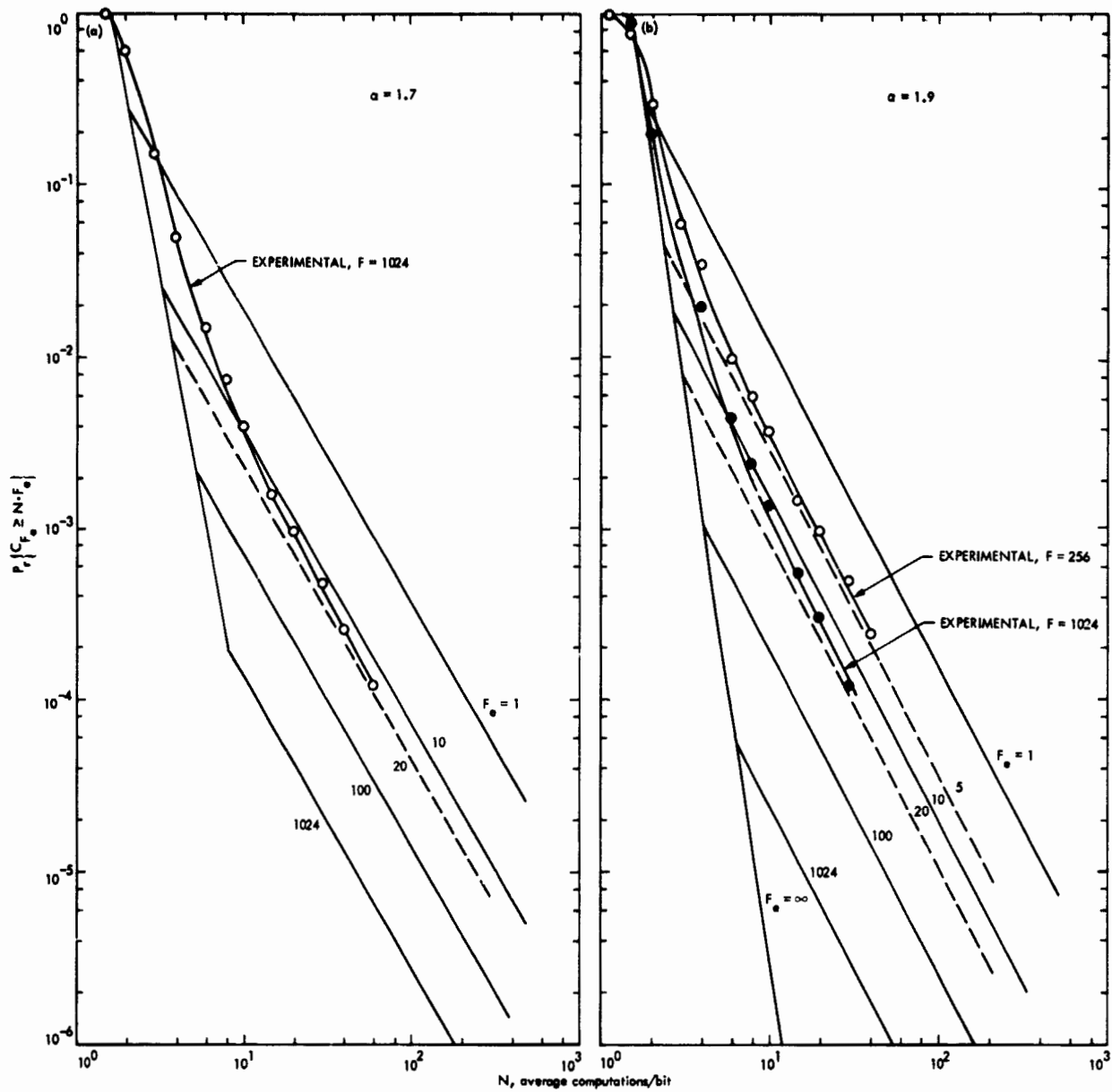
Fig. 6. Comparison of actual decoder computations distribution with straight-line model for (a) $F = 1024$, $\alpha = 1.7$, (b) $F = 256$ and $F = 1024$, $\alpha = 1.9$
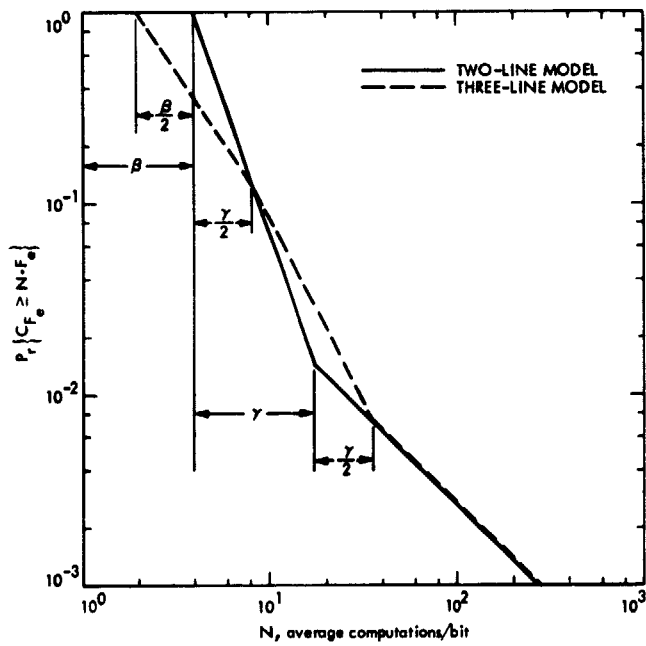
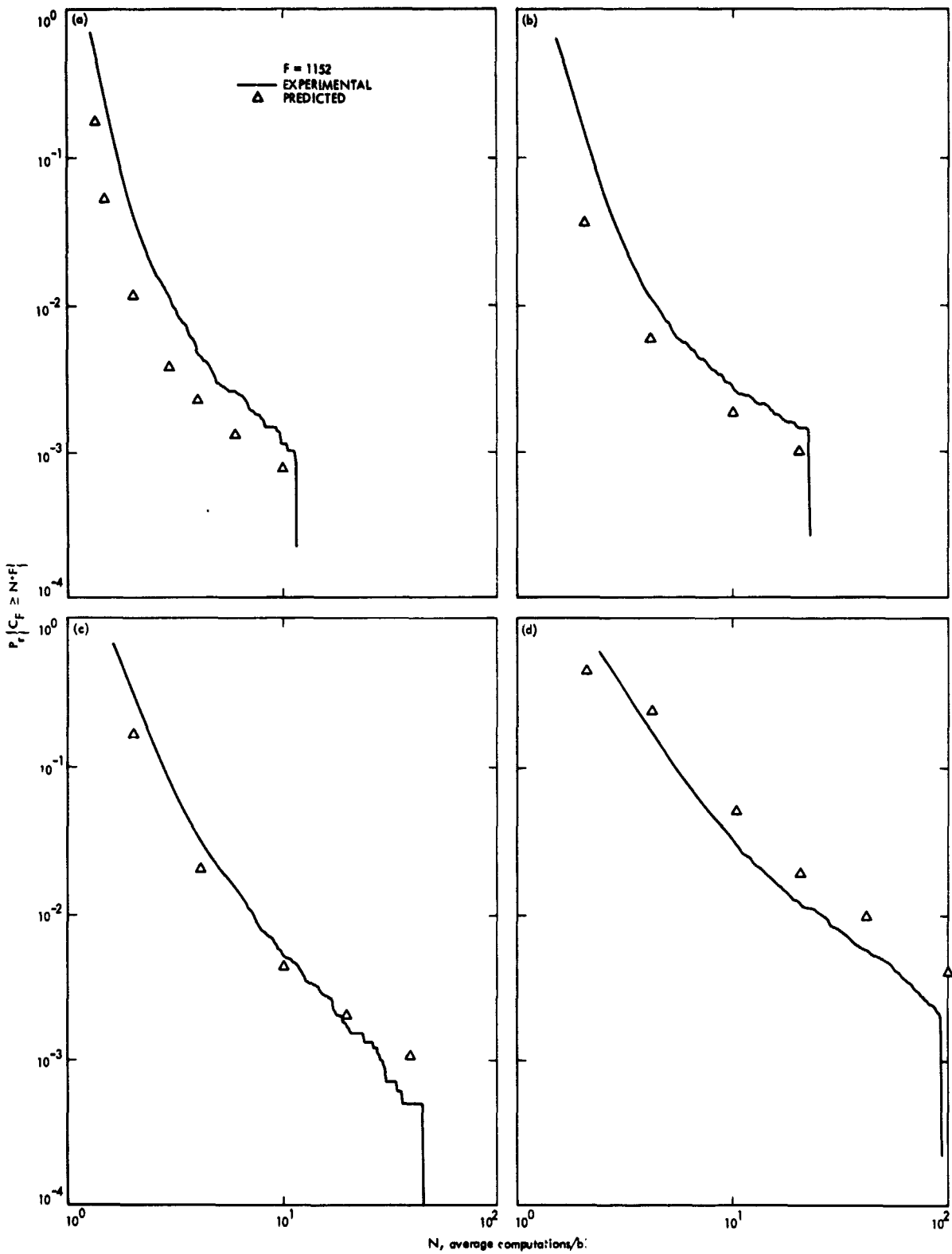Fig. 7. Construction method for three-line model

Fig. 8. Comparison of medium-rate model with actual noisy reference decoder for frame length 1152 and (a) 2048 bps, $P_T/N_0 = 39.1$ dB, mod index = 67.5 deg, (b) 1024 bps, $P_T/N_0 = 36.3$ dB, mod index = 60.0 deg, (c) 512 bps, $P_T/N_0 = 34.1$ dB, mod index = 48.0 deg, (d) 256 bps, $P_T/N_0 = 31.4$ dB, mod index = 42.0 deg
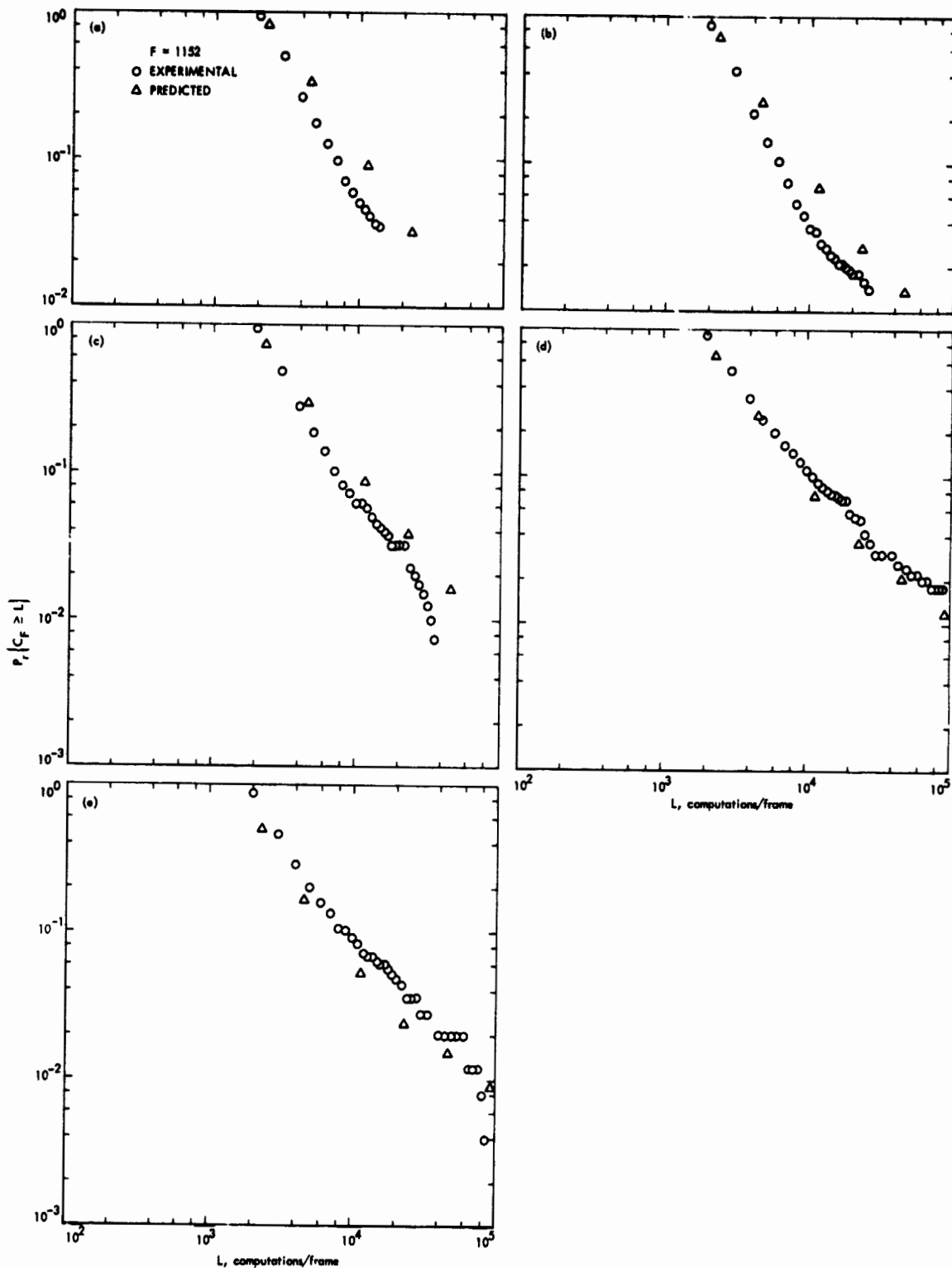
Fig. 9. Comparison of medium-rate model with actual noisy reference decoder for frame length 1152 and
(a) 2048 bps, SER = 8.0%, mod index = 54.6 deg, (b) 1024 bps, SER = 7.7%, mod index = 54.6 deg,
(c) 512 bps, SER = 7.9%, mod index = 54.6 deg, (d) 256 bps, SER = 7.9%, mod index = 54.6 deg,
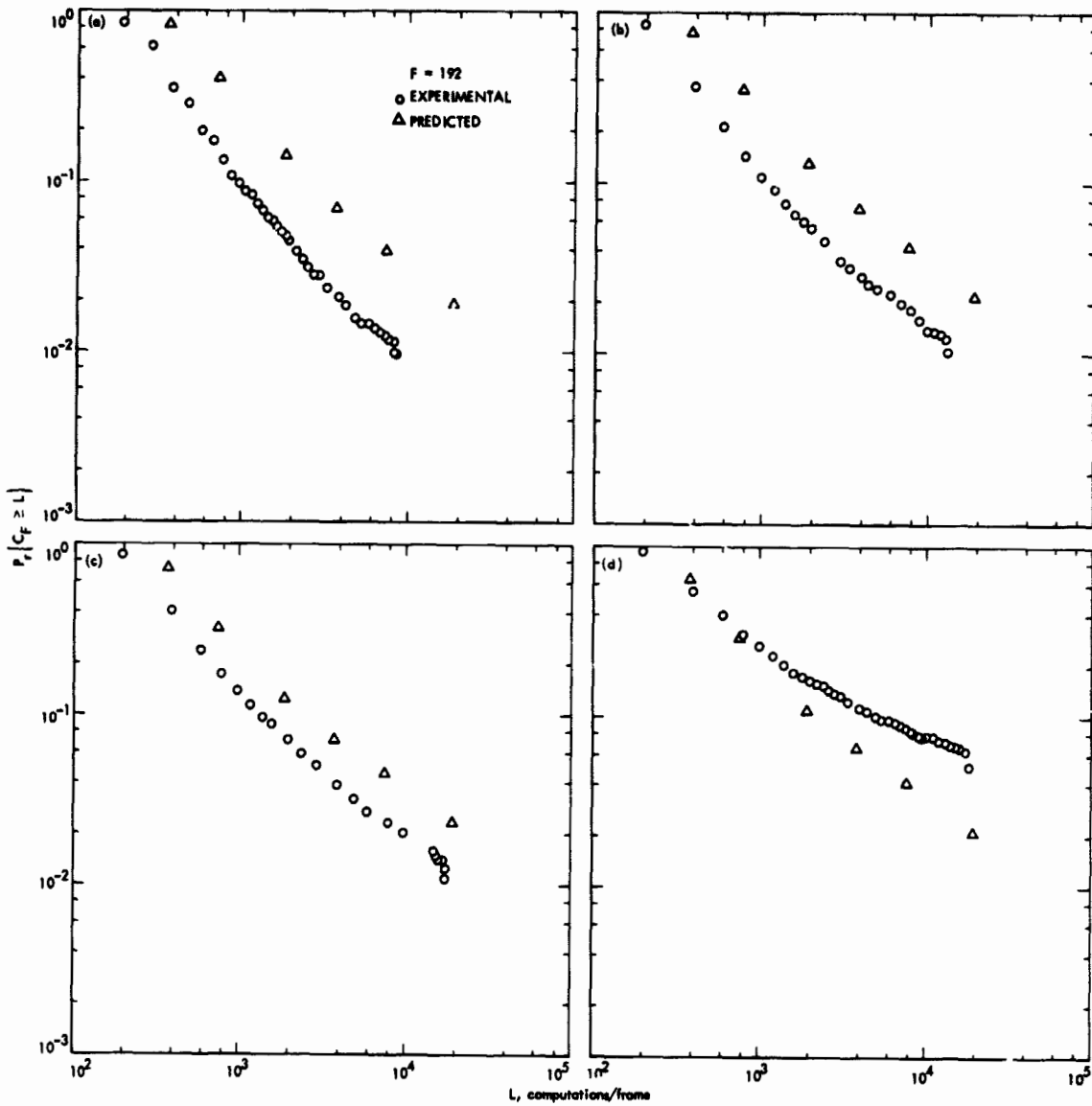(e) 128 bps, SER = 7.5%, mod index = 54.6 deg

Fig. 10. Comparison of medium rate model with actual noisy reference decoder for frame length 192 and (a) 2048 bps, SER = 8.2%, mod index = 66.5 deg, (b) 1024 bps, SER = 8.1%, mod index = 66.5 deg, (c) 512 bps, SER = 8.2%, mod index = 66.5 deg, (d) 256 bps, SER = 8.5%, mod index = 66.5 deg

Real-Time High-Rate Telemetry Support of Mariner 10 Operations

J. T. Hatch
J. W. Capps
Network Operations

Television pictures from the Mariner 10 spacecraft were received and displayed in real-time at JPL during important phases of the MVM'73 mission. In order for the DSN to support this activity, the telemetry data processing equipment at DSS 14 had to be modified and a special microwave super group channel established between the station and JPL to handle transmission of the high rate (117.6 kbps) data. How this capability was implemented and operated by the DSN is described in this article.

I. Introduction

The approved Mariner Venus/Mercury 1973 (MVM'73) mission profile established a requirement for real-time evaluation at JPL of spacecraft uncoded 117.6-kbps high-rate telemetry data (video pictures). Mission events which called for real-time transmission of the 117.6-kbps data were as follows:

Mission event	Date or period
Earth-Moon television system calibration	Mid-November 1973
TV scan calibrations	November through January 1974
Kohoutek comet pictures	January 1974
Venus encounter	February 1974
Mercury encounter	March 1974

To meet the requirement, the DSN established a 230.4-kbps data transmission capability between DSS 14 and JPL, with the Western Union (WU) leased portion of this capability being known as the 240-kHz super group microwave channel.

At DSS 14, a word formatter assembly was provided by the project to receive the 117.6-kbps data from the symbol synchronizer assembly (SSA) of the Telemetry and Command Data (TCD) Subsystem and arrange the data in a nonblocked, synchronous word-formatted mode for forwarding to the station's Ground Communications Facility (GCF) interface. The data were then transmitted via the GCF and the WU-leased super group microwave channel to the Mission Control and Computing Center (MCCC) at JPL for processing and display of the pictures on television monitors.

As an added feature, during the Mercury encounter the capability was provided to transmit the pictures from JPL

to NASA Headquarters and Goddard Space Flight Center (GSFC), where they were also displayed on television monitors in real-time.

II. Description of Capabilities

A. Basic Data Handling Configuration

The basic configuration of this real-time data handling capability is depicted in Fig. 1 and includes the DSS 14, MVM'73 Project, GCF and MCCC equipment and interfaces indicated below.

(1) DSS 14

    (a) Symbol Synchronizer Assembly (SSA).

    (b) SSA word formatter switch and word formatter (Project-supplied).

    (c) 230.4-kbps Wideband Data Assembly (WBDA) which included wideband (WB) patch panels, General Electric Time Division Multiplex (GE TDM) 522 data set/modems, and bit error rate tester (BERT) 901.

(2) GCF switching center at Goldstone (GCF 10).

    (a) Dual Area Microwave Assembly (AMWA) radio channels.

    (b) 230.4-kbps WBDA (same as DSS 14).

    (c) Western Union (WU) leased GE TDM 501 data sets.

    (d) WU-leased GE TDM 520 modems.

(3) GCF 10 to GCF 20 intersite transmission (WU-leased 240-kHz super group microwave channel).

(4) GCF switching center at JPL (GCF 20).

    (a) WU-leased GE TDM 501 data sets.

    (b) WU-leased GE TDM 520 data sets.

    (c) 230.4-kbps WBDA, which included WB patch panels, BERT 901, and line driver amplifiers.

(5) MCCC

    (a) Mission Test Computer Facility (MTCF) communications interface patch panel.

    (b) Word deformatter.

    (c) MTCF 1230 computer.

    (d) Project/Mission Control Computing Facility (MCCF) Television Assembly (TVSA).

B. Wideband Data Transmission Capability

The wideband portion of the capability depicted in Fig. 1 was engineered and installed by the Ground Communications System Engineering Group of the DSN Data Systems Development Section as the 230.4-kbps WBDA under Engineering Change Order (ECO) Number 72-224. It was used to support MVM'73 test and mission operations activities from July 1973 through April 1974. The main features of the 230.4-kbps WBDA are the following capabilities that it provided:

(1) A full duplex 230.4-kbps data transmission capability. The data were routed from DSS 14 to GCF 10, utilizing dual Area Microwave Assembly radio channels and a WU-leased 240-kHz super group microwave channel between GCF 10 and GCF 20.

(2) Redundant equipment to provide a backup to prime equipment.

(3) Full duplex end-to-end testing capability utilizing loopback techniques and special 230.4-kbps bit error rate testing equipment known as the BERT 901.

(4) Equipment necessary to provide a compatible interface with Project-supplied equipment and MCCC assemblies.

C. NASA Headquarters/GSFC Television Configuration

In March 1974, a requirement was established by the Office of Space Science Applications, NASA Headquarters, to provide some real-time Mercury encounter pictures to NASA Headquarters and GSFC. The configuration shown in Fig. 2 was used to meet this requirement. The system was active for a total of 10 h and 30 min, which included 2-½ h of testing and 8 h of prime Mercury encounter picture transmissions.

III. System Installation and Checkout

A. Schedules

The 230.4-kbps Wideband Data Assembly installation began approximately June 1, 1973. The GCF portion (WU-leased 240-kHz super group microwave channel and GCF MCCC/Project cable interface) was completed during the first week of July 1973. This wideband system, along with the DSS 14 GCF/Project word formatter and the JPL GCF/MCCC word deformatter interfaces, was tested during the last three weeks of July and declared operable on August 1, 1973.

B. Problem Areas

The GCF experienced almost no technical or installation problems in the establishment of the DSS 14-to-JPL 230.4-kbps capability. In fact, the hardware performance and test results exceeded all expectations. All GCF installation and checkout schedules were met; however, a minor problem was experienced with Western Union and General Electric in assuring that the July 1, 1973, committed date for completion of the GCF 10-to-JPL leased 240-kHz super group installation was met. A slip in the July 1, 1973, date was averted by the JPL Communications and Supply Section's direct coordination with the Vice Presidents of Western Union and General Electric, to effect a speedup of deliveries of the 230.4-kbps data set/modems from General Electric to Western Union.

C. Test Results

The GCF provided a full duplex end-to-end testing capability for the 240-kHz super group, with an additional microwave link test capability at GCF 10. BERT 901's were provided to DSS 14, GCF 10 and GCF 20. This test capability allowed the GCF to transmit a 2047-bit pseudo-random pattern in both directions for channel performance validation.

The GCF established an allowable bit error rate of 1×10^{-5} as the test criteria for circuit validation. To meet the bit error rate objective at a line transmission rate of 230.4 kbps, a 5-min bit error rate count end-to-end for both links could not exceed 700 bits in error. The following formula was used to calculate bit error rates:

$$\frac{\text{bit error count}}{\text{block count} \times \text{block size}} = \text{error rate}$$

(Note: block size equaled 99999 bits in each test.) Results of testing conducted on October 25, 1973, on the prime 230.4-kbps wideband circuit between DSS 14 and GCF 20 are tabulated in Table 1.

IV. Operational Performance

A. General

This mission-dependent high-rate telemetry data handling and transmission system performed exceptionally well. Of the approximately 9000 pictures obtained through the Mercury encounter, some 5000 were processed and displayed at JPL in real-time. Those pictures not received from DSS 14 via the 230.4-kbps Wideband System were received from the overseas 64-m stations (DSS 43 at Canberra, Australia, and DSS 63 at Madrid, Spain) via the 28.5-kbps wideband circuits, or were processed directly from the digital original data records that were shipped from the DSSs to JPL.

B. Data Quality

The quality of the pictures received during Venus encounter was excellent, averaging an approximate bit error rate of 1×10^{-5}, or one bit in error for every 100,000 bits received. For Mercury encounter, the bit error rate averaged approximately 2.5×10^{-5}. The 230.4-kbps Wideband System equaled or exceeded all established performance specification during both encounters. Had the system added significantly to the bit error rate, especially during periods of marginal spacecraft telecommunications performance at Mercury encounter, the Project would have had degraded data.

C. DSN Support

DSN support of the Mariner 10 real-time 117.6-kbps high-rate telemetry data retrieval effort was based on a "best efforts" commitment and low cost implementation. Nevertheless, during DSN/Ground Data System (GDS)/MCCC prelaunch testing, the only problems experienced were minor ones encountered at DSS 14 with the word formatter. Furthermore, throughout the mission and especially during the critical Venus and Mercury encounter sequences, the system functioned reliably and with a minimum amount of downtime.

The real-time 117.6-kbps high-rate telemetry data retrieval capability was de-implemented following Mercury encounter. Subsequently, however, the decision was made to provide the same support for the second Mercury encounter, the closest approach of which occurs on September 21, 1974. All equipment modifications and installations were completed at DSS 14 and DSC 10 by mid-August, and arrangements made for lease of the DSC 10 to the JPL 230.4-kbps super group microwave channel for the month of September 1974. DSN/GDS/MCCC testing is scheduled to be completed by September 15, 1974.

D. Operational Constraints

Despite the success indicated above, certain features of this capability were undesirable from an operations support standpoint. For example, at the station and throughout the GCF interfaces, little or no capability existed for on-line real-time monitoring of the system status; system design was such that standard DSN data and circuit

monitoring techniques could not be employed because of the nonstandard word formatted data transmission mode that was used.

These constraints required stopping the data flow and conducting off-line testing in order to troubleshoot the system when problems occurred. In addition, use of the mission-dependent word formatter assembly necessitated modifications at DSS 14 to interface this equipment with the SSAs and the 230.4-kbps WBDA. These nonstandard interfaces created an awkward operational situation at DSS 14 which was too troublesome to be acceptable on a long-term basis.

V. Conclusions

The MVM'73 high-rate telemetry data transmission system met its objectives in an impressive manner. Limitations and constraints imposed on the DSN by the system design were overcome and the system was operated successfully. If a similar system is to be used for future missions, then design and engineering effort should be expended in order to provide the DSN with a standard capability that is free of any constraints that could hamper successful DSN support of critical mission operations.

Table 1. 230.4-kbps wideband circuit test results

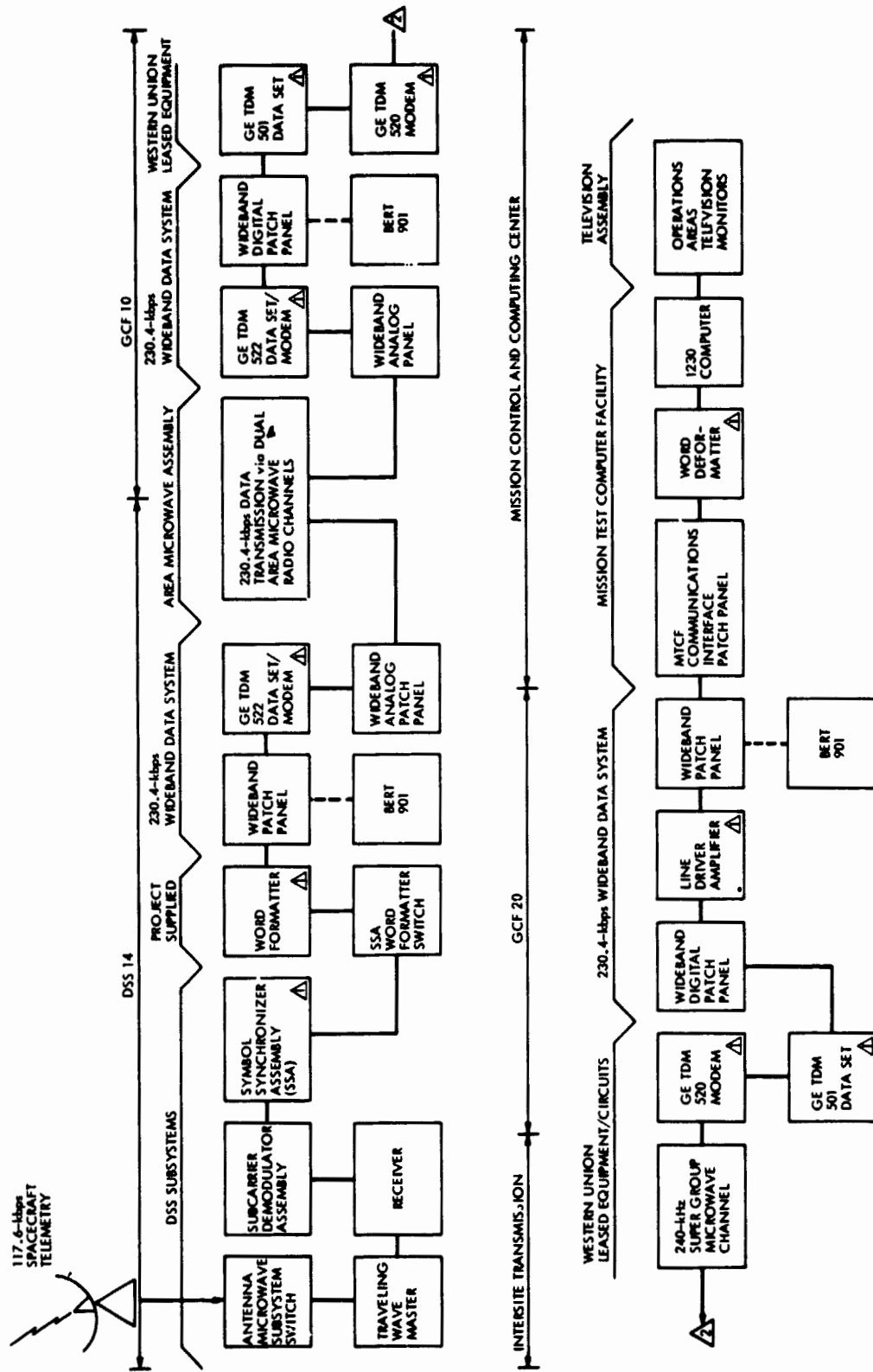| Test	Terminal	Duration, h	Bit error rate	Data, % throughout
Part 1	GCF 20	3	2.3×10^{-8}	99.999
Part 2	GCF 20	8	5.2×10^{-8}	99.998
Part 1	DSS 14	3	6.1×10^{-7}	99.975
Part 2	DSS 14	8	4.2×10^{-7}	99.983

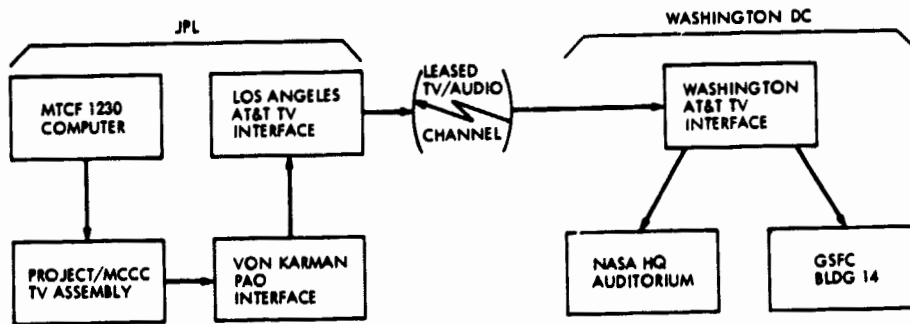Fig. 1. DSS 14 to JPL high-rate telemetry configuration

Fig.2. JPL-NASA Headquarters/GSFC real-time system configuration

Goldstone DSCC Energy Distribution Model

B. H. Chapman
TDA Planning Office

In expectation of increases in cost and decreases in supply of currently avail-able energy forms, the DSN is studying the installation of systems which will provide reliable Deep Space Communications Complex energy in stable amounts and at stable cost. One of the main factors in improving the economic viai.ility of such an installation is the efficiency with which the useful energy forms resulting from the conversion of the siable e.iergy form to be provided can be distributed to the consumers. The aim of the following general distribution model is to provide a method for the optimal design of a network for the distrib-tion of several different types of energy to users and for the optimal operation of such a network when installed. When such a network is operational the consumers' demand for energy can be ascertained by real-time sampling but during the design phase these energy demands are known only stochastically. The initial model below describes the case of known constant demand and will form the basis of a subse-quent model of the stochastic demand case. An algorithm to be used in the solution of this model problem is also outlined.

I. Mathematical Model I

In detail the situation to be modeled is as follows: Several plants and the related distribution system are to be constructed to serve the electrical, heating, and cooling needs of several established energy consumers whose demand for each energy form is constant and known. The possible locations of the plants are given, but the particular sites to be used are to be selected so as to result in the least total construction and operational cost. Each plant has a known cost function of its electrical capacity,

reflecting the initial capital cost plus the operational and maintenance cost over the expected lifetime of the plant. The heat output of each plant is the sum of two terms: (1) recovered waste heat, which is a known function of the plant's electrical output, and (2) heat obtained from fuel directly at a known cost. A portion of this heat output is then converted at a known cost and efficiency to chilled water for use in cooling. Each link of the distribution system has a known cost function of its capacity, and the losses in each link are known functions of the amount of energy traversing that link.

If a particular link is to be constructed, its capacity must lie between prescribed upper and lower bounds. The distribution system also allows for the transfer of electrical energy between plants, intermediate energy distribution nodes at various sites between plants and consumers, and substitution of electrical energy for heating and cooling energy at some known efficiencies and costs. Thus the problem is to determine which sites are to be used, what capacity plant to install at each selected site, and what the distribution pattern should be for each energy form. This is to be done so as to minimize the total construction and operational cost while satisfying the demands of each consumer and the capacity constraints on the distribution system.

In order to maintain a clear relationship between the physical problem and the following mathematical formulation, the variables and functions involved will all be triply subscripted. The first subscript refers to the level of the distribution system with which the variable or function is associated. The second and third subscripts refer, respectively, to the origin and destination within that level of the quantity described by the variable or function (Fig. 1).

A. System Variables

1. Level 0: Plant Variables. There are k possible sites for total energy plants (TEP) which derive electricity, heat, and chilled water from fuel. The variables are:

e_{00i} = electrical output of plant i

$H_{00i}(e_{00i})$ = recovered heat output function of plant i

h_{00i} = directly derived heat output of plant i

h_{0ii} = portion of heat output of plant i used for conversion to chilled water

$C_{0ii}(h_{0ii})$ = chilled water output function of plant i

e_{0ij} = electrical energy leaving plant i for plant j

$E_{0ij}(e)$ = electrical energy arriving at plant j when electrical energy e originated from plant i

2. Level 1: Primary Distribution Variables. The amounts of the three energy types leaving the plants and arriving at the l electrical consumers, m heating energy consumers, and n cooling energy consumers are:

e_{1ij} = electrical energy leaving plant i for electrical consumer j

$E_{1ij}(e)$ = electrical energy arriving at electrical consumer j when electrical energy e originated from plant i

c_{1ij} = cooling energy leaving plant i for cooling energy consumer j

$C_{1ij}(c)$ = cooling energy arriving at cooling energy consumer j when cooling energy c originated from plant i

h_{1ij} = heating energy leaving plant i for heating energy consumer j

$H_{1ij}(h)$ = heating energy arriving at heating energy consumer j when heating energy h originated from plant i

3. Level 2: Secondary Distribution Variables. Subsequent amounts of the three energy types distributed between consumers of the same energy type. The variables are:

e_{2ij} = electrical energy leaving electrical consumer i for electrical consumer j

$E_{2ij}(e)$ = electrical energy arriving at electrical consumer j when electrical energy e originated from electrical consumer i

c_{2ij} = cooling energy leaving cooling energy consumer i for cooling energy consumer j

$C_{2ij}(c)$ = cooling energy arriving at cooling energy consumer j when cooling energy c originated from cooling energy consumer i

h_{2ij} = heating energy leaving heating energy consumer i for heating energy consumer j

$H_{2ij}(h)$ = heating energy arriving at heating energy consumer j when heating energy h originated from heating energy consumer i

4. Level 3: Cooling Energy Substitution. Amounts of electrical energy from each electrical consumer used for substitution as cooling energy at each cooling energy consumer are:

e_{3ij} = electrical energy leaving electrical consumer i for substitution as cooling energy at cooling energy consumer j

$C_{3ij}(e)$ = cooling energy arriving at cooling energy consumer j when electrical energy e originated from electrical consumer i for substitution

5. Level 4: Heating Energy Substitution. Amounts of electrical energy from each electrical consumer used for substitution as heating energy at each heating energy consumer are:

e_{4ij} = electrical energy leaving electrical consumer i for substitution as heating energy at heating energy consumer j

$H_{4ij}(e)$ = heating energy arriving at heating energy consumer j when electrical energy e originated from electrical consumer i for substitution

B. Demands

e_j = electrical demand of electrical consumer j

c_j = cooling demand of cooling energy consumer j

h_j = heating demand of heating energy consumer j

It the energy input to a heating or cooling energy consumer exceeds the demand, the excess energy is dumped as waste. In order to keep the total system energy constant, this wasted energy is accounted for by the following *slack variables*:

c'_j = waste cooling energy dumped at cooling energy consumer j

h'_j = waste heating energy dumped at heating energy consumer j

(If consumer j is actually a dummy consumer representing a possible distribution node for electrical, cooling, or heating energy, then e_j or c_j and c'_j or h_j and h'_j, respectively, are set equal to 0).

C. Cost Functions

$\alpha_{00i}(e)$ = cost of installing electrical generation capacity e and waste heat recovery of capacity $H(e)$ at plant i

$\alpha_{0ij}(e)$ = cost of installing an electrical link of capacity e between plant i and plant j

$\alpha_{1ij}(e)$ = cost of installing an electrical link of capacity e between plant i and electrical consumer j

$\alpha_{2ij}(e)$ = cost of installing an electrical link of capacity e between electrical consumer i and electrical consumer j

$\alpha_{3ij}(e)$ = cost of installing an electrical substitution link taking electrical energy e from electrical consumer i to cooling energy consumer j and converting it to provide cooling energy $C_{3ij}(e)$

$\alpha_{4ij}(e)$ = cost of installing an electrical substitution link taking electrical energy e from electrical consumer i to heating energy consumer j and converting it to provide heating energy $H_{4ij}(e)$

$\beta_{00i}(h)$ = cost of installing direct heat generation of capacity h at plant i

$\beta_{0ii}(h)$ = cost of installing heat to chilled water conversion of capacity h at plant i to provide chilled water output $C_{0ii}(h)$

$\beta_{1ij}(h)$ = cost of installing a heating link of capacity h between plant i and heating energy consumer j

$\beta_{2ij}(h)$ = cost of installing a heating link of capacity h between heating energy consumer i and heating energy consumer j

$\gamma_{1ij}(c)$ = cost of installing a cooling link of capacity c between plant i and cooling energy consumer j

$\gamma_{2ij}(c)$ = cost of installing a cooling link of capacity c between cooling energy consumer i and cooling energy consumer j

All of the above functions include initial capital cost and installation cost plus the expected maintenance cost over the expected system lifetime.

II. Linearization of Functions

In general, all of the above cost, loss, and production functions will be nonlinear. In order to make the mathematical problem more tractable by current computational techniques, it is desirable to replace each of these functions by an approximating piecewise-linear function. This can be done to any desirable accuracy since, in general, the functions being approximated will be at least piecewise smooth. For example, consider the recovered heat and cost functions of the electrical generation capacity of a plant at site i (Fig. 2). It is then possible to approximate $H_{00i}(e_{00i})$ and $\alpha_{00i}(e_{00i})$ to within allowable error by functions which are linear on the intervals e^0_{00ik}, e^1_{00ik} for $k = 1 \ldots l_{00i}$ as in Fig. 3.

The partition values e^0_{00ik} and e^1_{00ik} and the approximating linear functions can be determined for example by a piecewise-linear least squares fit simultaneously on both functions.

The single plant in the description above with its upper and lower bounds on electrical generation capacity is then replaced by $l_{00i} = 3$ "pseudo-plants" with the rele-

vant upper and lower bounds to describe the capacity region in which each should operate.

The dichotomous variable λ_{00ik} is then introduced such that:

$\lambda_{00ik} = 1$ if pseudo-plant k is actually to be constructed at plant site i

$\lambda_{00ik} = 0$ if pseudo-plant k is not to be constructed

Since at most one of these pseudo-plants will be constructed at plant site i, we have the additional constraint:

$$\sum_{k=1}^{l_{00i}} \lambda_{00ik} \leq 1$$

Since the capacity of pseudo-plant k should be zero if it is not to be constructed and it should not be constructed if its capacity is zero, we have the following constraint to force the correct logical relationship between the dichotomous and capacity variables:

$$\lambda_{00ik}\, e^0_{00ik} \leq e_{00ik} \leq \lambda_{00ik}\, e^1_{00ik}$$

Each pseudo-plant will then have linear heat-recovery and cost functions in its limited capacity range:

$$H_{00ik}(e_{00ik}) = H_{00ik}\, e_{00ik} + H^*_{00ik} = H_{00ik}\, e_{00ik} + H^*_{00ik}\, \lambda_{00ik}$$

$$\alpha_{00ik}(e_{00ik}) = \alpha_{00ik}\, e_{00ik} + \alpha^*_{00ik} = \alpha_{00ik}\, e_{00ik} + \alpha^*_{00ik}\, \lambda_{00ik}$$

The same artifice may be used to piecewise-linearize each nonlinear function appearing in the model. This introduces the following bounds on the allowed operating capacities of the pseudo-system elements to be defined in doing so.

III. Upper and Lower Bounds on Capacities of Pseudo-system Elements

$e^1_{00ik},\, e^0_{00ik}$ = upper and lower bounds on electrical capacity of pseudo-plant k at plant site i, if built

$h^1_{00ik},\, h^0_{00ik}$ = upper and lower bounds on direct heat generation capacity of pseudo-plant k at plant site i, if utilized

$h^1_{0iik},\, h^0_{0iik}$ = upper and lower bounds on capacity of heat to chilled water conversion of pseudo-plant k at plant site i, if utilized

$e^1_{0ijk},\, e^0_{0ijk}$ = upper and lower bounds on capacity of pseudo-electrical link k between plant site i and plant site j if built

$e^1_{1ijk},\, e^0_{1ijk}$ = upper and lower bounds on capacity of pseudo-electrical link k between plant site i and electrical consumer j if built

$c^1_{1ijk},\, c^0_{1ijk}$ = upper and lower bounds on capacity of pseudo-cooling link k between plant site i and cooling energy consumer j if built

$h^1_{1ijk},\, h^0_{1ijk}$ = upper and lower bounds on capacity of pseudo-heating link k between plant site i and heating energy consumer j if built

$e^1_{2ijk},\, e^0_{2ijk}$ = upper and lower bounds on capacity of pseudo-electrical link k between electrical consumer i and electrical consumer j if built

$c^1_{2ijk},\, c^0_{2ijk}$ = upper and lower bounds on capacity of pseudo-cooling link k between cooling energy consumer i and cooling energy consumer j if built

$h^1_{2ijk},\, h^0_{2ijk}$ = upper and lower bounds on capacity of pseudo-heating link k between heating energy consumer i and heating energy consumer j if built

$e^1_{3ijk},\, e^0_{3ijk}$ = upper and lower bounds on capacity of pseudo-electrical substitution link k from electrical consumer i to cooling energy consumer j if utilized

$e^1_{4ijk},\, e^0_{4ijk}$ = upper and lower bounds on capacity of pseudo-electrical substitution link k from electrical consumer i to heating energy consumer j if utilized

As in the above example, the construction or non-construction of each pseudo-system element is controlled by the use of dichotomous variables.

$\lambda_{00ik} = 1$ if pseudo-plant k at plant site i is to be used for electrical generation $(k = 1 \ldots l_{00i})$

$\mu_{00ik} = 1$ if pseudo-plant k at plant site i is to be used for direct heat generation $(k = 1 \ldots m_{0ci})$

$\mu_{0iik} = 1$ if pseudo-plant k at plant site i is to be used for production of chilled water $(k = 1 \ldots m_{0ii})$

$\lambda_{0ijk} = 1$ if plant site i is to be connected to plant site j by a pseudo-electrical link with capacity between e^0_{0ijk} and e^1_{0ijk} $(k = 1 \ldots l_{0ij})$

$\lambda_{1ijk} = 1$ if plant site i is to be connected to electrical consumer j by a pseudo-electrical link with capacity between e^0_{1ijk} and e^1_{1ijk} $(k = 1 \ldots \ell_{1ij})$

$\mu_{1ijk} = 1$ if plant site i is to be connected to heating energy consumer j by a pseudo-heating link with capacity between h^0_{1ijk} and h^1_{1ijk} $(k = 1 \ldots m_{1ij})$

$\nu_{1ijk} = 1$ if plant site i is to be connected to cooling energy consumer j by a pseudo-cooling link with capacity between c^0_{1ijk} and c^1_{1ijk} $(k = 1 \ldots n_{1ik})$

$\lambda_{2ijk} = 1$ if electrical consumer i is to be connected to electrical consumer j by a pseudo-electrical link with capacity between e^0_{2ijk} and e^1_{2ijk} $(k = 1 \ldots \ell_{2ij})$

$\mu_{2ijk} = 1$ if heating energy consumer i is to be connected to heating energy consumer j by a pseudo-heating link with capacity between h^0_{2ijk} and h^1_{2ijk} $(k = 1 \ldots m_{2ij})$

$\nu_{2ijk} = 1$ if cooling energy consumer i is to be connected to cooling energy consumer j by a pseudo-cooling link with capacity between c^0_{2ijk} and c^1_{2ijk} $(k = 1 \ldots n_{2ij})$

$\lambda_{3ijk} = 1$ if substitution from electrical consumer i to cooling energy consumer j is to be provided by a pseudo-electrical substitution link with capacity between e^0_{3ijk} and e^1_{3ijk} $(k = 1 \ldots \ell_{3ij})$

$\lambda_{4ijk} = 1$ if substitution from electrical consumer i to heating energy consumer j is to be provided by a pseudo-electrical substitution link with capacity between e^0_{4ijk} and e^1_{4ijk} $(k = 1 \ldots \ell_{4ij})$

The constant demand problem can then be formulated as the following mixed integer linear program:

Minimize

$$\sum_{i=0}^{4} \sum_{j} \sum_{k} \sum_{l=1}^{\ell_{ijk}} \{\alpha_{ijkl} e_{ijkl} + \alpha^*_{ijkl} \lambda_{ijkl}\}$$

$$+ \sum_{i=0}^{2} \sum_{j} \sum_{k} \sum_{l=1}^{m_{ijk}} \{\beta_{ijkl} h_{ijkl} + \beta^*_{ijkl} \mu_{ijkl}\}$$

$$+ \sum_{i=1}^{2} \sum_{j} \sum_{k} \sum_{l=1}^{n_{ijk}} \{\gamma_{ijkl} c_{ijkl} + \gamma^*_{ijkl} \nu_{ijkl}\}$$

where the sums over j and k are taken over all possible combinations corresponding to the value of the distribution level subscript i and the type of the variable (e, h, or c).

This will give the minimum *total* cost of the system with the following constraints:

Subject to

$$\lambda_{ijkl}, \mu_{ijkl}, \nu_{ijkl} = 0 \text{ or } 1$$

$$h'_j, c'_j, e_{ijkl}, h_{ijkl}, c_{ijkl} \geqslant 0$$

The following constraints arise from the energy balance (energy flowing in equals energy flowing out) at each node of the distribution system:

$$\sum_{\kappa=1}^{\ell_{00j}} e_{00j\kappa} + \sum_{\substack{i=1 \\ i \neq j}}^{k} \sum_{\kappa=1}^{\ell_{0ij}} \{E_{0ij\kappa} e_{0ij\kappa} + E^*_{0ij\kappa} \lambda_{0ij\kappa}\}$$

$$= \sum_{\substack{r=1 \\ r \neq j}}^{k} \sum_{\kappa=1}^{\ell_{0jr}} e_{0jr\kappa} + \sum_{r=1}^{l} \sum_{\kappa=1}^{\ell_{1jr}} e_{1jr\kappa} \qquad \text{for } j = 1 \ldots k$$

$$\sum_{\kappa=1}^{\ell_{00j}} \{H_{00j\kappa} e_{00j\kappa} + H^*_{00j\kappa} \lambda_{00j\kappa}\} + \sum_{\kappa=1}^{m_{00j}} h_{00j\kappa}$$

$$= \sum_{\kappa=1}^{m_{0jj}} h_{0jj\kappa} + \sum_{r=1}^{m} \sum_{\kappa=1}^{m_{1jr}} h_{1jr\kappa} \qquad \text{for } j = 1 \ldots k$$

$$\sum_{\kappa=1}^{m_{0jj}} \{C_{0jj\kappa} h_{0jj\kappa} + C^*_{0jj\kappa} \mu_{0jj\kappa}\}$$

$$= \sum_{r=1}^{n} \sum_{\kappa=1}^{n_{1jr}} c_{1jr\kappa} \qquad \text{for } j = 1 \ldots k$$

$$\sum_{i=1}^{k} \sum_{\kappa=1}^{\ell_{1ij}} \{E_{1ij\kappa} e_{1ij\kappa} + E^*_{1ij\kappa} \lambda_{1ij\kappa}\}$$

$$+ \sum_{\substack{i=j \\ i \neq j}}^{l} \sum_{\kappa=1}^{\ell_{2ij}} \{E_{2ij\kappa} e_{2ij\kappa} + E^*_{2ij\kappa} \lambda_{2ij\kappa}\}$$

$$= e_j + \sum_{\substack{r=1 \\ r \neq j}}^{l} \sum_{\kappa=1}^{\ell_{2jr}} e_{2jr\kappa} + \sum_{r=1}^{n} \sum_{\kappa=1}^{\ell_{3jr}} e_{3jr\kappa} + \sum_{r=1}^{m} \sum_{\kappa=1}^{\ell_{4jr}} e_{4jr\kappa}$$

$$\text{for } j = 1 \ldots l$$

$$\sum_{i=1}^{k} \sum_{\kappa=1}^{m_{1ij}} \{H_{1ij\kappa} h_{1ij\kappa} + H^*_{1ij\kappa} \mu_{1ij\kappa}\}$$

$$+ \sum_{\substack{i=1 \\ i \neq j}}^{m} \sum_{\kappa=1}^{m_{2ij}} \{H_{2ij\kappa} h_{2ij\kappa} + H^*_{2ij\kappa} \mu_{2ij\kappa}\}$$

$$+ \sum_{i=1}^{l} \sum_{\kappa=1}^{\ell_{4ij}} \{H_{4ij\kappa} e_{4ij\kappa} + H^*_{4ij\kappa} \lambda_{4ij\kappa}\}$$

$$= h_j + h'_j + \sum_{\substack{r=1 \\ r \neq j}}^{m} \sum_{\kappa=1}^{m_{2jr}} h_{2jr\kappa} \qquad \text{for } j = 1 \ldots m$$

$$\sum_{i=1}^{k}\sum_{\kappa=1}^{n_{1ij}}\{C_{1ij\kappa}c_{1ij\kappa} + C_{1ij\kappa}^{*}v_{1ij\kappa}\}$$

$$+ \sum_{\substack{i=1 \\ i \neq j}}^{n}\sum_{\kappa=1}^{n_{2ij}}\{C_{2ij\kappa}c_{2ij\kappa} + C_{2ij\kappa}^{*}v_{2ij\kappa}\}$$

$$+ \sum_{i=1}^{l}\sum_{\kappa=1}^{h_{ij}}\{C_{3ij\kappa}e_{3ij\kappa} + C_{3ij\kappa}^{*}\lambda_{3ij\kappa}\}$$

$$= c_j^l + c_j' + \sum_{\substack{r=1 \\ r \neq j}}^{n}\sum_{\kappa=1}^{n_{2jr}} c_{2jr\kappa} \qquad \text{for } j = 1 \ldots n$$

The following constraints, besides keeping the capacity of each pseudo-system element between the relevant upper and lower bounds if it is to be constructed, also force the correct logical relationships between the capacity variables and the associated dichotomous variables.

$$\lambda_{ij\kappa l} e_{ij\kappa l}^{0} \leqslant e_{ij\kappa l} \leqslant \lambda_{ij\kappa l} e_{ij\kappa l}^{1}$$

$$\mu_{ij\kappa l} h_{ij\kappa l}^{0} \leqslant h_{ij\kappa l} \leqslant \mu_{ij\kappa l} h_{ij\kappa l}^{1}$$

$$v_{ij\kappa l} c_{ij\kappa l}^{0} \leqslant c_{ij\kappa l} \leqslant v_{ij\kappa l} c_{ij\kappa l}^{1}$$

where the subscripts i, j, κ, and l run over all allowable combinations, depending on the type of variable.

The remaining set of constraints insures that at most one of the possible pseudo-system elements in each case is to be constructed as an element of the real system.

$$\sum_{l=1}^{l_{ij\kappa}} \lambda_{ij\kappa l} \leqslant 1$$

$$\sum_{l=1}^{m_{ij\kappa}} \mu_{ij\kappa l} \leqslant 1$$

$$\sum_{l=1}^{n_{jk}} v_{ij\kappa l} \leqslant 1$$

where the subscripts i, j, and κ run over all allowable combinations depending on the type of the associated capacity variable.

IV. Method of Solution

The most favorable results in solving large mixed integer linear programs like the above are currently given by branch and bound methods (or specialized methods which utilize branch and bound methods as part of their procedure.) The method is a search procedure which estimates or evaluates the maximum objective function value for all possible combinations of values of the integer restricted variables. It begins with a large set of

possible combinations of values for the integer-restricted variables and then divides this set into successively smaller subsets.

At each step an estimate is made of the maximum objective function value given that the combination of values of the integer restricted variables lies in each subset. Also at each step this estimate of the maximum objective function value for each subset is compared with the objective function value of a solution which satisfies the constraints and has integer values for the integer-restricted variables. Subsets whose maximum objective function values cannot exceed the value of the best current integer solution are then no longer considered as candidates for containing the optimum combination of values of the integer-restricted variables.

If at any step an integer solution is found whose evaluated objective function value is larger than that of the current best integer solution then it is taken as the updated best integer solution. Continuing in this manner the subsets are partitioned more and more finely and are eliminated as their maximum possible objective function values fall below the increasing objective function value of the best current integer solution. Eventually a point is reached where one of the subsets will contain only the optimum combination of values of the integer-restricted variables and this solution will then become the current best integer solution. From this point on, the comparison of objective function values will eliminate all the remaining subsets of possible combinations of values of the integer-restricted variables and establish this solution as the true optimum.

In more detail, the method is illustrated by the accompanying structured Level 1 flowchart. When the given mixed-integer linear program is feasible, it is solved as a linear program neglecting the integer constraints to obtain the objective function value $\bar{a}_{00}$. Prior to solving this problem there was no current feasible solution in which the integer-restricted variables took on integer values; so the objective function value of the current best integer solution x_{0c} is set equal to $-\infty$. Likewise before this problem was solved there was no estimate of an upper bound on its objective function value so UB_P was set equal to ∞.

If the solution of this problem is such that all integer-restricted variables have integer values, the optimal solution has been found immediately. If not, one of the variables whose integer constraint is not satisfied in the current solution is chosen for the branching process. Here

two new subproblems are created by restricting the value of the unsatisfied variable to be greater than the integer immediately above its current value and to be less than the integer immediately below its current value. The initial feasible region is then divided into two disjoint regions, one of which must contain the optimum solution, since the branching variable must be integer-valued and only a non-integer portion of feasible region has been removed between these two disjoint regions. One of these subproblems is then chosen to be solved immediately as a linear programming problem neglecting the integer constraints. The other subproblem is stored in a list with an upper bound on its objective function value to be solved later. This process is then repeated with the solved subproblem becoming the current problem at each step until one of its branched descendants yields a solution whose integer-restricted variables have integer values. The value of the objective function of this solution is recorded as x_{0c} and any subproblem in the stored list whose upper bound is less than x_{0c} can be eliminated since its feasible region could not have contained the optimum solution. The method then backtracks by choosing a problem from the stored list to begin the procedure again.

At each branching step the feasible region is split into two disjoint regions and the non-integer region between them is removed from the feasible region. Hence, at any point in the procedure, exactly one of the subproblems contains the optimal solution (if it is unique). In cases where one of the integer restricted variables is not constrained above but the problem does have a finite optimum solution, the method will keep reducing the infinite portion of the feasible region until the upper bound on the objective function value associated with that region falls below the objective function value of the current best integer solution at which time it can be eliminated. This leaves only the disjoint finite feasible regions which the procedure continues to divide while eliminating the non-integer regions of the integer restricted variables until the objective function values of all remaining feasible regions have been examined and the optimum solution found or infeasibility demonstrated.

The details of the methods used in the branching and backtracking subroutines to determine which of the problems is to be solved next and in finding upper bounds on the objective function values are given in an appendix. This procedure has been used successfully on large mixed integer programming problems with on the order of one hundred 0-1 integer variables and several thousand continuous variables (Refs. 1, 2), and hence will be effective in dealing with problems having a few consumers and plants and involving mildly non-linear cost and production functions.

In cases where there are many consumers and plants and more non-linear functions, however, the number of 0-1 integer variables increases enormously to the point where branch and bound methods cannot solve the problem within a reasonable amount of computer time even if many of the obviously uneconomical combinations of values of these variables have been eliminated beforehand. In cases such as this, a refined procedure utilizing "Bender's decomposition" can be used. This is an iterative procedure which at each step deals only with decoupled problems describing the distribution of individual commodities (here, energy types). Besides being able to deal with much larger problems (problems having about two thousand 0-1 integer variables and about twenty thousand continuous variables have been solved (Ref. 3)). The fact that at each step the procedure deals with only the usual "transportation problem" involving a single commodity allows the problem of stochastic demand for these commodities to be dealt with much more simply than the case where the transportation problems are coupled together.

An important problem for DSN energy distribution is then the formulation of the full stochastic problem in terms of a Bender's decomposition algorithm.

References

1. Forrest, J. J. H., Hirst, J. P. H., and Tomlin, J. A., "Practical Solution of Large Mixed Integer Programming Problems," in *Management Science*, Vol. 20, No. 5, p. 736, 1974.

2. Tomlin, J. A., "Branch and Bound Methods for Integer and Non-convex Programming," in *Integer and Non-linear Programming*, p. 437, edited by J. Abadie. North Holland Pub. Co., Amsterdam, 1970.

3. Geoffrion, A. M., and Graves, G. W., "Multicommodity Distribution System Design," in *Management Science*, Vol. 20, No. 5, p. 822, 1974.
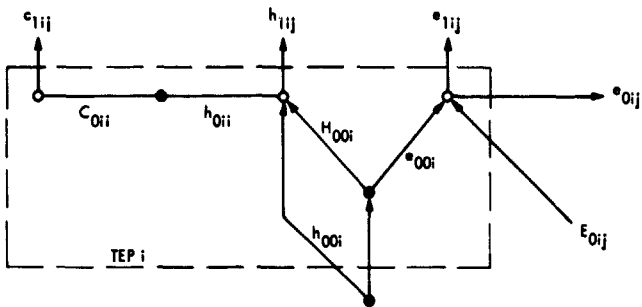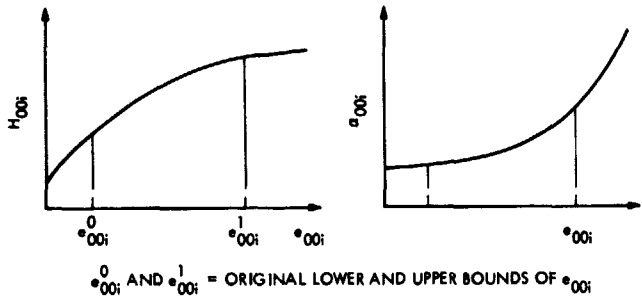
Fig. 1. Total energy plant

e^0_{00i} AND e^1_{00i} = ORIGINAL LOWER AND UPPER BOUNDS OF e_{00i}

Fig. 2. Original recovered heat and cost functions
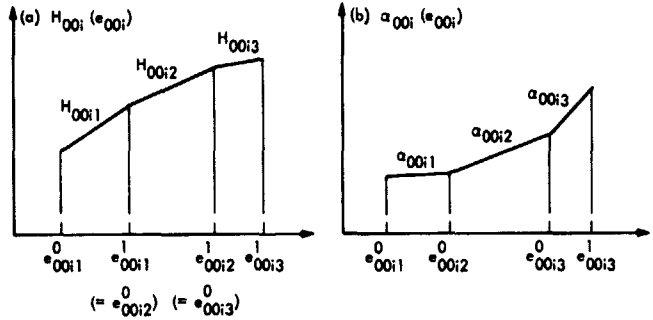
Fig. 3. Piecewise linear approximations to recovered heat and cost functions

BRNCHNBD

SET
 P = MIXED INTEGER PROBLEM
     TO BE SOLVED
 LIST = EMPTY
 $x_{0c} = -\infty$
 $UB_p = \infty$

SOLVELP
IF $UB_p < x_{0c}$ SET $\bar{a}_{00} = UB_p$
IF NOT SOLVE CURRENT PROBLEM
P AS A LINEAR PROGRAMMING
PROBLEM NEGLECTING INTEGER
CONSTRAINTS

P IS
INFEASIBLE
OR
$\bar{a}_{00} < x_{0c}$
?
NO   YES

ALL
INTEGER
RESTRICTED
VARIABLES
= INTEGER
?
NO   YES

BACKTRAK
IF LIST IS NONEMPTY
CHOOSE FROM LIST
THE NEXT SUBPROBLEM
TO BE SOLVED AND
SET IT EQUAL TO P

BRANCH
CHOOSE AN UNSATISFIED INTEGER
VARIABLE x_p WITH CURRENT VALUE
$\bar{a}_{p0} = n_{p0} + f_{p0}$ WHERE n_{p0} IS
AN INTEGER AND $0 < f_{p0} < 1$

CREATE TWO NEW SUBPROBLEMS BY
APPENDING TO THE CURRENT
PROBLEM P THE CONSTRAINTS:
$x_p \geq n_{p0} + 1$ AND $x_p \leq n_{p0}$

CALCULATE UPPER BOUNDS ON THE
OBJECTIVE FUNCTIONS OF THESE
NEW SUBPROBLEMS

SET CURRENT PROBLEM P = ONE OF
THESE NEW SUBPROBLEMS AND PLACE
THE OTHER IN LIST WITH ITS UB

NEW INTEGER SOLUTION:
RECORD VALUE OF THE
OBJECTIVE FUNCTION x_{0c}

BACKTRAK
IF LIST IS NONEMPTY
CHOOSE FROM LIST
THE NEXT SUBPROBLEM
TO BE SOLVED AND
SET IT EQUAL TO P
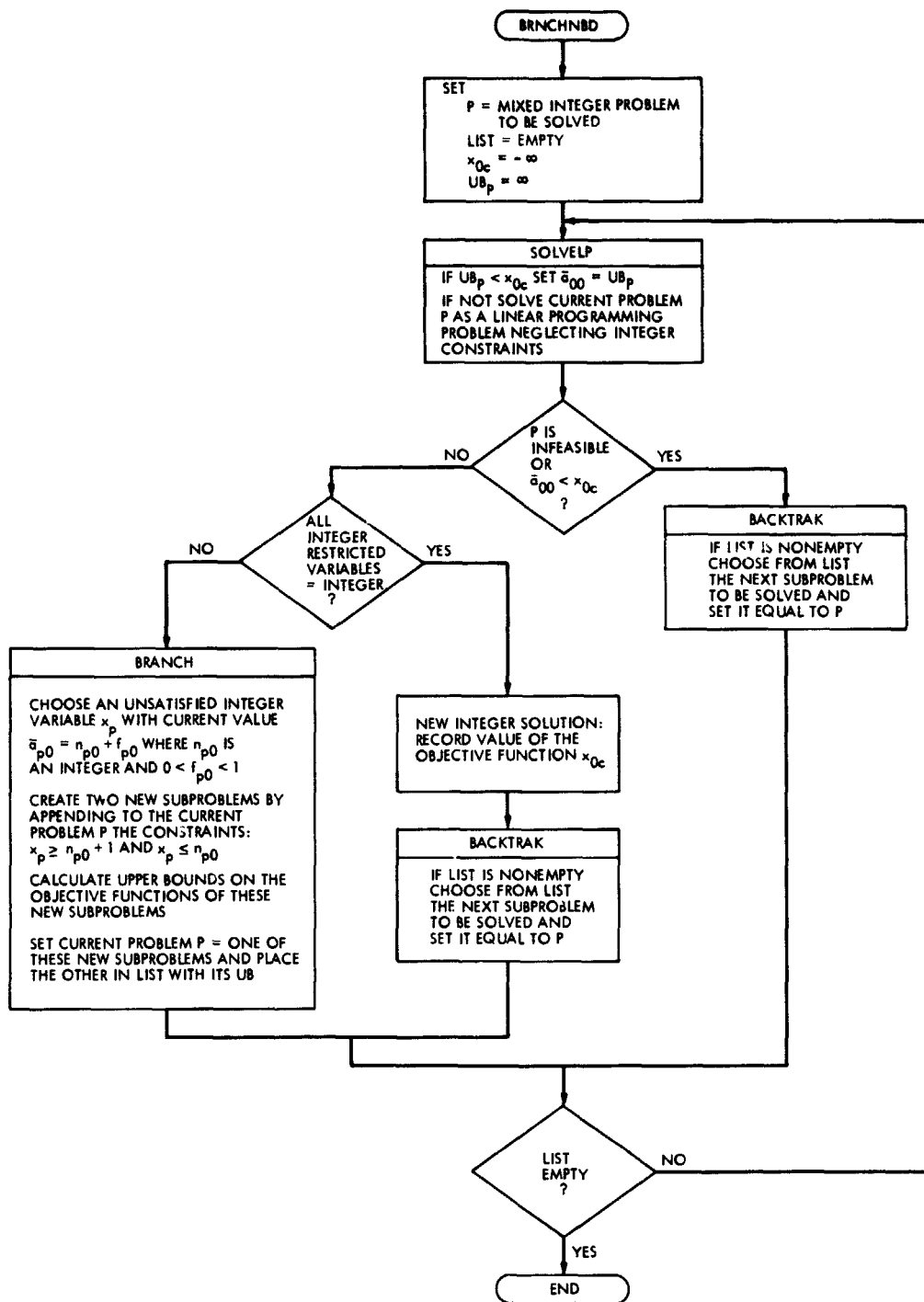
LIST
EMPTY
?
NO

YES

END

Fig. 4. Flowchart for BRNCHNBD

Appendix A

Details of Methods Which Can Be Used in BRANCH and BACKTRAK Routines

I. BRANCH

In the optimal solution of the current linear programming (LP) subproblem some of the integer-restricted-variables will take on non-integer values. In order to force these variables toward integer values, two more tightly constrained subproblems are formed. Let the integer-restricted variable x_p have $\bar{a}_{p0} = n_{p0} + f_{p0}$ (where n_{p0} is an integer and $0 \leqslant f_{p0} < 1$) as its value in the current optimal solution. The feasible set for the current subproblem is then reduced by appending the further constraint: $x_p \geqslant n_{p0} + 1$ to yield one subproblem and by appending $x_p \leqslant n_{p0}$ to yield the other subproblem. The decision of which unsatisfied integer variable to choose for this branching process is often based on the calculation of *penalties* which estimate the change in objective function value due to the newly appended constraints.

A. Simplex Algorithm

As a preface to the following procedures, some of the salient points of the simplex algorithm will be described. Suppose we have the standard linear programming problem:

Maximize the linear form

$$\sum_{j=1}^{n} \bar{a}_{0j} x_j$$

where the $\bar{a}_{0j}$ are constants, subject to

$$Ax = b$$
$$x_j \geqslant 0 \qquad j = 1 \ldots n$$

where

$$x = (x_1, x_2, \ldots, x_n)$$
$$b = (b_1, b_2, \ldots, b_m)$$

and $A = (a_{ij})$ is an $m \times n$ matrix. Suppose also that we have m linearly independent columns of A which yield the following feasible linear combinations:

$$a_{.l_1} \bar{a}_{10} + a_{.l_2} \bar{a}_{20} + \cdots + a_{.l_m} \bar{a}_{m0} = b$$

where

$$\bar{a}_{j0} \geqslant 0$$

when

$$l_j \epsilon J^c = \{l_1, l_2, \ldots, l_m\} \subset \{1, \ldots, n\}$$

The $x_j = x_{l_j}$ are called the current basic variables. If we then set the values of the remaining variables equal to zero:

$$x_{k_i} = 0 \qquad \text{for } k_i \epsilon J$$

we obtain a current basic feasible solution. The x_{k_i} are called the current non-basic variables. The value of the objective function for this current basic feasible solution is:

$$\bar{a}_{00} = \sum_{j=1}^{m} a_{0l_j} \bar{a}_{j0}$$

The columns corresponding to current non-basic variables can then be expressed as linear combinations of the columns corresponding to the current basic variables. This can conveniently be recorded in tableau form, i.e.,

$$\bar{a}_{.k_i} = \sum_{j=1}^{m} \bar{a}_{ji} a_{.l_j} \qquad (\text{synthetic } x_{k_i})$$

$$b = \sum_{j=1}^{m} \bar{a}_{j0} a_{.l_j}$$

can be represented as

	b	x_{k_1}	x_{k_2}	....	x_{k_i}	....	$x_{k_{n-m}}$
x_0	$\bar{a}_{00}$	$\bar{a}_{01}$	$\bar{a}_{02}$	....	$\bar{a}_{0i}$	....	$\bar{a}_{0, n-m}$
X_1	$\bar{a}_{10}$	$\bar{a}_{11}$	$\bar{a}_{12}$	....	$\bar{a}_{1i}$	....	$\bar{a}_{1, n-m}$
.	.	.	.		.		.
.	.	.	.		.		.
.	.	.	.		.		.
.	.	.	.		.		.
.	.	.	.		.		.
X_m	$\bar{a}_{m0}$	$\bar{a}_{m1}$	$\bar{a}_{m2}$	....	$\bar{a}_{mi}$	....	$\bar{a}_{m, n-m}$

Appended to the tableau is a row of reduced costs denoted by $\bar{a}_0, \bar{a}_{0i}$ giving the decrease in objective function value when one unit of synthetic x_{k_i} in the current basic feasible solution is replaced by one unit of real x_{k_i}. If an arbitrary amount of synthetic x_{k_i} is replaced in this manner, the resulting solution may be infeasible or feasible but not a basic feasible solution. However, the simplex algorithm introduces as much as possible some currently non-basic variable x_{k_i}, which has a negative reduced cost, while still retaining feasibility. This results in a new basic feasible solution as follows. If the value of x_{k_i} is increased from 0 to v_{k_i} then to maintain feasibility:

$$a_{.1_1}\bar{a}_{10} + a_{.1_2}\bar{a}_{20} + \cdots + a_{.1_m}\bar{a}_{m0} + a_{.k_1}v_{k_i} = b$$

the value of the basic variable X_p must change to:

$$\bar{a}'_{p0} = \bar{a}_{p0} - \bar{a}_{pi}v_{k_i}$$

If it is assumed that the problem has a finite solution, then at least one of the $\bar{a}_{p_i}$ must be greater than zero. Since the value of all basic variables must be greater than or equal to zero, v_{k_i} can be increased until $\bar{a}'_{r0} = 0$ for some basic variable X_r. Then x_{l_r} becomes a non-basic variable and $x_{k_i} = X_r$ enters the basis in the amount $\bar{a}_{r0} = v_{k_i}$. The value of the objective function is then increased from $\bar{a}_{00}$ to $\bar{a}_{00} - \bar{a}_{0i}v_{k_i}$ (recall that $\bar{a}_{0i} < 0$).

Since b is represented by a unique linear combination of the columns of A corresponding to the current basis, and since (in the non-degenerate case) the value of the objective function increases with each change to a new basic feasible solution, there must be a unique objective function value associated with each basic feasible solution. Hence, the algorithm can never return to the same basis twice and as the procedure is repeated, for problems assumed to have finite optimum, each basic feasible solution is examined until in a finite number of steps one is found for which all the reduced costs are positive. For this solution no currently non-basic variable can be introduced into the basis without decreasing the objective function value; hence, this must be the optimal solution.

B. Penalties

Suppose we have solved the following mixed integer linear program:

Maximize

$$x_0 = \sum_{j=1}^{n} a_{0j}x_j$$

subject to $Ax = b$, where A is an $(m \times n)$ matrix

$$x_j \geq 0$$

$$x_j = \text{integer} \quad \text{for } j \in I \subset \{1 \dots n\}$$

but as a linear program neglecting the integer constraints. Regardless of the LP method used in the solution the final simplex tableau can still be obtained. Let

$$\{x_{k_i}\} \quad \text{for } k_i \in J \subset \{1 \dots n\}$$

be the set of non-basic variables and

$$\{X_j = x_{l_j}\} \quad \text{for } l_j \in J^c$$

be the set of basic variables. The tableau is then given as follows:

	b	x_{k_1}	x_{k_2}	....	x_{k_i}	....	$x_{k_{n-m}}$
x_0	$\bar{a}_{00}$	$\bar{a}_{01}$	$\bar{a}_{02}$	....	$\bar{a}_{0i}$	....	$\bar{a}_{0,n-m}$
X_1	$\bar{a}_{10}$	$\bar{a}_{11}$	$\bar{a}_{12}$	....	$\bar{a}_{1i}$	....	$\bar{a}_{1,n-m}$
.	.	.	.		.		.
.	.	.	.		.		.
.	.	.	.		.		.
.	.	.	.		.		.
X_m	$\bar{a}_{m0}$	$..\bar{a}_{m1}$	$\bar{a}_{m2}$	....	$\bar{a}_{mi}$	....	$\bar{a}_{m,n-m}$

(1) The column of A corresponding to the non-basic variable x_{k_i} is expressed as a linear combination of the columns of A corresponding to the basic variables (synthetic x_{k_i})

$$a_{k_i} = \sum_{j=1}^{m} \bar{a}_{ji}\, a_{.l_j}$$

(2) The first column of the tableau gives the values of the objective function and the basic variables in the final solution

$$\bar{a}_{00} = \sum_{j=1}^{m} a_{0l_j}\bar{a}_{j0}$$

(3) If the non-basic variables x_{k_i} are changed in value from zero to v_{k_i}, then in order to maintain feasi-

bility the value of the basic variables X_p must change to

$$\bar{a}'_{p0} = \bar{a}_{p0} - \sum_{i=1}^{n-m} \bar{a}_{pi}\, v_{k_i} \qquad \text{for } p = 1 \ldots m$$

(4) The decrease in the objective function value when one unit of synthetic x_{k_i} in the optimal solution is replaced by one unit of τ_{k_i} is given by $\bar{a}_{0i}$ (the reduced cost of x_{k_i}), and since the solution is optimal the reduced costs must all be positive.

Suppose that the basic variable X_p has the current optimal value $\bar{a}_{p0}$. If a new problem is created by appending to the current problem the constraint: $X_p \geqslant \bar{a}_{p0} + \alpha$ then the value of the objective function must decrease since the feasible region has been reduced. Since the number of constraints has been increased by one in the new problem, one of the currently non-basic variables x_{k_q} must enter the basis of the new problem.

If the value of α is small enough the rest of the basic variables will remain the same as in the current optimal solution. From the current tableau the minimum amount in which x_{k_q} may be introduced can be determined (as in 3 above)

$$\bar{a}'_{p0} = \bar{a}_{p0} - \bar{a}_{pq} v_{k_q} \geqslant \bar{a}_{p0} + \bar{\alpha}$$

$$v_{k_q} \geqslant -\frac{\alpha}{\bar{a}_{pq}}$$

since x_{k_q} must be introduced in a positive amount must have $a_{pq} < 0$

The decrease in objective function value from the current optimum when x_{k_q} is introduced in the amount v_{k_q} can then be determined from the reduced cost:

$$D \geqslant \bar{a}_{0q}\left[-\frac{\alpha}{\bar{a}_{pq}} \right]$$

Considering all of the non-basic variables which may enter the basis of the new problem in this manner, the current objective function value must be decreased by at least:

$$D_u = \alpha \min_{\substack{j \\ \bar{a}_{pj} < 0}} \left[-\frac{\bar{a}_{0j}}{\bar{a}_{pj}} \right]$$

and if this minimum is taken for $j = q$ then the amount of the non-basic variable x_{k_q} in the solution must increase

from zero to

$$v_{k_q} = -\frac{\alpha}{\bar{a}_{pq}}$$

Similarly, if a new problem is created by appending to the current problem the further constraint: $x_p \leqslant a_{p0} - \beta$ the degradation of the objective function value must be at least

$$D_d = \beta \min_{\substack{j \\ \bar{a}_{pj} > 0}} \left[\frac{\bar{a}_{0j}}{\bar{a}_{pj}} \right]$$

and if this minimum is taken for $j = r$, then the amount of the non-basic variable x_{k_r} in the solution must increase from zero to

$$v_{k_r} = \frac{\beta}{\bar{a}_{pr}}$$

These results may now be applied to an integer-restricted basic variable x_p which has the current optimal value

$$\bar{a}_{p0} = n_{p0} + f_{p0}$$

where n_{p0} is an integer and $0 < f_{p0} < 1$.

Setting

$$\alpha = 1 - f_{p0}$$

(corresponding to adding the constraint $X_p \geqslant n_{p0} + 1$)

$$\beta = f_{p0}$$

(corresponding to adding the constraint $X_p \leqslant n_{p0}$)

the degradations of the objective functions must be at least

$$D_u = (1 - f_{p0}) \cdot \min_{\substack{j \\ \bar{a}_{pj} < 0}} \left[-\frac{\bar{a}_{0j}}{\bar{a}_{pj}} \right]$$

$$D_d = f_{p0} \cdot \min_{\substack{j \\ \bar{a}_{pj} > 0}} \left[\frac{\bar{a}_{0j}}{\bar{a}_{pj}} \right]$$

If the minima are taken for $j = q$ and $j = r$ respectively, then the amounts of the currently non-basic variables x_{k_q} and x_{k_r} must have increased in the optimal solutions of the new problems. However, if either x_{k_q} or x_{k_r} is an integer restricted variable, its amount in any integer solution of the new problem must have increased from its

current zero value by an integer amount of at least one. The degradations of the current objective function value must therefore be at least equal to the reduced costs $\bar{a}_{0q}$ or $\bar{a}_{0r}$.

Thus, we can formulate two penalties which can be used to find upper bounds on the objective functions of the more tightly constrained problems created from the original problem.

$$P_u^p = \min_{\substack{j \\ \bar{a}_{pj} < 0}} \begin{cases} (1 - f_{p0})\left[-\dfrac{\bar{a}_{0j}}{\bar{a}_{pj}}\right] & j \notin I \quad (\text{i.e., } x_{k_j} \neq \text{integer}) \\ \max\left\{(1 - f_{p0})\left[-\dfrac{\bar{a}_{0j}}{\bar{a}_{pj}}\right], \bar{a}_{0j}\right\} & j \in I \end{cases}$$

which gives as an upper bound on the objective function for the original problem with the appended constraint $X_p \leqslant n_{p0}$ the value

$$UB = \bar{a}_{00} - P_u^p$$

$$P_d^p = \min_{\substack{j \\ \bar{a}_{pj} > 0}} \begin{cases} f_{p0}\left[\dfrac{\bar{a}_{0j}}{\bar{a}_{pj}}\right] & j \notin I \\ \max\left\{f_{p0}\left[\dfrac{\bar{a}_{0j}}{\bar{a}_{pj}}\right], \bar{a}_{0j}\right\} & j \in I \end{cases}$$

which gives as an upper bound on the objective function for the original problem with the appended constraint: $X_p \leqslant n_{p0}$ the value

$$UB - \bar{a}_{00} = P_d^p$$

A stronger upper bound on the value of the objective function of a subproblem which was obtained by more tightly constraining the current problem can be obtained by a Gomory cut. Gomory showed that if the integer-restricted variable X_p is unsatisfied in the LP solution of the current problem and has the value $\bar{a}_{p0} = n_{p0} + f_{p0}$, then any feasible integer solution of the current problem (and hence any feasible integer solution of a more tightly constrained subproblem) must satisfy the following additional inequality:

$$-f_{p0} - \sum_{j=1}^{n} f_{pj}^{*}(-x_j) \geqslant 0$$

where

$$\bar{a}_{pj} = n_{pj} + f_{pj}$$

and

$$f_{pj}^{*} = \begin{cases} \bar{a}_{pj} & \bar{a}_{pj} \geqslant 0 \text{ and } j \notin I \\ \dfrac{f_{p0}(-\bar{a}_{pj})}{(1 - f_{p0})} & \bar{a}_{pj} < 0 \text{ and } j \notin I \\ f_{pj} & f_{pj} \leqslant f_{p0} \text{ and } j \in I \\ \dfrac{f_{p0}(1 - f_{pj})}{(1 - f_p)} & f_{pj} > f_{p0} \text{ and } j \in I \end{cases}$$

If this inequality is appended as a constraint to the current problem, then the degradation of the objective function for this subproblem from the dual-simplex method must be at least

$$D_G = \min_{j \in \{1 \ldots n\}} \bar{a}_{0j}\left[\dfrac{f_{p0}}{f_{pj}^{*}}\right]$$

Using this value it is now possible to give a penalty for satisfying the integer requirement of any currently unsatisfied basic integer restricted variable:

$$P_G^p = \min_{j \in \{1 \ldots n\}} \begin{cases} f_{p0}\dfrac{\bar{a}_{0j}}{\bar{a}_{pj}} & \bar{a}_{pj} \geqslant 0 \text{ and } j \notin I \\ (1 - f_{p0})\left[-\dfrac{\bar{a}_{0j}}{\bar{a}_{pj}}\right] & \bar{a}_{pj} < 0 \text{ and } j \notin I \\ \bar{a}_{0j}\dfrac{f_{p0}}{f_{pj}} & f_{pj} \leqslant f_{p0} \text{ and } j \in I \\ \bar{a}_{0j}\dfrac{(1 - f_{p0})}{(1 - f_{pj})} & f_{pj} > f_{p0} \text{ and } j \in I \end{cases}$$

An upper bound on the value of the objective function of any integer solution attainable from the current problem is then given by

$$UB = \bar{a}_{00} - P_G^p$$

A choice may now be made, based on these penalties, as to which unsatisfied integer restricted variable is to be used for branching. The most commonly followed procedures are as follows:

1) Calculate the penalties P_u^p and P_d^p for all currently unsatisfied integer restricted variables.

   –Choose the variable associated with the smallest penalty as the branching variable.

   –Create two new subproblems by appending to the current problem the constraints: $X_p \geqslant n_{p0} + 1$ and $X_p \leqslant n_{p0}$

−Choose the new subproblem associated with the smaller penalty for immediate solution.

−Place the other new subproblem in LIST with its upper bound (determined from P_u^p or P_d^p and P_0^p).

This procedure is based on the assumption that in most cases the smaller penalty will reflect the smaller true degradation, and hence that an integer solution will be reached along this branch with a high objective function value. If this assumption is not justified, a refinement of the above procedure known as node swapping can be used:

1a) Compare the true degradation of the subproblem which was solved immediately with the penalty of the postponed subproblem.

−If the true degradation exceeds the penalty, solve the postponed subproblem to find its true degradation, then choose the subproblem with the lower true degradation as the problem from which to continue branching.

−If the true degradation of the immediately solved subproblem is less than the penalty of the postponed subproblem, then the subproblem solved must have the lower true degradation and is the problem from which branching should continue.

Or better still

2) Calculate the penalties P_u^p and P_d^p for all currently unsatisfied integer-restricted variables.

−Choose the variable associated with the largest penalty as the branching variable.

−Create two new subproblems by appending to the current problem the constraints: $X_p \geq n_{p0} + 1$ and $X_p \leq n_{p0}$

−Place the new subproblem associated with the larger penalty in LIST with its upper bound (determined from P_u^p or P_d^p and P_0^p).

−Choose the other new subproblem for immediate solution.

This procedure has the advantage of postponing the problems which are known to have the smallest objective function values until later in the search when presumably there will be an integer solution available with a larger objective function value in which case the postponed subproblem need not be solved at all! since it could not possibly be optimal.

C. Shortcomings of the Penalty Approach

In cases where the number of constraints is very large, however, the penalty method of directing the search for an optimal integer solution breaks down and the search becomes essentially random. The reason for this is that a calculated penalty will not represent in any manner the true degradation of the associated subproblem. In fact, the larger penalty may be in the direction of the much smaller true degradation. This is illustrated in Fig. A-1 where the feasible set of the current problem has been projected on the (X_p, x_0) plane.

To direct the search in these cases, branching can be based on priorities. The branching variable is chosen as the unsatisfied integer-restricted variable in the solution of the current problem which is highest on a priority list supplied exogenously by the user. The postponement or solution of the newly created subproblems is then based on penalties (perhaps with node swapping). The priority list may be determined from the user's knowledge of which variables will have the greatest effect on the overall system or, failing this, priorities may be assigned in order of the cost coefficient values in the original objective function.

See the Level 2 flowcharts in Fig. A-1 that describe the above methods (note that the flowchart for BRANCH1A utilizes the flowchart for BRANCH1 as a Level 3 flowchart)

II. BACKTRAK

In most cases the procedure of further constraining unsatisfied integer-restricted variables will eventually lead to a point where the subproblem chosen for branching cannot usefully be further constrained. This can happen if it becomes infeasible or if its value falls below the value of the best integer solution currently available or if it yields a new best integer solution. In these cases it is necessary to have a procedure for choosing a problem from the stored list from w   to continue the search. The earliest such procedure u   d was LIFO (last in–first out) in which the next problem chosen was the last problem placed in the list which has an upper bound greater than the current best integer solution value and

was dictated by the serial access nature of the storage devices available when it was first implemented.

In general, such a choice of procedure may be far from optimal. An improved procedure is to choose as the next problem the problem in the stored list which has the largest upper bound on its objective function value. This procedure takes advantage of the newer random access storage devices but still not in the most efficient manner. The disadvantage of this procedure is that it takes into account only the objective function value and excludes other, perhaps equally important, properties of the stored problems: primarily, the amount of work necessary to bring the chosen problem to an integer solution. A current method which takes both of these factors into account is the best projection criterion.

A. Best Projection Criterion

Let the optimal value of the objective function for the original mixed-integer problem with the integer requirements relaxed be x_0^0 and the value of the objective function of the latest integer solution found be x_0^l. If the first integer solution has not been reached, some estimate, possibly inaccurate, of the value of x_0^l may be given. Define the sum of integer infeasibilities

$$s = \sum_{\substack{p \, 1 \\ i_p \in I}}^{m} \min \{f_{p0}, 1 - f_{p0}\}$$

as a measure of how much the integer restricted variables in the problem differ from integer values in the solution. If the objective function value x_0^k of each outstanding problem presently stored in the list is plotted against its sum of integer infeasibilities s^k and then projected parallel to the line between (s^0, x_0^0) and $(0, x_0^l)$ onto the line $s = 0$ we get as the projected value

$$p_k = x_0^k - \frac{x_0^0 - x_0^l}{s^0} s^k$$

See Fig. A-3.

Here

$$\lambda = \frac{x_0^0 - x_0^l}{s^0}$$

gives an estimate of the marginal degradation of the objective function value for a unit decrease in the sum of integer infeasibilities and hence p_k is an estimate of the objective function value which can be obtained in an integer solution ($s = 0$) attainable from the current outstanding problem k and is of course more accurate when s^k is small. The potential objective function value of a problem can be estimated from its upper bound while an estimate of its sum of integer infeasibilities can be obtained from its value in the parent problem which branched to yield the stored problem. The next problem chosen for solution is then the one with the largest projected integer solution value p^k. If the value of λ is overestimated, more weight is placed on objective function value in deciding which outstanding problem is to be chosen next for solution. If the value of λ is underestimated, more weight is placed on the proximity to an integer solution in this decision.
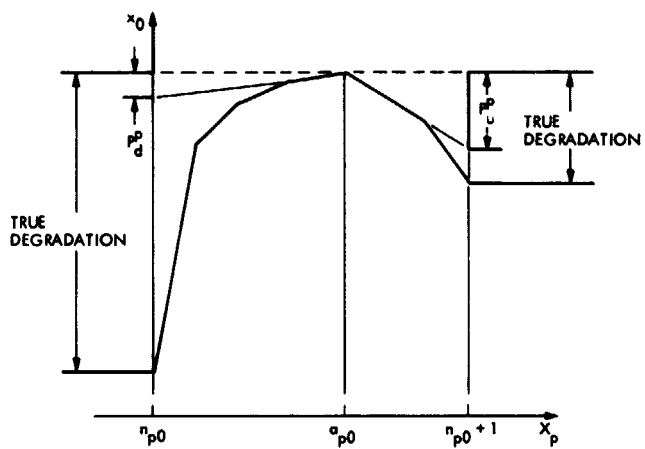
Fig. A-1. A larger penalty in the direction of
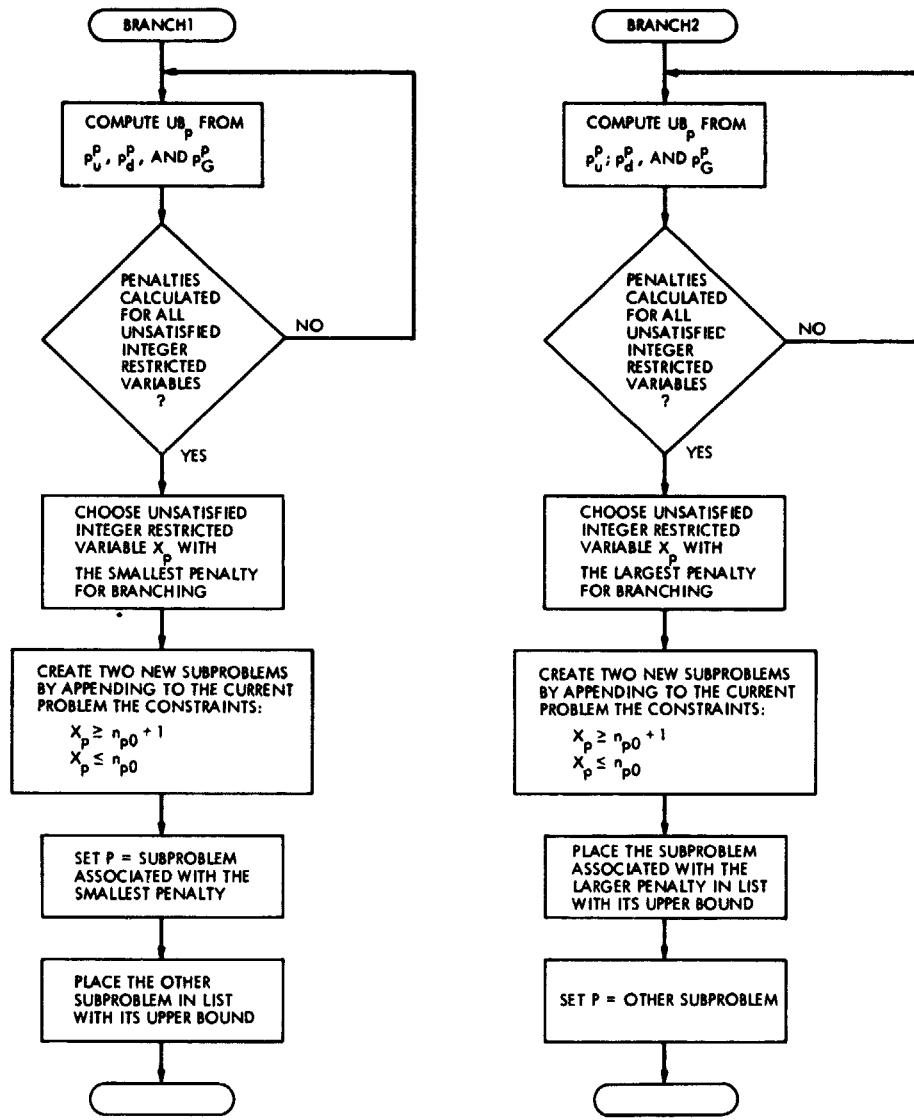smaller degradation

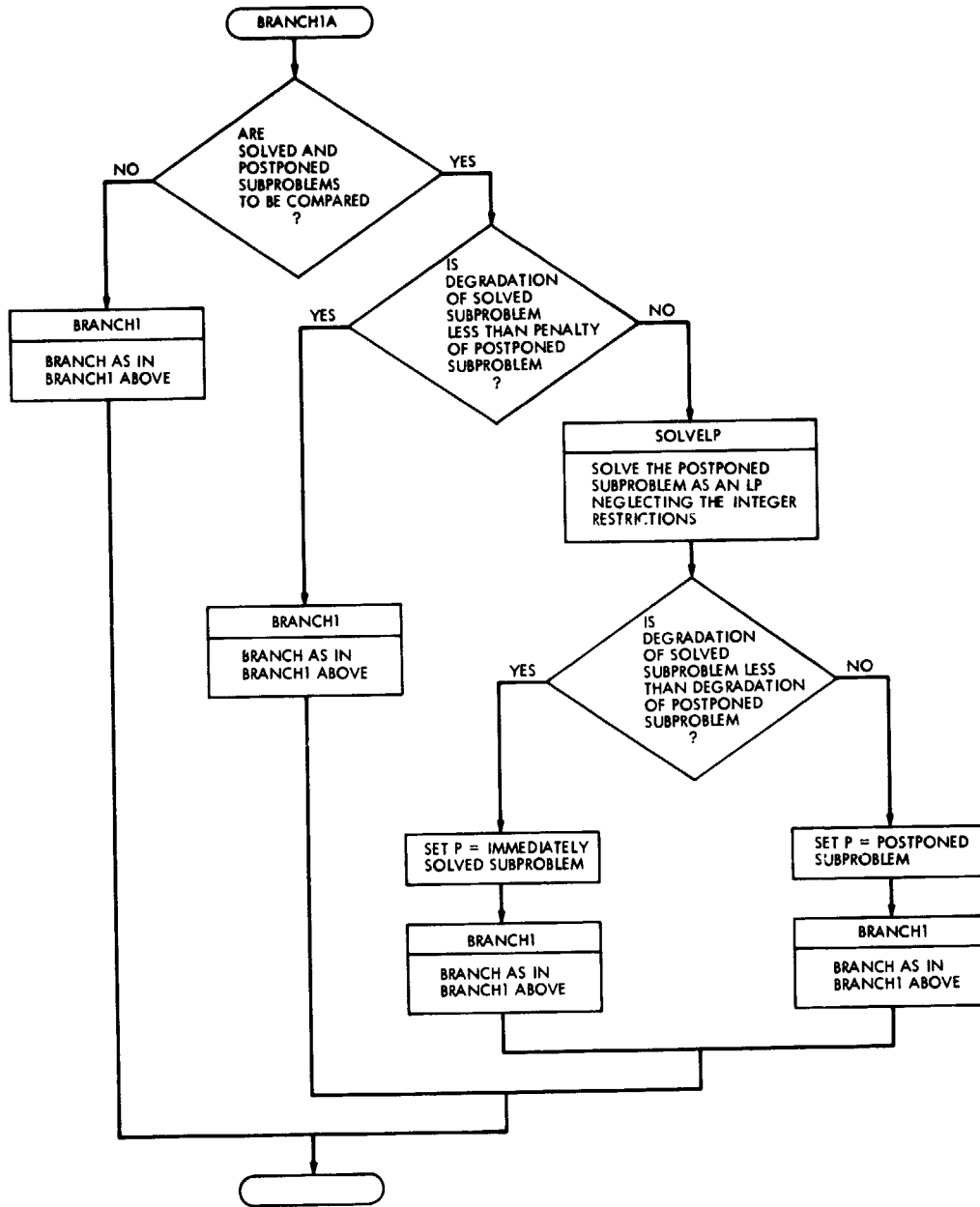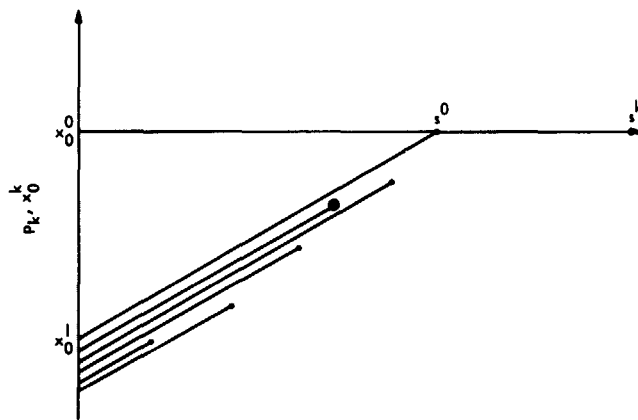Fig. A-2. Flowcharts for BRANCH1, BRANCH2, and BRANCH1A

Fig. A-2 (contd)

Fig. A-3. Objective function versus sum of infeasibilities